Comput Geosci (2008) 12:47–82
DOI 10.1007/s10596-007-9060-z

ORIGINAL PAPER

A dual-porosity model for ionic solute transport in expansive clays

Márcio A. Murad · Christian Moyne

Received: 30 May 2007 / Accepted: 24 October 2007 / Published online: 7 December 2007

Abstract A microstructure model of dual-porosity type is proposed to describe contaminant transport in fully-saturated swelling clays. The swelling medium is characterized by three separate-length scales (nano, micro, and macro) and two levels of porosity (nano- and micropores). At the nanoscale, the medium is composed of charged clay particles saturated by a binary monovalent aqueous electrolyte solution. At the intermediate (micro) scale, the two-phase homogenized system is represented by swollen clay clusters (or aggregates) with the nanoscale electrohydrodynamics, local charge distribution, and disjoining pressure effects incorporated in the averaged constitutive laws of the electro-chemo-mechanical coefficients and the swelling pressure, which appear in Onsager's reciprocity relations and in a modified form of Terzaghi's effective principle, respectively. The microscopic coupling between aggregates and a bulk solution lying in the micropores is ruled by a slip boundary condition on the tangential velocity of the fluid, which captures the effects of the thin electrical double layers surrounding each clay cluster. At the macroscale, the system of clay clusters is homogenized with the bulk fluid. The resultant macroscopic picture is governed by a dual-porosity model wherein macroscopic flow and ion transport take place in the bulk solution and the clay clusters act as sources/sinks of mass of water and solutes to the bulk fluid. The homogenization procedure yields a three-scale model of the swelling medium by providing new nano and micro closure problems, which are solved numerically to construct constitutive laws for the effective electro-chemo-hydro-mechanical coefficients. Considering local instantaneous equilibrium between the clay aggregates and micropores, a quasisteady version of the dual-porosity model is proposed. When combined with the three-scale portrait of the swelling medium, the quasisteady model allows us to build-up numerically the constitutive law of the equilibrium adsorption isotherm, which governs the instantaneous immobilization of the solutes in the clay clusters. Moreover, the constitutive behavior of the retardation coefficient is also constructed by exploring its representation in terms of the local profile of the electrical double layer potential of the electrolyte solution, which satisfies the Poisson–Boltzmann problem at the nanoscale.

Keywords Swelling clay · Homogenization · Dual porosity · Pollutant · Transport · Onsager's relations · Adsorption isotherm · Slip boundary condition · Electro-chemo-mechanical couplings · Retardation coefficient · Disjoining (swelling) pressure · Poisson–Boltzmann

M. A. Murad (✉)
Laboratório Nacional de Computação Científica
LNCC/MCT, Av Getúlio Vargas 333,
25651–070 Petrópolis, Rio de Janeiro, Brazil
e-mail: murad@lncc.br

C. Moyne
LEMTA, Nancy-University, CNRS 2,
avenue de la Forêt de Haye,
54504 Vandoeuvre les Nancy Cedex, France
e-mail: Christian.Moyne@ensem.inpl-nancy.fr

1 Introduction

Swelling porous media such as 2–1 lattice clays, hydrophilic polymers, shales, corneal endothelium, and

connective biological tissues exhibit a wide range of applications in almost all aspects of life. For example, smectite 2:1 clay particles saturated by saline solutions have been studied for decades and consist of one of the most traditional materials whose applications have played important roles throughout human history. Phenomena such as dehydration and rehydration of smectites, which are tied up directly to the electrochemical properties of the clay/water interface, have a profound impact on a wide variety of geotechnical and geoenvironmental problems. In agriculture, water adsorption by the clay determines the ability of soils to transport and supply water, nutrients, and pesticides. Owing to its low hydraulic conductivity, plasticity, and swelling properties along with the adsorptive capacity for contaminants, compacted clays (bentonites) have been suggested as appropriate buffer materials in geological disposal facilities against chemical or nuclear contamination including exposure to nuclear waste heat. In this particular application, swelling is a desirable property, as the swollen macromolecules are expected to fill-up the voids between the canisters containing the waste and the surrounding ground. Likewise, compacted soil liners have been used as earthen barriers to minimize the leakage from landfills to the subsurface environment. On the other hand, swelling and shrinkage are serious challenges the foundation engineer faces because of the potential danger of unpredictable upward movements of structures founded on expansive soils. Damage induced by swelling also occurs during well drilling operations where borehole stability in clay-rich shales is profoundly affected by the complex physicochemical interactions between the shaly formation and the aqueous drilling fluid.

The interplay between hydraulic-driven flow and charge transport, commonly referred to as electrokinetic coupling, has widespread applications in environmental science and geophysics, particularly in electrokinetic remediation of metal-contaminated soils and in measurements of electrokinetic signals to map groundwater flow in clay-rich formations. Beyond applications in natural geomaterials, electro-chemo-mechanical interactions between fluids and swelling polymers/biopolymers exhibit numerous technological applications such as in controlled drug release, in the design of contact lenses, in semiconductor manufacturing, and in food stuffs. In biomedical technology, electrical interactions between ions and negatively charged proteoglycans rule the deformation of cartilaginous soft hydrated tissues as load-bearing structures. The swelling property of the tissue plays an important role in articulating joint lubrication and damping of dynamic forces in the human body. Other applications of electro-chemo-mechanical couplings near charged surfaces involve the design of artificial membranes with high ion-exchange capacity, filtration processes, drying, ceramic science, and stress-crack prediction. As such, it is imperative that any macroscopic model describing the complex electro-chemo-mechanical interactions inherent to this type of system contains accurate constitutive relations.

Expansive materials have in common a structure that can be loosely identified as a mixture of macromolecules or colloidal particles (polymers, clay particles, proteoglycans) and solvent (water, hydrocarbons). The solvent is either adsorbed to the macromolecules forming an electrolyte solution with dissociated ionic species or in a bulk state, wherein cation and anion concentrations are locally equal. For simplicity we henceforth restrict our discussion to clay–water–electrolyte mixtures. The reader must be aware that the approach developed herein can also be applied to most colloidal systems.

Clay particles are mostly colloidal aluminosilicates lamellae. A typical 2:1 smectite such as montmorillonite is composed of two structural units: a sheet of aluminia octahedra sandwiched between two sheets of silica tetrahedra that stack by sharing exchangeable cations between their faces. The result of this arrangement is a flat composite layer exhibiting tremendous surface area with the flakes separated by aqueous layers forming stable aggregates. Crystal imperfections and isomorphous substitutions of some aluminum or silicon atoms by lower valence cations in the octahedral and tetrahedral sites of the clay sheets produce a negative surface charge. When exposed to polar liquids this charge is compensated by counter-ions in the electrolyte solution forming the classical Gouy–Chapman–Stern model commonly referred to as electrical double layer (EDL) theory (Van Olphen [56], Hunter [34], Mitchell [46]). The layers of fluid adjacent to the solid are denoted as the Stern or compact layer, whereas the more distant mobile part is the Gouy or diffuse layer. Macroscopic evidences of the clay/water electro-chemo-mechanical interactions are manifested in many observed phenomena such as electro-osmosis, chemico-osmosis, streaming potentials, conduction Ohmic current, streaming current, and electrophoresis (Lyklema [45]).

Montmorillonite clays often shrink/swell in response to changes in fluid content or chemical composition of the pore fluid. When water comes in contact with a mass of clay crystals, it solvates the counter-ions and penetrates between the layers, forcing them apart.

When hydration progresses, the crystals expand to several times their original thickness. In the characterization of swelling, a distinction is commonly made between short-range crystalline swelling, typically associated with adsorption of the first two to three molecular layers of water, and long-range osmotic swelling, which arises from the overlapping between adjacent diffuse double layers. Stable arrangement of clay particles and the spacing between individual lamellae are dictated by the disjoining pressure, which is defined by the excess in the normal fluid stress relative to the bulk phase pressure of the outer solution (Derjaguin et al. [18]).

Like most natural porous media, smectitic clays exhibit a hierarchy of scales and often there is a distinct scale separation. The finest scale of this hierarchy is the nanoscale, wherein the portrait of the soil fabric is an assembly of colloidal-size particles with lamellar structure. A typical characteristic length associated with this scale, where multiscale continuum descriptions can still be adopted, is the Debye's screening length $\mathcal{O}(10^{-9}m)$, which measures the effective thickness of the EDL (Hunter [34]). At this scale, the electrolyte solution can still be regarded as a continuum fluid with flow governed by the electrohydrodynamics coupled with Nernst–Planck and Poisson–Boltzmann equations governing flow, transport of mobile charges, and electric potential distribution (see Moyne and Murad [47, 49, 50], Gross and Osterlé [29], Fair and Osterlé [28], Sasidhar and Ruckenstein [60, 61], Yang and Li [68]).

At the microscale (the homogenized nanoscale), the typical length of which is of $\mathcal{O}(10^{-6}m)$, the highly heterogeneous solid–fluid interactions are represented in an averaged fashion, with electrolyte solution and particles viewed as overlaying continua forming swollen clay clusters (or aggregates) with averaged properties established at every point of the mixture (Bennethum and Cushman [9]). Under near-equilibrium isothermal conditions, the simultaneous movements of fluid, ions, and electric current are linearly coupled with the conjugated gradients of hydraulic head, concentration, and electric potentials through Onsager's reciprocity relations (see, e.g., Lai et al. [39], Huyghe and Janssen [36], Gu et al. [30, 31], Heidug and Wong [32], Moyne and Murad [49], Rosanne et al. [57]). The thermodynamics of irreversible processes underlying Onsager's reciprocity relations provides a comprehensive framework for describing the coupling between fluxes and driving forces (Yeung and Mitchell [69]). The coefficients appearing in the Onsager's matrix reflect (in the averaged sense) the nanoscopic electro-hydro-chemical interactions that take place in the electrolyte solution (see Fair and Osterlé [28], Moyne and Murad [49, 50], Looker and Carnie [42]).

The mechanisms governing the deformation of the solid matrix are ruled by the averaged stress partitioning rules, which are dictated by the modified form of Terzaghi's effective stress principle (Hueckel [33], Achari and Joshi [1]). In addition to the well-known stresses of direct contact (Terzaghi's effective stresses and pore pressure), an additional electrochemical component incorporating the net repulsive (R) and attractive (A) forces, commonly denoted by $(R-A)$ (see Sridharan and Rao [66], Lambe [38], Hueckel [33]), plays an important role in the expansion/shrinking of the aggregates. This stress has been identified with the swelling pressure (the averaged Derjaguin's disjoining pressure), which can be measured through the overburden pressure excess that must be applied to a well-ordered clay–water mixture separated from bulk water by a semipermeable membrane to prevent further uptake of water (Low [44]).

The microscopic two-scale electro-chemo-mechanical model for the clay clusters is coupled with the equations governing flow and solute transport in the bulk solution lying in the micropore system. Owing to the coarser structure of the micropores with larger size void spaces and characteristic length much greater than the Debyes length, the equations governing the bulk fluid are free of EDL effects. This particular feature distinguishes properties of a bulk fluid from an electrolyte solution and further implies in a pointwise form of the electroneutrality condition with local equality between co- and counterion concentrations (Newman [54]).

Application of the second level of up-scaling to the cluster/microvoid coupled microscopic model leads to the macroscopic description of the swelling medium wherein the two systems are represented in a homogenized fashion. The resultant effective model resembles in form the well-established dual-porosity models for fissured media (Barenblatt et al. [8], Warren and Root [70], Wilson and Aifantis [72]). In the macroscopic picture of a dual-porosity model, an interconnected network of micropores (or fissures) provides most of the global conductivity for flow and transport, whereas most of the storage takes place in the relatively low permeability matrix blocks. Here, we identify matrix block and fissure systems with the clay clusters and micropores, respectively. An essential feature underlying the accuracy of dual-porosity models is the correct description of the constitutive response of the coupling between the two media. Classically, this coupling

is incorporated pointwisely via transfer functions that quantify mass, momentum, and energy interchange between them. In the so-called lumped-parameter formulations, the transfer functions are represented by classical exchange terms, assumed proportional to the difference between the potentials in the two systems [8, 70, 72]. More recently, more realistic descriptions of such coupling have been proposed based on two-scale formulations that aim at capturing the influence of the microstructure upon the constitutive response of the transfer function. Notably, the so-called microstructural dual-porosity approaches proposed by Arbogast and coworkers [2, 3, 24] for rigid fractured media (see also Bourgeat et al. [13]) have established a direct correlation between the mass transfer term and the microstructural behavior of the fractured media. The two-scale portrait underlying this approach is a continuous family of microscopic matrix blocks with prescribed geometry distributed over the macroscopic domain occupied by the fractures, with each block identified to a macroscopic location. In contrast to lumped-parameter models, the transfer functions are explicitly calculated by solving and averaging the microscale closure problems in the matrix blocks. The down-scaling procedure inherent to this approach represents a way to capture the influence of the geometry of the microstructure and the multiple space and time scales involved in the problem upon the effective medium behavior (Showalter [63]).

The framework of microstructural dual-porosity models for rigid media has been extended to deformable poroelastic media by Murad and Cushman [51] and Murad et al. [52]. The novelty in this approach is that, in addition to the mass transfer function, a distributed momentum interchange term between global and local systems also appears in the homogenized model. Furthermore, application of the modified Green's function technique shows direct correlation between the transient poroelastic closure in the matrix blocks and a single effective viscoelastic constitutive law for the macroscopic effective stress tensor exhibiting fading memory effects (Murad et al. [52]). The history dependency in the effective stress/strain constitutive law aims at capturing secondary consolidation and hereditary creep phenomena, which arise from the delayed drainage of the fluid in the secondary level of pores after the fluid pressure in the coarser voids of the primary structure has been somewhat dissipated (see Murad et al. [52] for details).

The generalization of the three-scale dual-porosity approach developed by Murad and Cushman [51] and Murad et al. [52] to incorporate electro-chemo-hydro-mechanical couplings in swelling porous media still

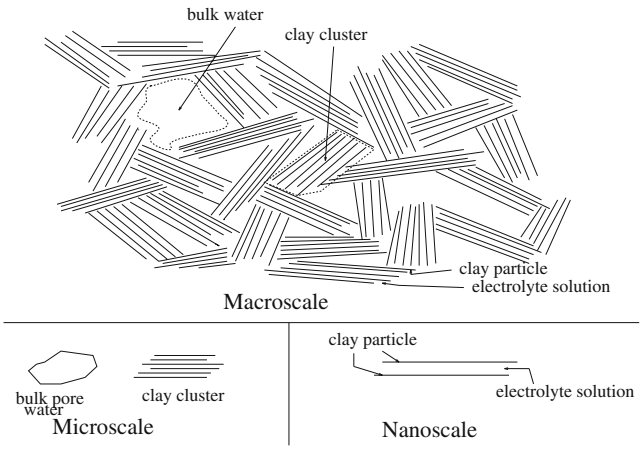

Fig. 1 Three-scale model for clay

remains an open issue. The goal of this contribution is to fill this gap. We develop herein a three-scale dual-porosity model for expansive clays based on a rigorous up-scaling of the nanoscale description (Fig. 1). To accomplish this task we begin by presenting the microscale electro-chemo-mechanical model for the clay clusters based on a modified form of Terzaghi's decomposition coupled with the Onsager's reciprocity relations. To evaluate the magnitude of the Onsager's coefficients, we consider a particular form of nanostructure wherein each clay cluster is composed of parallel particles of close face-to-face contact. In this simplified arrangement, we establish precise correlations between the averaged electrochemical coefficients and the nanoscopic electrokinetics of the electrolyte solution lying in the nanopores. We also formulate the microscopic equations governing flow and transport in the micropore domain occupied by the bulk solution. As mentioned before, owing to the coarser structure of the micropores, the equations governing the bulk fluid do not incorporate EDL effects. Nevertheless, the microscopic hydrodynamic coupling between clusters and micropores is dictated by a slip boundary condition in the fluid tangential velocity owing to the presence of the thin EDLs surrounding each clay cluster. This suggests that, unlike what happens in the nanopores, the effect of the EDL upon the bulk fluid acts in a short range fashion remaining restricted to the cluster/micropore interface, giving rise to a discontinuity in the tangential velocity of the fluid.

Assuming local periodicity of the aggregates, we apply the homogenization procedure to up-scale the coupled cluster/micropore model to the macroscale. This yields a microstructure model of dual-porosity type with macroscopic bulk fluid flow and transport equations coupled with generalized mass transfer

functions to local microscale problems posed in each clay cluster domain. By exploring the closure problems arising from the homogenization procedure, we provide microscopic representations for the effective coefficients, such as swelling pressure and chemico- and electro-osmotic conductivities in Darcy's law. In particular, the three-scale representation of the swelling pressure obtained herein furnishes more refined information compared to its well-known two-scale formula seated on the EDL theory for parallel particles (Derjaguin and Churaev [18], Israelachvili [37], Van Olphen [56]). The novelty is the appearance of an additional component in the constitutive law, which captures the transmissibility of the electro-chemo-mechanical stresses between adjacent clusters.

A simplified version of the dual-porosity model is derived by postulating local thermodynamic equilibrium between clusters and micropores. This leads to the appearance of a *quasisteady* approach characterized by a time-scale assumption wherein the macroscopic medium follows a regular evolution process with its thermodynamic states at local equilibrium with the clay clusters. Under this assumption, the microscopic transient closure problems become stationary and, consequently, the constitutive law of the distributed mass transfer function gives rise to a retardation coefficient, which governs the instantaneous electrochemical immobilization of the species in the aggregates. In this scenario we exploit the notable feature of the three-scale approach in providing a double nano/micro representation for the retardation coefficient, yielding an accurate constitutive law for this parameter built-up from the electrochemistry of the electrolyte solution in the nanopores, whose electric potential and charge distribution satisfy the Poisson–Boltzmann problem. This framework is further explored to reconstruct the adsorption isotherm, whose form resembles that of a generalized nonlinear power-law curve of Freundlich type with the exponent depending on bulk concentration.

In the stratified nanostructure of clay clusters composed of parallel particles of face-to-face contact, the Poisson–Boltzmann equation reduces to a one-dimensional nonlinear problem in the direction normal to the clay surface. Using a well-known change of variables the problem is reduced to a formulation based on the computation of elliptic integrals, whose numerical solution can easily be obtained [18, 50]. Making use of this discretization technique, we compute the nanoscopic profile of the electric potential and further use it as input data in the numerical solution of the closure problems for the effective electrochemical coefficients to build-up their constitutive laws. Finally, our simulations illustrate the potential of the three-scale approach in providing a first step towards the derivation of reliable effective constitutive laws arising from bridging nano, micro, and macro electro-chemo-mechanical phenomena in swelling systems.

2 Microscopic electro-chemo-hydro-mechanical model

We begin by presenting the microscale electro-chemo-hydro-mechanical model governing averaged fluid flow, ion transport, electric current, and particle deformation in the clay clusters. The aggregates are treated as a water-saturated charged porous deformable continuum composed of two overlapping phases: the clay particles (solid phase) and the aqueous electrolyte solution consisting of water solvent and a single binary monovalent salt with fully dissociated 1:1 electrolytes (Na^+/Cl^- or K^+/Cl^-). The microscopic governing equations can be derived within the framework of the mixture theory in conjunction with the linearized thermodynamics of irreversible processes (see, e.g., Lai et al. [39], Huyghe and Janssen [36], Gu et al. [30, 31] Heidug and Wong [32]), or alternatively by averaging the nanoscopic model in the nanopores (Moyne and Murad [49, 50]). In the former procedure, one makes use of Onsager's reciprocity relations to obtain near equilibrium couplings between driving forces and conjugated fluxes, whereas in the latter approach, the up-scaled model is derived by homogenizing the continuum nanoscopic description of the electrolyte solution in the nanopores given by the electrohydrodynamics coupled with Nernst–Planck and Poisson–Boltzmann equations governing flow, ion movement, and local electric potential distribution (see [49, 50] for details).

For the sake of simplicity, we consider fluid and nanoscale particles incompressible and gravity/inertial effects negligible. Particles are assumed elastic undergoing quasistatic small deformations from an arbitrary reference configuration and contain a uniformly distributed surface charge density, which is neutralized by the excess of positively charged dissociated ions to fulfill the electroneutrality condition. Steric and hydration effects are neglected and, consequently, throughout the paper, the liquid phase is treated a structureless Newtonian electrolyte solution with ions treated as point charges.

2.1 Microscopic formulation in primitive variables

We begin by presenting some of the microscopic averaged governing equations for the clay clusters

formulated in primitive unknowns (e.g., ion concentrations, thermodynamic pressure). Furthermore, we illustrate that this formulation is not natural for enforcing boundary conditions with the outer bulk fluid in the micropores. By invoking the well known continuity of the electrochemical potentials at the interface, we rephrase the model in terms of alternative "hidden" bulk variables defined in the sense of Moyne and Murad [47, 49], which are more appropriate for imposing boundary conditions.

Let $\Omega_s \subset R^n\,(1 \le n \le 3)$ be the microscale region occupied by the clay aggregates. For each time $t \in (0, \infty)$, the subset of governing equations formulated in primitive unknowns read as follows [49].

Total momentum

$$\nabla \cdot \boldsymbol{\sigma}_t = 0 \tag{2.1}$$

where $\boldsymbol{\sigma}_t$ is the overall averaged stress tensor of the aggregates.

Modified Terzaghi's decomposition

$$\boldsymbol{\sigma}_t = -P_l\,\boldsymbol{I} + \boldsymbol{\sigma}_e + \boldsymbol{E}_M \tag{2.2}$$

where $\boldsymbol{I}$ is the identity tensor, P_l and $\boldsymbol{\sigma}_e$ the averaged thermodynamic pressure of the electrolyte solution and Terzaghi's contact stress tensor between particles, and $\boldsymbol{E}_M$ a coupling electromechanical tensor that represents the averaged counterpart of the nanoscopic Maxwell stress tensor of the electrolyte solution (see [47, 49] and, further, Section 2.2.5). In the above decomposition, chemical effects are lumped in the thermodynamic pressure P_l, whose magnitude incorporates the sum of the bulk phase pressure of the outer solution and Donnan osmotic pressure (see [49]). For dilute solutions, the osmotic pressure is given by the well known Van't Hoff relation (see, e.g., [20, 36]).

Linear elastic constitutive law for the contact stresses

$$\boldsymbol{\sigma}_e = \boldsymbol{C}\boldsymbol{\mathcal{E}}(\mathbf{u}) \tag{2.3}$$

where $\mathbf{u}$ is the averaged displacement of the solid phase, $\boldsymbol{\mathcal{E}}(\mathbf{u}) = 1/2(\nabla\mathbf{u} + \nabla\mathbf{u}^T)$ the linearized strain tensor, and $\boldsymbol{C}$ the elastic modulus (fourth-rank tensor) of the aggregates.

Overall mass balance for locally incompressible phases

$$\nabla \cdot \mathbf{v}_D + \nabla \cdot \frac{\partial \mathbf{u}}{\partial t} = 0 \tag{2.4}$$

where $\mathbf{v}_D$ is the Darcy velocity of the electrolyte solution relative to the movement of the solid phase.

Mass balance of the solid phase

$$\frac{\partial}{\partial t}(1-\phi) + \nabla \cdot \left((1-\phi)\frac{\partial \mathbf{u}}{\partial t}\right) = 0 \tag{2.5}$$

where ϕ is the intracluster porosity.

Mass balances of the ions

$$\frac{\partial}{\partial t}(\phi\, C_\pm) + \nabla \cdot \boldsymbol{J}_\pm = 0 \tag{2.6}$$

where C_+ and C_- are the averaged concentration of cations (Na^+) and anions (Cl^-) and $\{\boldsymbol{J}_+, \boldsymbol{J}_-\}$ the corresponding fluxes. The notation $\pm$ aims at representing the two mass balances in a single set.

Constitutive law for the ion fluxes

To present the constitutive laws for $\boldsymbol{J}_\pm$, denote F and R as the Faraday and ideal gas constants, T the absolute temperature (assumed constant), and $\mu_\pm$ the averaged molar electrochemical potentials of cations and anions. Under the dilute solution approximation, for monovalent ions of unitary valence, $\mu_\pm$ are defined as (see e.g. Callen [14], Lyklema [45])

$$\mu_\pm := \overline{\mu}_\pm \pm F\Phi_* + RT \ln C^*_\pm \tag{2.7}$$

where Φ_* is the microscale electric potential, $\overline{\mu}_\pm$ the reference values of the chemical potential (depending on pressure and temperature), and $C^*_\pm$ an apparent ion concentration, which, as we shall further illustrate in Section 2.2.3, is directly related to $C_\pm$. The difference between $C_\pm$ and $C^*_\pm$ stems from the averaging of the nonlinearity in the constitutive law of the nanoscale electrochemical potential, which, due to the noncommuting property, differs from the logarithm of the averaged concentration.

Denoting $\boldsymbol{D}^\star_\pm$ and $\boldsymbol{V}_\pm$ the averaged apparent diffusion coefficients and advection velocities, the ionic fluxes are given by [49]

$$\boldsymbol{J}_\pm = C_\pm \boldsymbol{V}_\pm - \frac{\boldsymbol{D}^\star_\pm C^*_\pm}{RT}\nabla\mu_\pm\,. \tag{2.8}$$

The reader may verify that, unlike the advection of nonionic species, which is solely driven by the Darcy's seepage flux $\mathbf{v}_D$, the convective velocities for cation and anion transport are not equal. The difference stems from the electrochemical interactions between the movement of the fluid and the EDLs, which have different influence upon cations and anions. In addition, the tensors $\boldsymbol{D}^\star_\pm$ do not play the role of real diffusivities, as they appear multiplied by the gradient of the apparent ion concentrations $\nabla\mu_\pm(C^*_\pm)$. Subsequently,

by exploring the correlations with the nanoscale behavior of the electrolyte solution, direct relations between $C_{\pm}^{\star}$ and $C_{\pm}$ along with $\boldsymbol{D}_{\pm}^{\star}$ and the ionic diffusivities $\boldsymbol{D}_{\pm}$ for $\nabla C_{\pm}$ will be derived.

Neglecting the pressure–diffusion effect associated with the variability of the reference electrochemical potentials induced by pressure gradient, under isothermal conditions, $\overline{\mu}_{\pm}$ are constants. Denoting $\overline{\Phi}_{*} = F\Phi_{*}/RT$, the dimensionless electric potential, using Eqs. 2.7 and 2.8 in Eq. 2.6, we obtain

$$\frac{\partial}{\partial t}\left(\phi C_{\pm}\right) + \nabla\cdot\left(C_{\pm}\boldsymbol{V}_{\pm}\right) = \nabla\cdot\left[\boldsymbol{D}_{\pm}^{\star}\left(\nabla C_{\pm}^{*} \pm C_{\pm}^{*}\nabla\overline{\Phi}_{*}\right)\right]. \tag{2.9}$$

The right-hand side (RHS) of Eq. 2.9 shows ion diffusion governed by the sum of a Fickian term and an electromigration component, which governs the movement of the ions under the electric potential gradient. Together with the relation between $\{C_{\pm}^{*}, \boldsymbol{D}_{\pm}^{\star}\}$ and $\{C_{\pm}, \boldsymbol{D}_{\pm}\}$, the above result represents the upscaled form of the Nernst–Planck equations (Samson et al. [58]).

2.2 Boltzmann transformations and bulk properties

By invoking the classical Donnan equilibrium between the electrolyte solution in the nanopores and the outer bulk fluid in the micropores, it is well known that the electrochemical potentials are continuum across the interface (Callen [14]). According to the classical EDL theory at the nanoscale, for a given concentration of species in the bulk solution, ion concentrations vary strongly in the nanopores according to Boltzmann distributions resulting from the equality between the electrochemical potentials [21]. Therefore, to fulfill the electroneutrality condition with the surface charge density, the averaged ion concentration $C_{\pm}$ is discontinuous across the interface with the outer saline bath, and consequently, boundary conditions are not naturally enforced in terms of these unknowns (see [47, 49]).

2.2.1 Equilibrium bulk concentrations

To recast the microscopic problem in a more appropriate manner for enforcing boundary conditions with the outer bulk fluid, we adopt a change of variables by replacing $C_{\pm}$ and $C_{\pm}^{\star}$ by an auxiliary bulk concentration to be further defined pointwisely in Ω_s. To this end, we begin by invoking the classical nanoscopic EDL theory describing the thermodynamic equilibrium between an electrolyte solution delimited by two parallel charged particles and an outer bulk fluid. Denoting $\{c^{\pm}, \mu^{\pm}, \Phi^{*}\}$ as the nanoscopic counterpart of $\{C_{\pm}, \mu_{\pm}, \Phi_{*}\}$, the thermodynamic equilibrium between the electrolytes and the species in the bulk fluid is dictated by the equality of the electrochemical potentials (Dormieux et al. [21]). Denoting $\mu_f = \mu_f^{+} = \mu_f^{-}$ and $C_f = C_f^{+} = C_f^{-}$ as the chemical potential and bulk concentration of the species in the bulk fluid, at equilibrium, these are homogeneous quantities. We then have

$$\mu^{\pm} = \overline{\mu}^{\pm} \pm F\Phi^{*} + RT\ln c^{\pm} = \mu_f := \overline{\mu}^{\pm} + RT\ln C_f \tag{2.10}$$

which yields the classical Boltzmann distributions of the EDL theory (see [35, 46, 56])

$$c^{\pm} = C_f \exp\left(\mp\overline{\Phi}^{*}\right) \tag{2.11}$$

with $\overline{\Phi}^{*} := F\Phi^{*}/RT$ denoting the dimensionless nanoscopic EDL potential. To up-scale this result to the microscale, denote $\langle\cdot\rangle_z := |Z|^{-1}\int_{Z_\alpha}\cdot\,\mathrm{d}Z_\alpha$ and $\langle\cdot\rangle_z^{\alpha} := |Z_\alpha^{-1}|\int_{Z_\alpha}\cdot dZ_\alpha$ $(\alpha = l, s)$ as the volume average and intrinsic volume average operators $(\langle\cdot\rangle_z^{l} = \phi\langle\cdot\rangle_z^{l})$ over a nanoscopic cell Z composed of subdomains Z_s and Z_l occupied by the parallel particles and nanopores, respectively (see Fig. 2). By averaging Eq. 2.11 over Z_l and noting that, by definition, $C_{\pm} := \langle c^{\pm}\rangle_z^{l}$, because C_f is a homogeneous quantity, the discontinuity in the averaged concentrations across the interface is given by

$$C_{\pm} - C_f = C_f\left[\left\langle\exp\left(\mp\overline{\Phi}^{*}\right)\right\rangle_z^{l} - 1\right]. \tag{2.12}$$

The above result motivates the necessity of rephrasing the model in terms of alternative concentrations to whom Dirichlet boundary conditions representing continuity with the bulk fluid in the micropores can naturally be enforced.

2.2.2 Streaming potential

To define bulk concentration in Ω_s, we begin by extending the above Boltzmann distributions to nonequilibrium conditions induced by flow and charge transport. To this end, consider a simple nanoscopic picture of one-dimensional flow of an electrolyte solution in an idealized array of nanopores with geometry composed of long channels delimited by parallel particles or capillary tubes (Fig. 3). The movement of the electrolyte solution induced by a pressure gradient carries the counter-ions in the diffuse layer towards the downstream end. This leads to the appearance of the so-called streaming current, which gives rise to an electrokinetic potential, commonly referred to as streaming

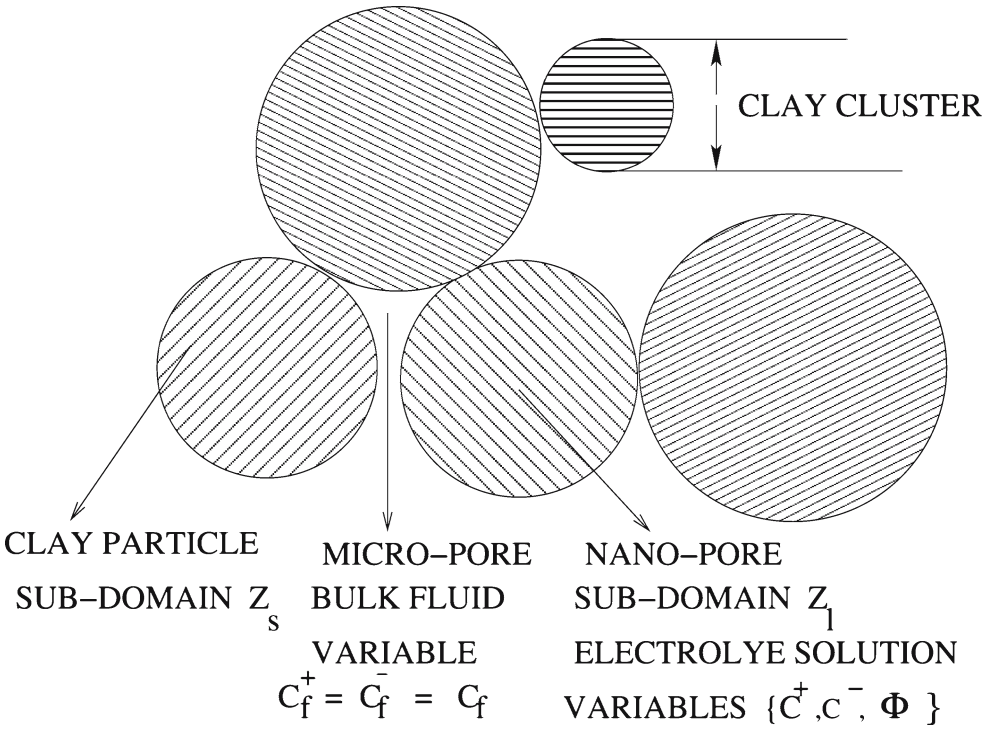

Fig. 2 Microscopic portrait of the clay fabric

potential [10, 60, 61, 68]. The gradient of this latter quantity acts to drive the counterions of the diffuse layer in the opposite direction to the pressure driven flow generating a conduction current and a counter electro-osmotic flow acting to slow down the movement of the liquid (see, e.g., Li [41] and references therein). Under the open-circuit condition, which is characterized by the absence of an external electric field when the outer solutions are isolated from each other, the balance between pressure-driven and counter electro-osmotic flow stabilizes when the net electric current vanishes (see [10, 60, 61, 68] for details).

By invoking the aforementioned discussion, we postulate that, under nonequilibrium conditions, the total electric potential $\Phi^\star$ incorporates the EDL component φ associated with local charge distribution in the nanopores and the streaming potential Ψ_b, herein denoted with the subscript "b" to designate its "bulk nature", i.e., not associated with EDL effects. By making use of this decomposition, we then split the nanoscopic overall potential in the form (see also [10, 60, 61, 67])

$$\Phi^* = \varphi + \Psi_b \,. \tag{2.13}$$

As mentioned before, to characterize φ and Ψ_b, the former potential aims at representing a fluctuating EDL component varying strongly in the nanopore domain, whereas the latter plays the role of the streaming potential under the open-circuit assumption. In the one-dimensional setting, Ψ_b varies axially with flow and transport, whereas φ fluctuates transversally according to the Boltzmann distribution of the EDL theory (see Fig. 3 and [28, 60, 61, 68]). Because Ψ_b does not vary in the transversal direction, it is treated as a pure microscopic quantity [50]. Whence, by averaging Eq. 2.13

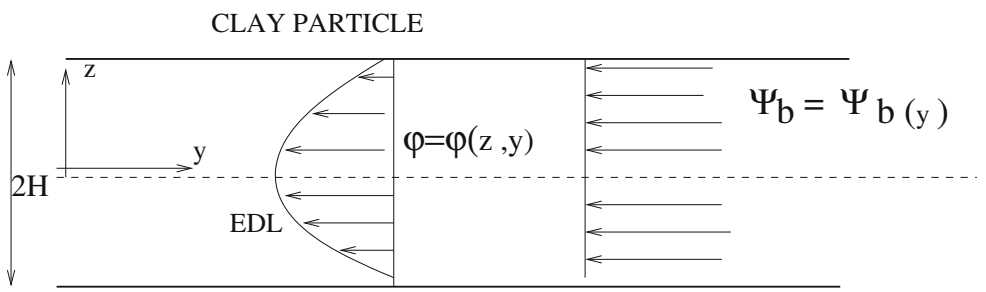

Fig. 3 Nanoscopic portrait of the dependence of the EDL and streaming potentials

across the nanopore domain, the microscopic decomposition reads

$$\Phi_* := \langle \Phi^* \rangle_z^l = \langle \varphi \rangle_z^l + \Psi_b \,. \tag{2.14}$$

2.2.3 Nonequilibrium bulk concentrations

To extend the Boltzmann distributions (Eq. 2.12) to nonequilibrium conditions towards the characterization of local bulk concentrations $C_b^{\pm}$, one needs to incorporate the effects of the streaming potential. For thin double layers, bulk properties are nothing but those measured away from the particle surface. Conversely, when the EDLs span the entire nanopores, bulk properties become "hidden" and their pointwise characterization requires the more elaborated analysis presented next (see also [49]).

Following Newman [54], the characterization of a bulk medium is seated on the absence of EDL effects and net charge density $\left(q_b := F\left(C_b^+ - C_b^-\right) = 0\right)$, which implies in local equality between co- and counterion concentrations $\left(C_b^+ = C_b^- = C_b\right)$. We then adapt Newman's conjecture to our picture by defining a hidden bulk solution in the clay cluster domain as a fluid characterized by local equality between co- and counterion concentrations at local thermodynamic equilibrium with the cations and anions of the electrolyte solution. To define mathematically thermodynamic properties associated with the hidden bulk solution, we make use of the decomposition (Eq. 2.13) and define the electrochemical potential of the species in the bulk fluid $\left(\mu_b^{\pm}\right)$ by setting $c^+ = c^- = C_b$ and $\Phi^* = \Psi_b$ (or $\varphi_b = 0$) in Eq. 2.10, which gives $\mu_b^{\pm} := \overline{\mu}_{\pm} \pm F\Psi_b + RT \ln C_b$. This local characterization is based on neglecting the EDL potential and the net charge density in a bulk fluid. By construction, the thermodynamic equilibrium between the species in the electrolyte solution and in the hidden bulk fluid is governed by the equality $\mu_b^{\pm} = \mu^{\pm}$. Using the above definition along with Eq. 2.10, we have

$$\mu_b^{\pm} = \overline{\mu}_{\pm} \pm F\Psi_b + RT \ln C_b = \mu^{\pm} = \overline{\mu}_{\pm} \pm F\Phi^* + RT \ln c^{\pm} \tag{2.15}$$

which, using Eq. 2.13, leads to the nonequilibrium version of the Boltzmann distributions (Eq. 2.11)

$$c^{\pm} = C_b \exp\left(\mp \overline{\Phi}^* \pm \overline{\Psi}_b\right) = C_b \exp(\mp \overline{\varphi}) \tag{2.16}$$

with $\overline{\varphi} := F\varphi/RT$ and $\overline{\Psi}_b := F\Psi_b/RT$ the corresponding dimensionless quantities. Like the streaming potential Ψ_b in Fig. 3 and unlike the EDL variables $\{c^{\pm}, \overline{\varphi}\}$, the bulk concentration is not directly affected by the surface charge of the particles and, consequently, does not fluctuate transversally, varying only axially [50]. Using this result by averaging Eq. 2.16, we obtain

$$C_{\pm} := \left\langle c^{\pm} \right\rangle_z^l = C_b \, G_{\pm} \,. \tag{2.17}$$

with $G_{\pm} := \langle \exp(\mp \overline{\varphi}) \rangle_z^l$. An important consequence of Eq. 2.17 is the extension of Eq. 2.12 to the nonequilibrium case, provided the pair $\{C_f, \langle \exp(\mp \overline{\Phi}^*) \rangle_z^l\}$ is locally replaced by $\{C_b, G_{\pm}\}$ with C_b varying across the cluster domain. Thus, unlike $\overline{\Psi}_b$, which only appears at nonequilibrium conditions, $\overline{\varphi}$ plays the role of an EDL potential, which dictates the Boltzmann distributions for ion concentration in general thermodynamic conditions. When the electrolyte solution is at equilibrium with an outer saline bath of uniform concentration $C_b = C_f$, the classical equilibrium distributions Eq. 2.12 are recovered by simply setting $\overline{\Psi}_b = 0$ and $\overline{\varphi} = \overline{\Phi}^{\star}$.

One may clearly observe that, when the EDLs overlap, C_b becomes a hidden quantity in the sense that only indirect measurements based on Eq. 2.17 can be used to evaluate it for given values of $\{C_{\pm}, G_{\pm}\}$. One may interpret C_b as an apparent concentration (same for Na^+ and Cl^-), which is asymptotically achieved locally by freezing each fluid particle instantaneously with an isolating wall and letting the EDL potential $\overline{\varphi} \to 0$. For a precise characterization of C_b in general nanopore domains of nonparallel particles, we refer to the two-scale homogenization analysis developed in Moyne and Murad [49].

It remains to rephrase the averaged Nernst–Planck equation (Eq. 2.9) in terms of C_b. This can be accomplished by making use of the averaged Boltzmann transformations for $C_{\pm}$ and $C_{\pm}^{\star}$. The former is represented by Eq. 2.17, whereas the latter can be derived by up-scaling the equality between the nanoscale electrochemical potentials (Eq. 2.15). Thus, denoting $\mu_{b\pm} := \left\langle \mu_b^{\pm} \right\rangle_z^l$ and $\mu_{\pm} := \left\langle \mu^{\pm} \right\rangle_z^l$ using Eq. 2.7 and recalling that C_b and Ψ_b are independent of the nanoscopic coordinate, we have

$$\mu_{b\pm} = \overline{\mu}_{\pm} \pm F\Psi_b + RT \ln C_b = \mu_{\pm} = \overline{\mu}_{\pm} \pm F\Phi_* + RT \ln C_{\pm}^*$$

which implies

$$C_{\pm}^* = C_b \exp\left(\mp \overline{\Phi}_* \pm \overline{\Psi}_b\right) = C_b \, G_{\pm}^* \tag{2.18}$$

where $G_{\pm}^* := \exp(\mp \langle \overline{\varphi} \rangle_z^l)$. Note that, due to the noncommuting property of the mean value operator of a nonlinear function, $G_{\pm}^* \neq G_{\pm}$, which implies $C_{\pm}^* \neq C_{\pm}$. Conversely, under the linearized Debye–Huckel approximation of the Boltzmann distribution, valid for low electric potentials (Hunter [35]), we have $G_{\pm} \approx \langle 1 \mp \overline{\varphi} \rangle_z^l = 1 \mp \langle \overline{\varphi} \rangle_z^l \approx G_{\pm}^*$, and consequently, the two ion concentrations coincide.

Making use of the above generalized Boltzmann distributions, we are now ready to derive the relation between $C^*_\pm$ and $C_\pm$. From Eqs. 2.17 and 2.18, we have

$$C^*_\pm = C_b G^*_\pm = C_\pm G^{-1}_\pm G^*_\pm .$$

with shows $C^*_\pm$ and $C_\pm$ simply related by the correction factor $G^*_\pm G^{-1}_\pm$. In an analogous manner, we define the diffusion coefficient for $\nabla C_\pm$ in the form $\boldsymbol{D}^\star_\pm := G^{*-1}_\pm G_\pm \boldsymbol{D}_\pm$. Therefore, using Eq. 2.17 and the decomposition Eq. 2.14, one can rephrase Eq. 2.9 in terms of $C_b, \overline{\varphi}, \overline{\Psi}_b$, and $\boldsymbol{D}_\pm$ as

$$\frac{\partial}{\partial t}\left(\phi\, G_\pm C_b\right) + \nabla \cdot \boldsymbol{J}_\pm = 0 \tag{2.19}$$

$$\boldsymbol{J}_\pm = C_b G_\pm \boldsymbol{V}_\pm - \boldsymbol{D}_\pm G_\pm \left(\nabla C_b \pm C_b \nabla \overline{\Psi}_b\right) \tag{2.20}$$

which shows the same form of the averaged Nernst–Planck derived in Moyne and Murad [49] by homogenizing the nanostructure. The reader may verify that, within the two-scale model discussed in Moyne and Murad [49], the diffusivities admit the nanoscopic representation $\boldsymbol{D}_\pm G_\pm = \left\langle \mathcal{D}^\pm \exp(\mp\overline{\varphi})(1+\chi^\pm)\right\rangle^l_z$, where $\mathcal{D}^\pm$ and $\chi^\pm$ denote the binary ion–water nanoscopic diffusion coefficients and $\chi^\pm$ the effective tortuosity factors for each solute.

The replacement of the unknowns $\{C_\pm, C^\star_\pm\}$ by $\{C_b, \overline{\Psi}_b\}$ results in the appearance of the capacities $G_\pm = \langle \exp(\mp\overline{\varphi})\rangle^l_z$, which measure the storativity of the ions in the EDL. The retardation factor G_+ for the cations is much larger than G_-, owing to the high concentration of positive charges in the EDL (recall that $\overline{\varphi} < 0$).

2.2.4 Bulk phase pressure

Like the ion concentrations $c^\pm$ in the EDL picture, the nanoscopic counterpart of the fluid thermodynamic pressure varies drastically in the fluid domain and behaves discontinuously across the interface with the bulk solution [47]. The magnitude of the microscopic fluid pressure P_l incorporates the bulk phase pressure of the outer solution P_f and the averaged Donnan osmotic pressure $\pi_\star := P_l - P_f$, which, for dilute solutions under equilibrium conditions, is classically defined by Van't Hoff relation $\pi_\star := RT(C_+ + C_- - 2C_f)$ (Donnan [20], Huyghe and Janssen [36]). In a similar fashion to the pointwise characterization of C_b, define the averaged hidden bulk pressure P_b in the clay cluster domain by subtracting $\pi_\star$ from P_l. By extending pointwisely Van't Hoff relation to nonequilibrium conditions with C_f replaced by C_b, using the Boltzmann distributions Eq. 2.17, we have

$$\begin{aligned} P_b :&= P_l - \pi_\star = P_l - RT(C_+ + C_- - 2C_b) \\ &= P_l - RTC_b(G_+ + G_- - 2) \\ &= P_l - 2RTC_b\left(\langle \cosh\overline{\varphi}\rangle^l_z - 1\right). \end{aligned} \tag{2.21}$$

The hidden bulk phase pressure P_b exhibits the same nonoscillatory properties of C_b and Ψ_b [47, 49] and equalizes with the outer bulk phase pressure P_f under equilibrium conditions. Like the local characterization of C_b in Eq. 2.17, the above result provides indirect measurement of P_b through the triplet $\{P_l, \langle\cosh\overline{\varphi}\rangle^l_z, C_b\}$.

2.2.5 Alternative Terzaghi's decomposition

Using Eq. 2.21 in the modified Terzaghi's effective stress principle Eq. 2.2, we obtain

$$\boldsymbol{\sigma}_t = -P_b\, \boldsymbol{I} + \boldsymbol{\sigma}_e - \boldsymbol{\Pi} \quad \text{with} \quad \boldsymbol{\Pi} := \pi_\star \boldsymbol{I} - \boldsymbol{E}_M . \tag{2.22}$$

The above decomposition provides an alternative representation of the Terzaghi's effective stress principle with P_l replaced by P_b. The additional electrochemical stress $\boldsymbol{\Pi}$ is commonly referred to as swelling stress tensor [47, 49, 53] and can be viewed as the total stress in the aggregates ($\boldsymbol{\sigma}_t$) relative to the sum of contact stress and bulk phase pressure ($P_b\boldsymbol{I} - \boldsymbol{\sigma}_e$). This quantity may be regarded as a tensorial generalization of the experimentally observed swelling pressure Π, defined by the difference between the overburden normal stress ($-1/3\mathrm{tr}\boldsymbol{\sigma}_t$) and bulk phase pressure P_b in a well-ordered parallel particle arrangement where $\boldsymbol{\sigma}_e = 0$ [44]. For a nanostructure composed of parallel particles within each cluster, the swelling pressure is nothing but the projection of $\boldsymbol{\Pi}$ normal to the particle surface [47, 49]. At equilibrium where $C_b = C_f$ and $P_b = P_f$, the constitutive law $\Pi = \Pi(\phi, C_f)$ can easily be constructed by invoking the EDL theory (see [1, 49, 53] and Section 3).

2.3 Onsager's reciprocity relations

To complete the system of microscopic equations in the clay cluster domain, it remains to provide constitutive laws for the fluxes $\{\mathbf{v}_D, \boldsymbol{J}_+, \boldsymbol{J}_+\}$. To represent them properly within the thermodynamic context of Onsager's reciprocity relations, we replace $\boldsymbol{J}_\pm$ by the electric current $\boldsymbol{I}_e$ and the overall purely diffusive flux $\boldsymbol{J}_d$, both relative to the motion of the solid phase. This latter quantity is defined by subtracting the

purely advective flux of nonionic solutes induced by the Darcy's seepage velocity ($2C_b\mathbf{v}_D$) from the overall flux of ions $\boldsymbol{J}_t := \boldsymbol{J}_+ + \boldsymbol{J}_-$. Because this nonionic convective component differs from the sum of the first term in the RHS of Eq. 2.20 added over cations and anions (whose form is given by $C_b(G_+\boldsymbol{V}_+ + G_-\boldsymbol{V}_-)$), one may note that this latter component also exhibits a diffusive part.

Let $q_\star := F(C_+ - C_-)$ be the microscopic net charge density and $G_c := G_+ + G_-$, $G_s := G_+ - G_-$ the overall and net storativities of the ions in the EDL, respectively. Using the Boltzmann distributions, Eq. 2.17 gives $G_c = 2\langle\cosh\overline{\varphi}\rangle_z^l$, $G_s = -2\langle\sinh\overline{\varphi}\rangle_z^l$, $C_+ + C_- = G_cC_b$, and $q_* = FG_sC_b$. Therefore, by definition the new purely diffusive fluxes are given by

$$\begin{aligned}\boldsymbol{J}_d &:= \boldsymbol{J}_t - 2C_b\mathbf{v}_D - \phi(C_+ + C_-)\frac{\partial\mathbf{u}}{\partial t}\\ &= \boldsymbol{J}_t - 2C_b\mathbf{v}_D - \phi G_cC_b\frac{\partial\mathbf{u}}{\partial t},\end{aligned} \tag{2.23}$$

$$\begin{aligned}\boldsymbol{I}_e &:= F(\boldsymbol{J}_+ - \boldsymbol{J}_-) - F\phi(C_+ - C_-)\frac{\partial\mathbf{u}}{\partial t}\\ &= F(\boldsymbol{J}_+ - \boldsymbol{J}_-) - \phi FG_sC_b\frac{\partial\mathbf{u}}{\partial t}.\end{aligned} \tag{2.24}$$

The reciprocity relations express a linear law between $\{\mathbf{v}_D, \boldsymbol{J}_d, \boldsymbol{I}_e\}$ and the driving forces $\{\nabla P_b, RT\nabla\ln C_b, \nabla\Psi_b\}$ [49, 57]

$$\begin{pmatrix}\mathbf{v}_D\\ \boldsymbol{J}_d\\ \boldsymbol{I}_e\end{pmatrix} = -\begin{bmatrix}\boldsymbol{L}_{PP} & \boldsymbol{L}_{PC} & \boldsymbol{L}_{PE}\\ \boldsymbol{L}_{CP} & \boldsymbol{L}_{CC} & \boldsymbol{L}_{CE}\\ \boldsymbol{L}_{EP} & \boldsymbol{L}_{EC} & \boldsymbol{L}_{EE}\end{bmatrix}\begin{pmatrix}\nabla P_b\\ RT\nabla\ln C_b\\ \nabla\Psi_b\end{pmatrix} \tag{2.25}$$

where the matrix $\boldsymbol{L}_{IJ}$ $(I, J = P, C, E)$ is commonly referred to as Onsager's matrix. It is worth noting that, to embed the constitutive laws in the proper thermodynamic context, the bulk concentration was replaced by the Nernst potential $N = RT\ln C_b$, whose gradient is the driving force conjugated to the flux, which appears in the dissipative inequality.

The components $\{\boldsymbol{L}_{PP}, \boldsymbol{L}_{PE}\}$ of the first row of Onsager's matrix are nothing but the hydraulic and electro-osmotic conductivities for fluid flow, whereas $\boldsymbol{L}_{PC}$ is directly related to the chemico-osmotic permeability $\boldsymbol{K}_C := \boldsymbol{L}_{PC}RT/C_b$ [49]. The coefficient $\boldsymbol{L}_{EE}$ is commonly referred to as electric conductivity in Ohm's law, whereas $\boldsymbol{L}_{EP}$ and $\boldsymbol{L}_{CP}$ are the streaming current and ultrafiltration parameters, which reflect electric current and total ion flux driven by hydraulic gradients (see e.g. [16, 69]).

By adding and subtracting the transport equations in Eq. 2.19 over cations and anions and using the above Boltzmann distribution for q_* along with Eqs. 2.23 and 2.24, we obtain the overall movement of the species and charge conservation governed by

$$\frac{\partial}{\partial t}(\phi G_cC_b) = -\nabla\cdot\left(2C_b\mathbf{v}_D + \boldsymbol{J}_d + \phi G_cC_b\frac{\partial\mathbf{u}}{\partial t}\right) \tag{2.26}$$

$$\begin{aligned}F\frac{\partial}{\partial t}(\phi G_sC_b) &= \frac{\partial}{\partial t}(\phi q_*)\\ &= -\nabla\cdot\left(\boldsymbol{I}_e + \phi FG_sC_b\frac{\partial\mathbf{u}}{\partial t}\right).\end{aligned} \tag{2.27}$$

Furthermore, using the overall mass balance Eq. 2.4, we can rewrite Eq. 2.26 in the alternative form

$$\begin{aligned}&\frac{\partial}{\partial t}(\phi G_cC_b) + \frac{\partial\mathbf{u}}{\partial t}\cdot\nabla(\phi G_cC_b) - \phi G_cC_b\nabla\cdot\mathbf{v}_D\\ &\quad + \nabla\cdot(2C_b\mathbf{v}_D + \boldsymbol{J}_d) = 0\end{aligned} \tag{2.28}$$

The microscopic governing equations for the clay aggregates, formulated in terms of $\{\boldsymbol{\sigma}_t, \boldsymbol{\sigma}_e, \mathbf{u}, \phi, \boldsymbol{J}_d, \boldsymbol{I}_e, \mathbf{v}_D, P_b, C_b, \text{and } \Psi_b\}$, are given by Eqs. 2.1, 2.3–2.5, 2.22, 2.25, 2.26, and 2.27 supplemented by constitutive information on the coefficients $\{\boldsymbol{\Pi}, \boldsymbol{C}, G_c, G_s\}$, and $\{\boldsymbol{L}_{IJ}, I, J = P, C, E\}$. After solving for these primary unknowns, the averaged ion concentration $C_\pm$ and fluid thermodynamic pressure P_l, which appear in the primitive formulation, can be computed within a post-processing approach considering Eqs. 2.17 and 2.21.

2.4 Small advection induced by the solid movement

As we shall further observe, to maintain the local periodicity requirement for the subsequent homogenization process, Lagrangian coordinates tied up to the solid phase are more suitable for this task. Nevertheless, hereafter, we assume slow movement of the solid such that the material derivative following the solid velocity can be identified with the local Euler time derivative. Whence, we shall henceforth neglect the convection induced by the solid velocity by dropping terms involving $\partial\mathbf{u}/\partial t\cdot\nabla$. Under this assumption, the mass balances of particles (2.5) and species (2.28) reduce to

$$\frac{\partial\phi}{\partial t} - (1-\phi)\nabla\cdot\frac{\partial\mathbf{u}}{\partial t} = 0$$

$$\frac{\partial}{\partial t}(\phi G_cC_b) - \phi G_cC_b\nabla\cdot\mathbf{v}_D + \nabla\cdot(2C_b\mathbf{v}_D + \boldsymbol{J}_d) = 0$$

3 Nanoscopic representations

The magnitude of the Onsagers coefficients reflects the nanoscale behavior of the electrolyte solution in the nanopores. Electrochemical phenomena at these two separate-length scales are linked by the so-called closure problems arising from the homogenization procedure posed in each unit nanoscopic cell Z_l [49, 50]. Here, we present a particular form of the closure problems for the stratified nanostructure of parallel particles within each cluster depicted in Fig. 2. We also illustrate that the up-scaling of the compatibility condition between surface and net charged densities gives rise to the electroneutrality restriction, which further implies in a divergence-free electric current.

3.1 Nanoscopic governing equations

For each microscopic location, the nanoscopic governing equations of the electrolyte solution posed in the subdomain Z_l are represented in a local rectangular coordinate system $\boldsymbol{z}$. Whence, in what follows we adopt the subscript $\boldsymbol{z}$ to designate spatial derivative with respect to the nanoscopic coordinate to distinguish from the derivatives with respect to micro- and macrocoordinates denoted further by $\boldsymbol{y}$ and $\boldsymbol{x}$. Recalling that the reference hidden bulk potentials for fluid flow $\{P_b, C_b, \Psi_b\}$ do not fluctuate in the nanopores, they appear identical to their averaged values and therefore are independent of $\boldsymbol{z}$ [47]. Denoting $\{p^l, \pi^\star\}$ as the nanoscopic counterpart of $\{P_l, \pi_\star\}$, the nanoscale version of the Boltzmann distributions, Van Hoff relation, and the total electric potential decomposition, incorporating the dependence on $\boldsymbol{z}$ and $\boldsymbol{y}$, read as follows (see [49]):

$$\Phi^\star(\boldsymbol{y},\boldsymbol{z},t) = \varphi(\boldsymbol{y},\boldsymbol{z},t) + \Psi_b(\boldsymbol{y},t),$$
$$c^\pm(\boldsymbol{y},\boldsymbol{z},t) = C_b(\boldsymbol{y},t)\exp(\mp\overline{\varphi}) \tag{3.1}$$

$$\begin{aligned} p^l(\boldsymbol{y},\boldsymbol{z},t) &= P_b(\boldsymbol{y},t) + \pi^\star(\boldsymbol{y},\boldsymbol{z},t) \\ &= P_b + RT(c^+ + c^- - 2C_b) \\ &= P_b + 2RTC_b(\cosh\overline{\varphi} - 1)\,. \end{aligned} \tag{3.2}$$

Denoting $\boldsymbol{E} = -\nabla_z\Phi^* = -\nabla_z\varphi$ as the nanoscopic EDL electric field, $\tilde{\varepsilon}_0$ the vacuum permittivity, $\tilde{\varepsilon}$ the relative dielectric constant of the fluid (assumed constant), and $q^* := F(c^+ - c^-) = -2FC_b\sinh\overline{\varphi}$ the nanoscopic counterpart of the net charge density q_*, the variables $\{\boldsymbol{E}, \Phi^*, q^*\}$ fulfill the equations of electrostatic (see e.g. Landau and Lifshitz [40]).

$$\begin{aligned} &\tilde{\varepsilon}\tilde{\varepsilon}_0\nabla_z\cdot\boldsymbol{E} = -\tilde{\varepsilon}\tilde{\varepsilon}_0\triangle_{zz}\Phi^* = -\tilde{\varepsilon}\tilde{\varepsilon}_0\triangle_{zz}\varphi = q^* \quad \text{in} \quad Z_l \\ &\tilde{\varepsilon}\tilde{\varepsilon}_0\boldsymbol{E}\cdot\boldsymbol{n} = -\sigma \quad \text{on} \quad \partial Z_{ls} \end{aligned} \tag{3.3}$$

where $\sigma < 0$ is the surface charge density of the particles (assumed constant), Z_{ls} the interface between Z_l and Z_s, and $\boldsymbol{n}$ the unit normal exterior to Z_l. Using the above definitions for q^* and $\boldsymbol{E}$, we obtain the well-known Poisson–Boltzmann problem for the EDL potential

$$\begin{aligned} &\tilde{\varepsilon}\tilde{\varepsilon}_0\triangle_{zz}\varphi = 2FC_b\sinh\overline{\varphi} \quad \text{in} \quad Z_l \\ &\tilde{\varepsilon}\tilde{\varepsilon}_0\nabla_z\varphi\cdot\boldsymbol{n} = \sigma \quad \text{on} \quad \partial Z_{ls}. \end{aligned} \tag{3.4}$$

The electroneutrality condition imposes the following constraint between q^* and σ

$$\begin{aligned} \frac{1}{|Z|}\int_{Z_l} q^*\,\mathrm{d}Z &= \frac{\tilde{\varepsilon}\tilde{\varepsilon}_0}{|Z|}\int_{Z_l}\nabla_z\cdot\boldsymbol{E}\,\mathrm{d}Z = \frac{\tilde{\varepsilon}\tilde{\varepsilon}_0}{|Z|}\int_{\partial Z_{ls}}\boldsymbol{E}\cdot\boldsymbol{n}\,\mathrm{d}\Gamma \\ &= -\frac{1}{|Z|}\int_{\partial Z_{fs}}\sigma\,\mathrm{d}\Gamma\,. \end{aligned} \tag{3.5}$$

We now turn to the electrohydrodynamics. Following Eringen and Maugin [27] and Lyklema [45], the Stokesian flow of the electrolyte solution in the nanopores is strongly affected by the Coulombic body force $q^*\boldsymbol{E}$, which quantifies locally the viscous interaction between ions and solvent. Denoting μ and $\mathbf{v}$ as the viscosity and velocity of the liquid, neglecting gravity, convective, and inertial effects, the modified Stokes problem reads

$$\begin{aligned} &\mu\triangle_{zz}\mathbf{v} - \nabla_z p^l = -q^*\mathbf{E} = q^*\nabla_z\Phi^* \\ &\nabla_z\cdot\mathbf{v} = 0 \qquad \text{in} \quad Z_l \end{aligned} \tag{3.6}$$

The above momentum balance can also be rephrased in terms of the Cauchy stress tensor of the electrolyte solution $\boldsymbol{\sigma}^l$ in the form

$$\begin{aligned} &\nabla_z\cdot\boldsymbol{\sigma}^l = 0 \\ &\boldsymbol{\sigma}^l = -p^l\boldsymbol{I} + 2\mu\boldsymbol{\mathcal{E}}_z(\mathbf{v}) + \boldsymbol{\tau_M} \end{aligned} \tag{3.7}$$

where $\boldsymbol{\mathcal{E}}_z(\mathbf{v})$ is the nanoscopic strain rate tensor of the fluid and $\boldsymbol{\tau_M}$ the Maxwell stress tensor (Landau and Lifshitz [40])

$$\boldsymbol{\tau_M} := \frac{\tilde{\varepsilon}\,\tilde{\varepsilon}_0}{2}\left(2\,\boldsymbol{E}\otimes\boldsymbol{E} - E^2\,\mathbf{I}\right) \tag{3.8}$$

with $\otimes$ denoting the tensorial product between vectors. Using Eq. 3.3 in Eq. 3.8, one may easily note that $\nabla_z\cdot\boldsymbol{\tau_M} = q^*\boldsymbol{E}$, which shows that the divergence of the Maxwell stress tensor is nothing but the Coulomb force.

At the nanoscale, the expansion of the clay lattice is ruled by the disjoining stress tensor $\boldsymbol{\Pi}_d := \pi^\star \boldsymbol{I} - \boldsymbol{\tau}_{\boldsymbol{M}}$, defined by the difference between osmotic pressure and Maxwell stress tensor [18, 47]. Together with Eqs. 3.7, 3.2, and 3.8, this definition yields

$$\boldsymbol{\sigma}^l = -P_b\,\boldsymbol{I} + 2\mu\boldsymbol{\mathcal{E}}_z(\mathbf{v}) - \boldsymbol{\Pi}_d \tag{3.9}$$

with

$$\boldsymbol{\Pi}_d = 2RTC_b\,(\cosh\overline{\varphi}-1)\boldsymbol{I} - \frac{\tilde{\varepsilon}\,\tilde{\varepsilon}_0}{2} \times \left(2\,\boldsymbol{E}\otimes\boldsymbol{E} - E^2\,\mathbf{I}\right). \tag{3.10}$$

Like the second version of Terzaghi's decomposition (Eq. 2.22), the above result provides an alternative representation of the constitutive law for $\boldsymbol{\sigma}^l$, with p^l replaced by P_b.

Finally, the movement of the ions is governed by the nanoscopic counterpart of the Nernst–Planck equation (Eq. 2.9)

$$\frac{\partial c^\pm}{\partial t} + \nabla_z\cdot(c^\pm\mathbf{v}) = \nabla_z\cdot\left[\mathcal{D}^\pm\left(\nabla_z c^\pm \pm c^\pm\nabla_z\overline{\Phi}^*\right)\right] \tag{3.11}$$

where $\mathcal{D}^\pm$ denote the nanoscopic diffusion coefficients of the ions. It is worth noting that, unlike the averaged diffusivities tensors $\boldsymbol{D}_\pm$, which are strongly affected by the EDL potential and the tortuosity of the nanopores, $\mathcal{D}^\pm$ only depend on water–ion interactions. Using the nanoscopic Boltzmann distributions Eq. 2.16 along with the decomposition Eq. 3.1a, the above result can be rewritten in terms of the EDL dependent diffusivities $\mathcal{D}^\pm_*(\overline{\varphi}) := \mathcal{D}^\pm\exp(\mp\overline{\varphi})$ and hidden bulk properties in the form

$$\begin{aligned}&\frac{\partial}{\partial t}\left(\exp(\mp\overline{\varphi})\,C_b\right) + \nabla_z\cdot\boldsymbol{J}^\pm = 0 \quad \text{in} \quad Z_l\\ &\boldsymbol{J}^\pm = C_b\exp(\mp\overline{\varphi})\,\mathbf{v} - \mathcal{D}^\pm_*\left(\nabla_z C_b \pm C_b\nabla_z\overline{\Psi}_b\right).\end{aligned} \tag{3.12}$$

3.2 Consequence of the electroneutrality condition

We now aim at exploring the consequences of the electroneutrality condition. To this end, denote $c_s := |Z_s|^{-1}\int_{\partial Z_{ls}}\sigma\,\mathrm{d}\Gamma$ as the fixed charge density per unit of volume of the solid phase. Recalling that $q_* = \langle q^*\rangle^l_z = \phi^{-1}\langle q^*\rangle_z$, we have from Eq. 3.5 and the above definition

$$\langle q^*\rangle_z = \phi q_* = -\frac{1}{|Z|}\int_{\partial Z_{ls}}\sigma\,\mathrm{d}\Gamma = -\frac{(1-\phi)}{|Z_s|}\int_{\partial Z_{ls}}\sigma\,\mathrm{d}\Gamma = -(1-\phi)c_s \tag{3.13}$$

which yields $(1-\phi)c_s + \phi q_* = 0$. As the solid charge is tied-up directly to the mass of the solid and because particles are assumed nanoscopically incompressible, the intrinsic volume averaging of the surface charge does not vary, which implies c_s constant. Therefore, combining the previous relation with the mass and charge conservations Eqs. 2.5 and 2.26b, this latter balance can be rephrased as

$$\begin{aligned}\nabla\cdot\left(\boldsymbol{I}_e + \phi\,q_*\frac{\partial\mathbf{u}}{\partial t}\right) &= -\frac{\partial}{\partial t}(\phi\,q_*) = \frac{\partial}{\partial t}\left[(1-\phi)\,c_s\right]\\ &= -\nabla\cdot\left[(1-\phi)\,c_s\frac{\partial\mathbf{u}}{\partial t}\right]\\ &= \nabla\cdot\left(\phi\,q_*\frac{\partial\mathbf{u}}{\partial t}\right)\end{aligned}$$

which implies in a divergence free current

$$\nabla\cdot\boldsymbol{I}_e = 0\,. \tag{3.14}$$

Because the above result also incorporates the electroneutrality condition, we adopt Eq. 3.14 rather than Eq. 2.27 as a more accurate representation of conservation of charge.

3.3 Stratified nanostructures

Hereafter, we consider the one-dimensional representation of the aforementioned nanoscopic governing equations posed in the nanopore domain with geometry delimited of long parallel particles of close face-to-face contact separated by an interlayer spacing $2H$ (Fig. 3). In this simplified clay fabric arrangement, the average over the nanoscopic cell Z is nothing but the transversal averaging in the direction normal to the solid particles. In what follows, such transversal microscopization procedure is applied to the nanoscopic model to obtain representations for the Onsager's coefficients $\{\boldsymbol{L}_{IJ}, I, J = P, C, E\}$ and swelling stress tensor $\boldsymbol{\Pi}$ in terms of the local behavior of the EDL potential $\overline{\varphi}$. For simplicity and without loss of generality, we postulate a given microscopic elastic modulus $\boldsymbol{C}$ of the clay clusters with components given by the well-established micromechanics of linear elastic media (see, e.g., [59]).

3.3.1 Local electrostatics

In the one-dimensional setting depicted in Fig. 3, we adopt the notation y and z (without boldface) to represent the one-dimensional micro- and nanocoordinates in the axial (parallel to the particles) and transversal directions, respectively. For parallel particles, the one-dimensional flow and ion transport take place in the axial direction, whereas the EDL develops transversally in the z direction (Fig. 3) [50]. In the $\{y, z\}$ two-dimensional rectangular coordinate system, the local vectorial variables are represented in the form

$\mathbf{v} = \{v, 0\}$, $\boldsymbol{J}_d = \{J_d, 0\}$, $\boldsymbol{I}_e = \{I_e, 0\}$, $\boldsymbol{E} = \{0, E\}$, and $\mathbf{u} = \{0, u\}$, whereas the driving forces are represented as $\nabla P_b = \{\partial P_b/\partial y, 0\}$, $\nabla C_b = \{\partial C_b/\partial y, 0\}$, and $\nabla \Psi_b = \{\partial \Psi_b/\partial y, 0\}$. Recall that, unlike the local variables $\{\varphi, E, p^l, c^{\pm}\}$, which depend on z, the potentials for fluid flow $\{\partial P_b/\partial y, \partial C_b \partial y, \partial \Psi_b/\partial y\}$ do not fluctuate transversally and vary only in the axial direction with y ([50]). The pair $\{\varphi, E\}$ varies transversally and satisfies the one-dimensional version of the Poisson–Boltzmann problem Eq. 3.4

$$\begin{cases} \tilde{\varepsilon_0}\tilde{\varepsilon}\dfrac{d^2\varphi}{\mathrm{d}z^2} = -q^* = 2FC_b \sinh\overline{\varphi}; & E = -\dfrac{\mathrm{d}\varphi}{\mathrm{d}z} \\ E = 0 \qquad\qquad \text{at} \qquad z = 0, \\ E = -\dfrac{\sigma}{\tilde{\varepsilon}\,\tilde{\varepsilon_0}} \qquad \text{at} \qquad z = H, \end{cases} \tag{3.15}$$

The solution of the above problem can be represented in terms of the electric potential in the middle of the interlayer spacing $\overline{\varphi}_0 := \overline{\varphi}(z = 0)$. By multiplying Eq. 3.15 by $d\overline{\varphi}/dz$ and integrating from 0 to z, we obtain

$$\begin{aligned} \frac{\tilde{\varepsilon}\tilde{\varepsilon_0}}{2}\left(\frac{d\overline{\varphi}}{dz}\right)^2 &= \frac{2F^2C_b}{RT}\int_{\overline{\varphi}_0}^{\overline{\varphi}} \sinh\overline{\varphi}\, d\varphi \\ &= \frac{2F^2C_b}{RT}\left(\cosh\overline{\varphi} - \cosh\overline{\varphi}_0\right) \end{aligned} \tag{3.16}$$

which yields

$$\begin{aligned} E &= -\frac{RT}{F}\frac{d\overline{\varphi}}{dz} = 2\sqrt{\frac{RTC_b}{\tilde{\varepsilon}\tilde{\varepsilon_0}}(\cosh\overline{\varphi} - \cosh\overline{\varphi}_0)}; \\ \overline{\varphi} &= \overline{\varphi}_0 - 2F\int_0^z \sqrt{\frac{C_b}{\tilde{\varepsilon}\tilde{\varepsilon_0}RT}(\cosh\overline{\varphi} - \cosh\overline{\varphi}_0)}\, dz\,. \end{aligned} \tag{3.17}$$

Together with the boundary condition at $z = H$ in Eq. 3.15, the above result consists of the integral representation of the nonlinear, one-dimensional, Poisson–Boltzmann problem Eq. 3.15.

The axial movement of the ions is governed by the one-dimensional form of the Nernst–Planck equation (3.12)

$$\begin{aligned} &\frac{\partial}{\partial t}(\exp(\mp\overline{\varphi})C_b) + \frac{\partial}{\partial y}(\exp(\mp\overline{\varphi})C_b\, v) \\ &\quad = \frac{\partial}{\partial y}\left[\mathcal{D}_*^{\pm}\left(\frac{\partial C_b}{\partial y} \pm C_b\frac{\partial\overline{\Psi}_b}{\partial y}\right)\right]. \end{aligned} \tag{3.18}$$

Finally, to present the electrohydrodynamics in the stratified arrangement, we insert the decompositions Eqs. 3.1 and 3.2 in the two-dimensional Stokes problem Eq. 3.6. Together with the one-dimensional Poisson–Boltzmann problem (3.15), this yields

$$\mu\frac{\partial^2 v}{\partial z^2} - \frac{\partial P_b}{\partial y} - \frac{\partial\pi^\star}{\partial y} = q^*\left(\frac{\partial\varphi}{\partial y} + \frac{\partial\Psi_b}{\partial y}\right) \tag{3.19}$$

$$-\frac{\partial\pi^\star}{\partial z} = q^*\frac{\partial\varphi}{\partial z} = -\tilde{\varepsilon}\tilde{\varepsilon_0}\frac{\partial^2\varphi}{\partial z^2}\frac{\partial\varphi}{\partial z} = -\frac{\tilde{\varepsilon}\tilde{\varepsilon_0}}{2}\frac{\partial}{\partial z}\left(\frac{\partial\varphi}{\partial z}\right)^2 \tag{3.20}$$

Integrating Eq. 3.20 from the reference bulk state characterized by $p^l = P_b$ and $\pi^\star = \overline{\varphi} = \partial\overline{\varphi}/\partial z = 0$ and using Eq. 3.16 with $\overline{\varphi}_0 = 0$ gives

$$\begin{aligned} \pi^\star(y, z) = \frac{\tilde{\varepsilon}\tilde{\varepsilon_0}}{2}\left(\frac{\partial\varphi}{\partial z}\right)^2 &= 2RTC_b\int_0^{\overline{\varphi}} \sinh\overline{\varphi}\,\mathrm{d}\varphi \\ &= 2RTC_b\,[\cosh\overline{\varphi} - 1] \end{aligned} \tag{3.21}$$

which, as we may expect, shows $P - P_b$ varying in the transversal direction according to Van't Hoff relation. Using Eqs. 3.21 and 3.15 in Eq. 3.19, we obtain

$$\mu\frac{\partial^2 v}{\partial z^2} = \frac{\partial P_b}{\partial y} + 2\,R\,T\,(\cosh\overline{\varphi} - 1)\,\frac{\partial C_b}{\partial y} - \tilde{\varepsilon}\,\tilde{\varepsilon_0}\frac{\mathrm{d}^2\varphi}{\mathrm{d}z^2}\frac{\partial\Psi_b}{\partial y}\,. \tag{3.22}$$

Hence, given the driving forces $\{\partial P_b/\partial y, \partial C_b/\partial y, \partial\Psi_b/\partial y\}$ (independent of z), we have by linearity

$$v = -v_P\frac{\partial P_b}{\partial y} - v_C\frac{\partial C_b}{\partial y} - v_E\frac{\partial\Psi_b}{\partial y} \tag{3.23}$$

where the characteristic axial velocities $\{v_P, v_C, v_E\}$ correspond to fundamental solutions of Eq. 3.22 for unitary driving forces. In what follows, we exploit this result to derive nanoscopic representations for the axial components of the tensorial Onsager coefficients, herein denoted by L_{IJ} (without boldface). To embed Eq. 3.23 in the proper context of Onsager's reciprocity relations, we rewrite the chemico-osmotic term in terms of the Nernst potential $N := RT\nabla\ln C_b$, which furnishes the alternative representation $(v_C C_b/RT)\partial N/\partial y$ for the middle term in the RHS.

Recalling that $\mathbf{u} = \{0, u\}$, particles move transversally to the direction of the flow and, consequently, the axial component of the Darcy's velocity relative to the solid phase is nothing but $v_D := \langle v\rangle_z$. Thus, our nanoscopic representations read as follows.

3.3.2 Hydraulic conductivity

The axial component of the hydraulic conductivity L_{PP} is nothing but the transversal averaging of the local velocity v_P, solution of the Poiseuille flow (3.22) with

$\partial P_b/\partial y = -1$ and $\partial C_b/\partial y = \partial \Psi_b/\partial y = 0$. We then have $L_{PP} := \langle v_P \rangle_z = \phi \langle v_P \rangle_z^l$ with

$$\mu \frac{d^2 v_P}{dz^2} = -1 \,. \tag{3.24}$$

Denoting 2δ as the thickness of each clay particle, the nanoporosity is given by $\phi = H/(\delta + H)$. Hence, we have, after averaging,

$$L_{PP} = \frac{\phi}{H} \int_0^H v_P \mathrm{d}z = \frac{\phi H^2}{3\mu} = \frac{H^3}{3(\delta + H)\mu}. \tag{3.25}$$

3.3.3 Electro-osmotic permeability

In a similar fashion to L_{PP}, the axial component of the electro-osmotic permeability L_{PE} is the transversal averaging of the velocity profile $v_E = v_E(z)$ solution of the local problem

$$\mu \frac{\mathrm{d}^2 v_E}{\mathrm{d}z^2} = \tilde{\varepsilon}\, \tilde{\varepsilon_0} \frac{\mathrm{d}^2 \varphi}{\mathrm{d}z^2} \,. \tag{3.26}$$

After integration, exploring the symmetry at $z = 0$ along with the no-slip condition at $z = H$ gives

$$\mu \frac{\mathrm{d}v_E}{\mathrm{d}z}(z) = \frac{\tilde{\varepsilon}\, \tilde{\varepsilon_0}}{\mu} \frac{\mathrm{d}\varphi}{\mathrm{d}z}(z); \qquad v_E(z) = \tilde{\varepsilon}\, \tilde{\varepsilon_0} \left(\varphi(z) - \overline{\varphi}(H)\right) . \tag{3.27}$$

Hence, defining the zeta potential $\zeta := \varphi(H)$, we obtain after averaging

$$\begin{aligned} L_{PE} &= \frac{\phi}{H} \int_0^H v_E \,\mathrm{d}y = \frac{\phi\, \tilde{\varepsilon}\, \tilde{\varepsilon_0}}{H\mu} \int_0^H (\varphi(z) - \varphi(H))\, \mathrm{d}z \\ &= \frac{\phi \tilde{\varepsilon}\, \tilde{\varepsilon_0}}{\mu} \left(\langle \varphi \rangle_z^l - \zeta \right) . \end{aligned} \tag{3.28}$$

From Eq. 3.28, one may extract important information on the sources of electro-osmosis. The last term in the RHS involving the ζ-potential is commonly referred to as Helmholtz–Smoluchowski contribution and consists of a primary component relating electro-osmotic permeability to the ζ potential at the particle surface. This term establishes a direct correlation between the magnitude of L_{PE} and the EDL potential and dominates the conductivity for electro-osmotic flow for large particle distances $H >> \ell_D$ where $\ell_D := \left(\tilde{\varepsilon}\, \tilde{\varepsilon_0}\, R\, T/(2F^2 C_b)\right)^{1/2}$ is the Debye screening length (Hunter [35]). The secondary contribution involving the averaged EDL potential stems from the overlapping between adjacent EDLs and becomes relevant when $H = \mathcal{O}(\ell_D)$. This component acts to decrease the electro-osmotic permeability and has been incorporated in Smoluchowski's formula by means of a correction factor (see Hunter [34], Szymczyk et al. [67]).

When the thickness of the EDL is small compared to the interlayer spacing H, the Smoluchowski model for L_{PE} is recovered from Eq. 3.28 (Hunter [34], Coelho et al. [15], Shang [62]). Denoting $\{L_{PE}^{\infty}, \zeta^{\infty}, \overline{\varphi}^{\infty}\}$ the values of $\{L_{PE}, \zeta, \overline{\varphi}\}$ under the thin double layer assumption ($H \gg \ell_D$) the Smoluchowski's formula reads

$$L_{PE}^{\infty} = -\frac{\phi \tilde{\varepsilon} \tilde{\varepsilon_0} \zeta^{\infty}}{\mu} \,. \tag{3.29}$$

It is worth noting that by solving the Poisson–Boltzmann (Eq. 3.15) for $\overline{\varphi}^{\infty}$, parameterized by the bulk concentration considering noninteracting adjacent EDLs using the definition $\zeta^{\infty} := RTF^{-1}\overline{\varphi}^{\infty}(z = \pm H)$, one may easily build-up the constitutive laws $\zeta^{\infty} = \zeta^{\infty}(C_b)$ and $L_{PE}^{\infty} = L_{PE}^{\infty}(C_b)$.

3.3.4 Chemico-osmotic permeability

The axial component of the chemico-osmotic permeability $K_C := RTL_{PC}/C_b$ is the transversal averaging of the velocity v_C solution of

$$\mu \frac{\mathrm{d}^2 v_C}{\mathrm{d}z^2} = -2\, R\, T\, \left(\cosh \overline{\varphi} - 1\right) , \tag{3.30}$$

so that

$$L_{PC} = \frac{C_b \phi}{RTH} \int_0^H v_C dz \,. \tag{3.31}$$

In a similar fashion to Smoluchowski's regime, the asymptotic model of thin EDLs for the chemico-osmotic permeability can also be derived (Derjaguin [19] and Prieve et al. [55]) (Moyne and Murad [50]). Such derivation is presented in details in the Appendix. The asymptotic result reads as

$$\begin{aligned} L_{PC}^{\infty} &= -\frac{4 C_b \ell_D^2 \phi}{\mu} \ln\left(1 - \tanh^2\left(\frac{\overline{\zeta}^{\infty}}{4}\right)\right) \\ &= \frac{8 C_b \ell_D^2 \phi}{\mu} \ln\left(\cosh\left(\frac{\overline{\zeta}^{\infty}}{4}\right)\right) \quad \text{for} \quad \ell_D << H \,. \end{aligned} \tag{3.32}$$

where $\overline{\zeta} := \overline{\varphi}(H)$ is the dimensionless zeta potential. The above formula is consistent with the results obtained by Prieve et al. [55] and Moyne and Murad [50] relating fluid velocity with the $\overline{\zeta}$-potential considering flow near an infinite surface charged particle with thin EDLs.

3.3.5 Onsager's matrix

We now complete the derivation of the nanoscopic representations of the set of Onsager's coefficients L_{IJ}.

To this end we begin by recalling the two-scale representation of Darcy's law. Integrating Eq. 3.23 in the transversal direction z and using Eqs. 3.25, 3.28, and 3.31, we have

$$v_D := \langle v\rangle_z = -L_{PP}\frac{\partial P_b}{\partial y} - L_{PC}RT\frac{\partial \ln C_b}{\partial y} - L_{PE}\frac{\partial \Psi_b}{\partial y}$$

with

$$L_{PP} = \frac{\phi H^2}{3\mu}; \quad L_{PC} = \frac{C_b\phi}{RT}\langle v_C\rangle_z^l;$$

$$L_{PE} = \frac{\phi\,\tilde{\varepsilon}\,\tilde{\varepsilon_0}}{\mu}\left(\langle\varphi\rangle_z^l - \zeta\right) \tag{3.33}$$

In the parallel particle arrangement, the axial diffusive flux of ions J_d and electric current I_e (denoted without boldface) are given by $J_d = J_+ + J_- - 2\,C_b\,v_D$ and $I_e = F(J_+ - J_-)$. Inserting the local velocity decomposition Eq. 3.23 in Eq. 3.12 and using Eq. 3.33, we obtain after averaging

$$J_d = -L_{CP}\frac{\partial P_b}{\partial y} - L_{CC}\,RT\frac{\partial \ln C_b}{\partial y} - L_{CE}\frac{\partial \Psi_b}{\partial y}$$

$$I_e = -L_{EP}\frac{\partial P_b}{\partial y} - L_{EC}\,RT\frac{\partial \ln C_b}{\partial y} - L_{EE}\frac{\partial \Psi_b}{\partial y} \tag{3.34}$$

where the axial components L_{IJ} (I=C,E and J=P,C,E) of the Onsager's coefficients are given as

$$L_{CP} = 2C_b\,\langle(\cosh\overline{\varphi}\,-1)v_P\rangle_z;$$

$$L_{CC} = \frac{C_b}{RT}\left(2C_b\,\langle(\cosh\overline{\varphi}\,-1)v_C\rangle_z + \phi\,D^*\right)$$

$$L_{EP} = -2FC_b\,\langle\sinh\overline{\varphi}\,v_P\rangle_z;$$

$$L_{CE} = \frac{FC_b}{RT}\left(2\langle(\cosh\overline{\varphi}\,-1)v_E\rangle_z + \phi\Delta^*\right)$$

$$L_{EC} = \frac{FC_b}{RT}\left(-2C_b\,\langle\sinh\overline{\varphi}\,v_C\rangle_z + \phi\,\Delta^*\right);$$

$$L_{EE} = \frac{F^2\,C_b}{RT}\left(-2\langle\sinh\overline{\varphi}\,v_E\rangle_z + \phi D^*\right) \tag{3.35}$$

with $D^* := \langle\mathcal{D}^+\exp(-\overline{\varphi}) + \mathcal{D}^-\exp(\overline{\varphi})\rangle_z^l$ and $\Delta^* := \langle\mathcal{D}^+\exp(-\overline{\varphi}) - \mathcal{D}^-\exp(\overline{\varphi})\rangle_z^l$. By further manipulating the closure problems for the Onsager's coefficients in the parallel particle arrangement, one may show symmetry of the Onsager's matrix $L_{IJ} = L_{JI}$ [49].

3.3.6 Swelling stress tensor

To complete the two-scale model in the parallel particle arrangement, it remains to provide the nanoscopic representation for the swelling stress tensor $\boldsymbol{\Pi}$, which appears in the modified Terzaghi's decomposition Eq. 2.22. As mentioned before, $\boldsymbol{\Pi}$ plays the role of a tensorial generalization of the swelling pressure for a nanostructure composed of randomly oriented particles [47, 48, 53]. For stratified nanostructures of parallel particles, the scalar component of $\boldsymbol{\Pi}$ normal to the particle surface is the swelling pressure Π measured by Low [44] in a classical reverse osmosis experiment (see [47, 48, 53] for details). The swelling pressure may also be regarded as the intrinsic averaging of the nanoscopic disjoining pressure Π_d introduced by Derjaguin et al. [18]. In a similar fashion to Π, the electrostatic component of Π_d is locally defined as the normal projection of the tensor $\boldsymbol{\Pi}_d$ in Eq. 3.10 to the clay surface, i.e., $\Pi_d = \boldsymbol{\Pi}_d\boldsymbol{n}\cdot\boldsymbol{n}$.

Recalling the representation $\{0, E\}$ of the EDL electric field in the stratified arrangement, by invoking definition Eq. 3.8, the component of $\boldsymbol{\tau_M}$ normal to the clay surface is $\tau_M := \boldsymbol{\tau_M}\boldsymbol{n}\cdot\boldsymbol{n} = \tilde{\varepsilon}\tilde{\varepsilon_0}E^2/2 = \tilde{\varepsilon}\tilde{\varepsilon_0}(d\varphi/dz)^2/2$. Thus, using Eq. 3.16 in Eq. 3.10, by definition, the disjoining pressure is given by (Derjaguin et al. [18], Dahnert and Huster [17])

$$\begin{aligned}\Pi_d :&= \boldsymbol{\Pi}_d\boldsymbol{n}\cdot\boldsymbol{n} = \pi^\star - \tau_M\\ &= 2RTC_b(\cosh\overline{\varphi} - 1) - \frac{\tilde{\varepsilon}\tilde{\varepsilon_0}R^2T^2}{2F^2}\left(\frac{\mathrm{d}\varphi}{\mathrm{d}z}\right)^2\\ &= 2RTC_b\left(\cosh\overline{\varphi}_0 - 1\right).\end{aligned} \tag{3.36}$$

The above result is consistent with the EDL theory [35] and shows Π_d constant in the nanopore space, given only by the EDL potential $\overline{\varphi}_0$ in the middle of the interlayer spacing. The swelling pressure Π is nothing but the transversal averaging of the disjoining pressure in the direction normal to the particles. Because Π_d does not vary with z, we have

$$\Pi := \boldsymbol{\Pi}\boldsymbol{n}\cdot\boldsymbol{n} = \langle\boldsymbol{\Pi}_d\boldsymbol{n}\cdot\boldsymbol{n}\rangle_z^l = \langle\Pi_d\rangle_z^l = \Pi_d \tag{3.37}$$

which shows Π also given by Eq. 3.36. Unlike the disjoining pressure, the tangential component of $\boldsymbol{\Pi}$ varies

strongly with the local coordinate and gives rise to the interfacial tension of the electrolyte solution and to anisotropy of the stress tensor of the electrolyte solution [50]. Because the component does not produce any disjoining stress upon the solid particles, for simplicity, hereafter, we neglect this effect and adopt the representation $\boldsymbol{\Pi} = \Pi \boldsymbol{n} \otimes \boldsymbol{n}$. For a general representation of $\boldsymbol{\Pi}$ in randomly oriented particles including off-diagonal components, we refer to Moyne and Murad [47, 49] and Murad and Moyne [53].

3.4 Summary of the two-scale model for parallel particle arrangement

We are now ready to formulate the two-scale model for the clay aggregates composed of parallel particles of face-to-face contact. Recall that we have postulated a given averaged elastic modulus $\boldsymbol{C}$ with components calculated by the well-known micromechanics of linear elasticity (see, e.g., Sanchez-Palencia [59]).

Let $\Omega_s \subset R^n$ $(1 \leq n \leq 3)$ with smooth boundary Γ be the microscopic domain occupied by a clay cluster composed of parallel particles and let $\boldsymbol{n}$ and $\boldsymbol{t}$ be the unitary vectors normal and parallel to the particles within the cluster. The two-scale model consists in finding the microscopic variables $\{\boldsymbol{\sigma}_t, \mathbf{u}, \mathbf{v}_D, \boldsymbol{J}_t, \boldsymbol{J}_d, \boldsymbol{I}_e, P_b, C_b, \Psi_b, \phi\}$ satisfying

$$
\begin{cases}
\nabla \cdot \boldsymbol{\sigma}_t = 0 \\
\boldsymbol{\sigma}_t = -P_b \boldsymbol{I} + \boldsymbol{C}\boldsymbol{\mathcal{E}}(\mathbf{u}) - \boldsymbol{\Pi} \\
\nabla \cdot \mathbf{v}_D + \nabla \cdot \dfrac{\partial \mathbf{u}}{\partial t} = 0 \\
\dfrac{\partial \phi}{\partial t} = (1-\phi)\nabla \cdot \dfrac{\partial \mathbf{u}}{\partial t} \\
\dfrac{\partial}{\partial t}\left(\phi G_c C_b\right) + \nabla \cdot \boldsymbol{J}_t - \phi G_c C_b \nabla \cdot \mathbf{v}_D = 0 \\
\boldsymbol{J}_t = \boldsymbol{J}_d + 2C_b \mathbf{v}_D \\
\nabla \cdot \boldsymbol{I}_e = 0 \quad \text{in} \quad \Omega_s \\
\mathbf{v}_D = -\boldsymbol{L}_{PP} \nabla P_b - RT\, \boldsymbol{L}_{PC} \nabla \ln C_b - \boldsymbol{L}_{PE} \nabla \Psi_b \\
\boldsymbol{J}_d = -\boldsymbol{L}_{CP} \nabla P_b - RT\, \boldsymbol{L}_{CC} \nabla \ln C_b - \boldsymbol{L}_{CE} \nabla \Psi_b \\
\boldsymbol{I}_e = -\boldsymbol{L}_{EP} \nabla P_b - RT\, \boldsymbol{L}_{EC} \nabla \ln C_b - \boldsymbol{L}_{EE} \nabla \Psi_b
\end{cases}
\tag{3.38}
$$

where the swelling stress tensor $\boldsymbol{\Pi}$ and the Onsager's coefficients $\{\boldsymbol{L}_{IJ}(I, J = P, C, E)$ are represented as $\boldsymbol{\Pi} = \Pi \boldsymbol{n} \otimes \boldsymbol{n}$ and $\boldsymbol{L}_{IJ} = L_{IJ} \boldsymbol{t} \otimes \boldsymbol{t}$, with the corresponding scalars $\{\Pi, L_{IJ}\}$ and the retardation EDL parameter G_c admitting the nanoscopic representations in the subdomain Z_l of the unit cell Z

$$
\begin{aligned}
&G_c = 2\langle \cosh \overline{\varphi} \rangle_z^l; \qquad \Pi = 2RTC_b(\cosh \overline{\varphi}_0 - 1) \\
&L_{PP} = \frac{\phi H^2}{3\mu}; \quad L_{PC} = \frac{\phi C_b}{RT}\langle v_C \rangle_z^l; \quad L_{PE} = \frac{\phi \tilde{\varepsilon}\, \tilde{\varepsilon}_0}{\mu}\left(\langle \varphi \rangle_z^l - \zeta\right) \\
&L_{CP} = 2C_b \langle (\cosh \overline{\varphi} - 1) v_P \rangle_z; \\
&L_{CC} = \frac{C_b}{RT}\left(2C_b \langle (\cosh \overline{\varphi} - 1) v_C \rangle_z + \phi\, D^*\right) \\
&L_{EP} = -2FC_b \langle \sinh \overline{\varphi}\, v_P \rangle_z; \\
&L_{CE} = \frac{FC_b}{RT}\left(2\langle (\cosh \overline{\varphi} - 1) v_E \rangle_z + \phi \Delta^*\right) \\
&L_{EC} = \frac{FC_b}{RT}\left(-2C_b \langle \sinh \overline{\varphi}\, v_C \rangle_z + \phi\, \Delta^*\right); \\
&L_{EE} = \frac{F^2 C_b}{RT}\left(-2\langle \sinh \overline{\varphi}\, v_E \rangle_z + \phi D^*\right).
\end{aligned}
\tag{3.39}
$$

In the above nanoscopic representations, $2H$ and 2δ denote the interlayer spacing and particle thickness, $\phi = H/(H+\delta)$, the intracluster porosity, $\overline{\varphi} := F\varphi/RT$ the dimensionless EDL potential, $\zeta = \varphi(z = H)$ the zeta potential, and $\overline{\varphi}_0 = \overline{\varphi}(z = 0)$ the EDL potential in the middle of the interlayer spacing. The set of local variables $\{\overline{\varphi}, v_P, v_E, v_C\}$ satisfy the Poisson–Boltzmann problem Eq. 3.15 and the Stokes type flows Eqs. 3.24, 3.26, and 3.30. Finally, the EDL dependent diffusivities are defined as $D^* := \langle \mathcal{D}^+ \exp(-\overline{\varphi}) + \mathcal{D}^- \exp(\overline{\varphi}) \rangle_z^l$ and $\Delta^* := \langle \mathcal{D}^+ \exp(-\overline{\varphi}) - \mathcal{D}^- \exp(\overline{\varphi}) \rangle_z^l$, with $\mathcal{D}^{\pm}$ as the molecular binary water-ions diffusion coefficients.

From the Poisson–Boltzmann problem (3.15), the averaged EDL potential along with the pair $\{G_c, \Pi\}$ depend on $\{C_b, \phi\}$. Moreover, by invoking the above local representations for the axial components of the Onsagers coefficients and the local Stokes flows for the characteristic fluid velocities $\{v_P, v_E, v_C\}$, we obtain the same constitutive dependence of the Onsager parameters $L_{IJ} = L_{IJ}(\phi, C_b)$. It should be noted that, though the solid particles undergo small strains, if the local cell geometry induced by the deformation varies homothetically preserving symmetry (which is the case of parallel particles), by choosing the reference configuration of the solid equal to the current one, we may compute the constitutive dependence of the effective coefficients on a large range of intracluster porosities. Hence, we are constrained by the small strain assumption to construct locally the aforementioned constitutive laws.

Finally, after solving the two-scale formulation for the hidden bulk variables $\{P_b, C_b, \Psi_b\}$, the averaged

total electric potential Φ_*, ion concentrations $C_\pm$, and fluid thermodynamic pressure P_l can be recovered within a postprocessing approach considering Eqs. 2.14, 2.17, and 2.21.

4 Microscopic coupling between clay clusters and micropores

We shall henceforth discuss the up-scaling of the two-scale model to the macroscale and the derivation of the three-scale model of dual-porosity type. To this end, we begin by establishing the coupled cluster/micropore model at the microscale.

4.1 Hydrodynamics and transport in the micropores

The aforementioned two-scale model governs the behavior of the clay aggregates in Ω_s. In addition, let Ω_f be the micropore domain occupied by an aqueous incompressible Newtonian bulk solution containing the same monovalent ionic species with concentrations denoted by $C_f^\pm$. Like the hydrodynamics of the electrolyte solution, the movement of the bulk fluid is assumed slow so that inertial, convective, and gravity effects are omitted. Owing to the coarser structure of the larger-sized micropores, we adopt the thin double layer assumption where the thickness of the EDL around the clusters is considered small compared to a characteristic length scale of the micropores ℓ_f. Under this assumption, the action of the thin EDLs is restricted to the vicinity of the cluster/micropore interface, where it enforces slip boundary conditions in the tangential velocity of the liquid and screens the effective surface charge density, i.e., $(\sigma = 0)$ on Γ_{fs}. In addition, we neglect hydrodynamic dispersion effects, which entail the dependence of the diffusion coefficients on fluid velocity. Consequently, the only mechanisms governing the spreading of solutes in the bulk fluid are Fickian molecular diffusion and electromigration.

Let Φ_f be the total microscopic electric potential and Ψ_f the streaming potential of the bulk fluid. Adopting the Debye's length ℓ_D as the typical characteristic measure of the EDL thickness, under the assumption $\ell_f \gg \ell_D$, the order of magnitude of the left-hand side of the Poisson problem (3.3) is $\triangle\Phi_f \approx \mathcal{O}(\Phi_f/\ell_f^2) \approx 0$, which also implies in negligible RHS. Whence, the Poisson problem is naturally fulfilled with $q_f := F\big(C_f^+ - C_f^-\big) = 0$. Because $q_f = -FC_f \sinh\overline{\varphi}_f$ where $RTF^{-1}\overline{\varphi}_f := \Phi_f - \Psi_f$, this further implies $\overline{\varphi}_f = 0$, $\Phi_f = \Psi_f$, and $C_f^+ = C_f^- = C_f$, showing that the electroneutrality condition Eq. 3.5 is satisfied pointwisely. Whence, up to a boundary layer in the vicinity of the clusters, the bulk medium is characterized by local equality between co- and counterion concentrations.

Let $\{P_f, \boldsymbol{V}_f, \boldsymbol{\sigma}_f, \boldsymbol{J}_f, \boldsymbol{I}_f\}$ be the pressure, velocity, stress tensor, overall flux of species and electric current in the bulk fluid and let $\mu_f^+ = \mu_f^- = \mu_f = \overline{\mu}_\pm \pm F\Psi_f + RT\ln C_f$ be the electrochemical potential of the monovalent species given by Eq. 2.10 at equilibrium conditions.

Recalling that $q_f = 0$, the model in Ω_f reduces to the classical Stokes flow coupled with mass conservation of the ions with absence of EDL effects. Setting $\phi = 1$ (the micropores are totally open) along with $q_* = \boldsymbol{\tau_M} = \overline{\varphi} = 0$, $G_+ = G_- = G_c/2 = 1$, $\mathbf{v} = \boldsymbol{V}_f$, $\boldsymbol{J}_f = \boldsymbol{J}_f^+ + \boldsymbol{J}_f^-$, and $\mathcal{D}_\star^\pm = \mathcal{D}^\pm$ in Eqs. 3.7, 3.12 (added and subtracted over cations and anions), and (3.14), we obtain

$$\nabla\cdot\boldsymbol{\sigma}_f = 0$$

$$\boldsymbol{\sigma}_f = -P_f\boldsymbol{I} + 2\mu\boldsymbol{\mathcal{E}}(\boldsymbol{V}_f) \quad \text{in} \quad \Omega_f \tag{4.1}$$

$$\nabla\cdot\boldsymbol{V}_f = 0$$

$$2\frac{\partial C_f}{\partial t} + \nabla\cdot\boldsymbol{J}_f = 0 \tag{4.2}$$

$$\boldsymbol{J}_f = 2\,C_f\,\boldsymbol{V}_f + \boldsymbol{J}_{fd} \tag{4.3}$$

$$\boldsymbol{J}_{fd} := -\mathcal{D}_f\nabla C_f - \Delta_f\,C_f\nabla\overline{\Psi}_f \tag{4.4}$$

$$\nabla\cdot\boldsymbol{I}_f = 0 \tag{4.5}$$

$$\boldsymbol{I}_f = -F\left(\Delta_f\nabla C_f + \mathcal{D}_f\,C_f\nabla\overline{\Psi}_f\right) \tag{4.6}$$

where $\mathcal{D}_f := \mathcal{D}^+ + \mathcal{D}^-$, $\Delta_f := \mathcal{D}^+ - \mathcal{D}^-$, and $\overline{\Psi}_f := F\Psi_f/RT$. It should be noted that the diffusivities $\mathcal{D}^+$ and $\mathcal{D}^-$ are the same nanoscopic coefficients that appear in Eq. 3.11. Unlike the homogenized diffusivities $\boldsymbol{D}_\pm$ in Eq. 2.20, which vary strongly with the EDL potential, the pair $\{\mathcal{D}_f, \Delta_f\}$ is a pure binary water-solute property independent of φ.

In terms of $\{\boldsymbol{V}_f, P_f, C_f, \overline{\Psi}_f\}$, the above system can be rewritten in the form

$$\mu\triangle\boldsymbol{V}_f - \nabla P_f = 0$$

$$\nabla\cdot\boldsymbol{V}_f = 0 \quad \text{in} \quad \Omega_f$$

$$2\frac{\partial C_f}{\partial t} + 2\nabla\cdot(C_f\boldsymbol{V}_f) = \nabla\cdot\left(\mathcal{D}_f\nabla C_f + \Delta_f\,C_f\nabla\overline{\Psi}_f\right) \tag{4.7}$$

$$\nabla\cdot\left(\Delta_f\nabla C_f + \mathcal{D}_f\,C_f\nabla\overline{\Psi}_f\right) = 0 \tag{4.8}$$

4.2 Boundary conditions

The aforementioned microscopic equations are supplemented by boundary conditions on the cluster/

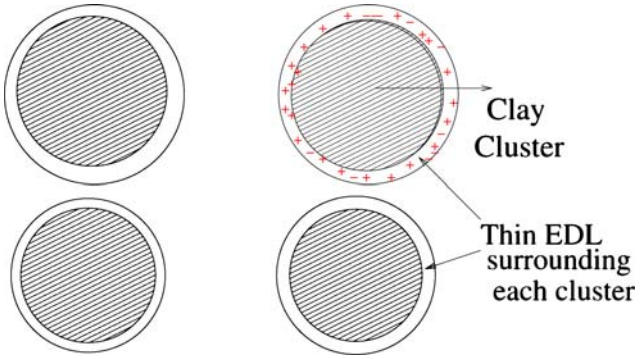

Fig. 4 Thin EDL surrounding each cluster responsible for the slip in the tangential component of fluid velocity

micropore interface Γ_{fs} and initial data. To match conditions on Γ_{fs}, we enforce continuity of the electrochemical potentials and the normal component of fluxes and stresses. Furthermore, we postulate an electrochemical slip in the velocity of the fluid tangential to the interface owing to the friction induced by the thin EDLs around the clusters (Fig. 4) (see, e.g., Edwards [26] Squiries and Bazant [65]).

4.2.1 Continuous interface conditions

Let $\boldsymbol{N}$ be the unit normal exterior to Ω_s and $\boldsymbol{V}_{fs} := \boldsymbol{V}_f - \partial\mathbf{u}/\partial t$ the velocity of the fluid in the micropores relative to the solid phase at the interface. Continuity of the normal component of the diffusive Onsager's fluxes, electrochemical potentials, and the normal component of overall and fluid stresses gives

$$\mathbf{v}_D \cdot \boldsymbol{N} = \boldsymbol{V}_{fs} \cdot \boldsymbol{N}, \quad \boldsymbol{J}_{fd} \cdot \boldsymbol{N} = \boldsymbol{J}_d \cdot \boldsymbol{N},$$

$$\boldsymbol{I}_e \cdot \boldsymbol{N} = \boldsymbol{I}_f \cdot \boldsymbol{N} \tag{4.9}$$

$$\boldsymbol{\sigma}_t \boldsymbol{N} = \boldsymbol{\sigma}_f \boldsymbol{N}, \quad \boldsymbol{\sigma}_f \boldsymbol{N} \cdot \boldsymbol{N} = -P_b,$$

$$\mu_f^{\pm} = \mu_{\pm} \quad \text{on} \quad \Gamma_{fs}. \tag{4.10}$$

Recalling that electrochemical potentials are not primary unknowns in our formulation, we eliminate these variables through their corresponding constitutive laws. Thus, the last condition in Eq. 4.10 is rewritten in terms of bulk concentrations and electric potentials. Together with the equality $\mu_{\pm} = \mu_{b\pm}$, this yields

$$\pm F\Psi_b + RT \ln C_b = \pm F\Psi_f + RT \ln C_f.$$

Adding the above results over cations and anions, we obtain

$$C_b = C_f, \qquad \Psi_b = \Psi_f \qquad \text{on} \quad \Gamma_{fs} \tag{4.11}$$

which shows continuity of the potentials for chemico- and electro-osmotic flows. An alternative form of representing continuity of the solute flux at the interface is in terms of conservation of the total ion flux relative to the movement of the solid. This form can be obtained by multiplying Eq. 4.9a by $2C_b$ adding to Eq. 4.9b, using the interface condition Eq. 4.11a along with the constitutive laws Eqs. 2.23 and 4.3. This yields

$$\begin{aligned}(\boldsymbol{J}_d + 2\mathbf{v}_D C_b) \cdot \boldsymbol{N} &= = \left(\boldsymbol{J}_{fd} + 2C_f \boldsymbol{V}_{fs}\right) \cdot \boldsymbol{N} \\ &= \left(\boldsymbol{J}_f - 2C_f \frac{\partial \mathbf{u}}{\partial t}\right) \cdot \boldsymbol{N} \quad \text{on} \quad \Gamma_{fs}\end{aligned} \tag{4.12}$$

4.2.2 Liquid slippage

The presence of the thin EDL around the clusters gives rise to a boundary layer with thickness of $\mathcal{O}(\ell_D)$ considered small compared to the characteristic length scale of the micropores ℓ_f. In this context, the shape of the velocity profiles shows a sharp layer in the vicinity of the solid particles where the chemico-osmotic and electro-osmotic tangential velocities exhibit high gradients in contrast with flat profiles away from the surface [6, 50]. Following Edwards [26], we postulate that the electrochemical component of the velocity averaged over the thin EDL thickness around the clusters, herein denoted by V_{match}, governs the jump in the fluid tangential velocities across the boundary. Whence the boundary layer is replaced by the following averaged slip condition in the tangential fluid velocities

$$(\boldsymbol{V}_{fs} - \mathbf{v}_D) \cdot \boldsymbol{\tau} = V_{\text{match}} \qquad \text{on} \quad \Gamma_{fs} \tag{4.13}$$

where $\boldsymbol{\tau}$ is the unit tangent vector to the boundary and V_{match} stems from the transversal averaging of the electro- and chemico-osmotic surface flows over the EDL thickness around Γ_{fs} (Fig. 4). By decomposing the RHS into its chemico- and electro-osmotic components, we have

$$V_{\text{match}} = V^C_{\text{match}} + V^E_{\text{match}}. \tag{4.14}$$

To derive the constitutive laws for the terms in the RHS, we postulate each component given by the transversal averaging of the one-dimensional velocities profiles in Eqs. 3.26 and 3.30 over the EDL thickness around the clusters. This gives a Darcy-type surface flow driven by concentration and electric potentials tangential gradients. Because the characteristic length of the micropores is much larger than the EDL thickness, one can make use of the asymptotic results for the electro-osmotic and chemico-osmotic conductivities in

Eqs. 3.29 and 3.32 under the regime of thin EDLs. Recalling that the micropores are totally open, we have

$$V^{E}_{\text{match}} = -L^{\infty}_{PE}\nabla\Psi_f\cdot\boldsymbol{\tau} \quad \text{with} \quad L^{\infty}_{PE} := \frac{\tilde{\varepsilon}\,\tilde{\varepsilon_0}\,\zeta^{\infty}}{\mu},$$

$$V^{C}_{\text{match}} = -\frac{RTL^{\infty}_{PC}}{C_f}\nabla C_f\cdot\boldsymbol{\tau} \quad \text{with}$$

$$L^{\infty}_{PC} := \frac{8\,C_f\ell_D^2}{\mu}\ln\left(\cosh\left(\frac{\overline{\zeta}^{\infty}}{4}\right)\right).$$

which, when combined with Eq. 4.14, yields

$$V_{\text{match}} = -\left(L^{\infty}_{PE}\nabla\Psi_f + \frac{RTL^{\infty}_{PC}}{C_f}\nabla C_f\right)\cdot\boldsymbol{\tau} \qquad \text{on} \quad \Gamma_{fs}\,. \tag{4.15}$$

Finally, assuming initially an incompressible response of the clay clusters, a given nanoporosity $\overline{\phi}$, and the equality between bulk concentration in the micropores and clusters, the initial conditions are

$$C_f = C_b = \overline{C}; \quad \nabla\cdot\mathbf{u} = 0 \qquad \phi = \overline{\phi} \qquad t = 0,\ .$$

5 Dual-porosity model derived by homogenization

The microscale interactions between aggregates and micropores are still fine structure phenomena that must be homogenized. We then up-scale to the macroscale using the homogenization procedure. In this framework, the swelling medium is idealized as a bounded domain with periodic structure. To deal with the micro- and macrostructures separately, we follow the general framework of Sanchez-Palencia [59] and introduce the microscopic characteristic length-scale ℓ of $\mathcal{O}(\ell_f)$, for which microscopic heterogeneities are relevant, and the macroscopic length-scale (L) of resolution size of the window of observation for which heterogeneities are invisible. Defining the ratio $\epsilon := l/L$ as the perturbation parameter inherent to the homogenization procedure, we make use of the scale-separation assumption, wherein l is much smaller than L so that $\epsilon << 1$. We then consider the perturbed domain Ω^{ϵ} reconstructed from a spatially repeated microcell Y^{ϵ}. Likewise, the subdomains Ω^{ϵ}_f and Ω^{ϵ}_s along with the interface Γ^{ϵ}_{fs} are formed by the union of Y^{ϵ}_f and Y^{ϵ}_s cell domains and $\partial Y^{\epsilon}_{fs}$ interfaces, respectively. Each cell Y^{ϵ} is congruent to a unitary parallelepiped period Y composed of subdomains Y_s and Y_f occupied by the aggregates and micropores, respectively, along with the interface ∂Y_{fs} (Fig. 5). Our starting point $\epsilon = 1$ corresponds to our microscopic model. The ϵ-model in Ω^{ϵ} consists of

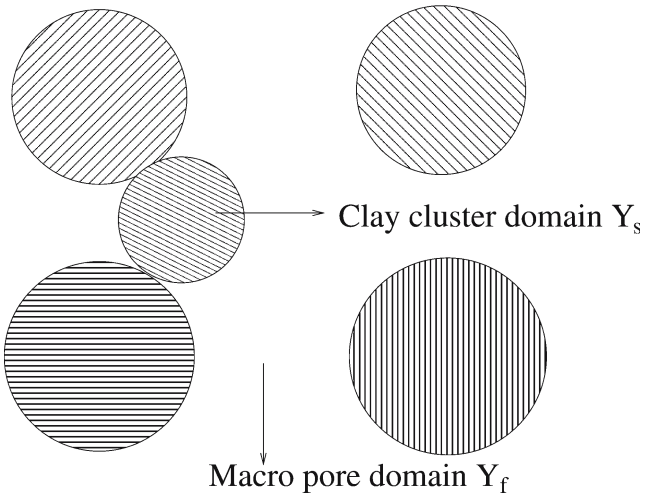

Fig. 5 Microscopic arrangement composed of a periodic cell (Y) composed of subdomains occupied by the clay clusters (Y_s) and micropores (Y_f)

properly scaled equations on the lattice of copies Y^{ϵ}. The basic problem is to investigate the asymptotics of the solution as $\epsilon \to 0$ and obtain the homogenized limit as the scale of the inhomogeneity tends to zero.

In our subsequent development, we make use of the classical spatial- and time-averaging theorems. Denoting f^{ϵ} and $\boldsymbol{g}^{\epsilon}$ as general scalar and vectorial functions defined in Y^{ϵ} and considering the velocity of the cluster/micropore interface given by $\partial\mathbf{u}^{\epsilon}/\partial t$, we have [64, 71]

$$\frac{\partial}{\partial t}\left(\frac{1}{|Y^{\epsilon}|}\int_{Y^{\epsilon}} f^{\epsilon}dY\right) = \frac{1}{|Y^{\epsilon}|}\int_{Y^{\epsilon}}\frac{\partial f^{\epsilon}}{\partial t}dy + \frac{1}{|Y^{\epsilon}|}\int_{\partial Y^{\epsilon}_{fs}} f^{\epsilon}\frac{\partial\mathbf{u}^{\epsilon}}{\partial t}\cdot\boldsymbol{N}\,\mathrm{d}\Gamma$$

$$\nabla\cdot\left(\frac{1}{|Y^{\epsilon}|}\int_{Y^{\epsilon}}\boldsymbol{g}^{\epsilon}dY\right) = \frac{1}{|Y^{\epsilon}|}\int_{Y^{\epsilon}}\nabla\cdot\boldsymbol{g}^{\epsilon}dY - \frac{1}{|Y^{\epsilon}|}\int_{\partial Y^{\epsilon}_{fs}}\boldsymbol{g}^{\epsilon}\cdot\boldsymbol{N}\,\mathrm{d}\Gamma\,. \tag{5.1}$$

5.1 Scaling analysis of the microscopic model

To describe the physics correctly, the coefficients of the microscopic model must be properly scaled. From the well-established homogenization of the Stokes problem, the viscosity μ of the bulk fluid is rescaled by ϵ^2 (Auriault [7], Sanchez-Palencia [59]). Furthermore, denoting v_{ref} and $\mathcal{D}_{ref}$ as reference values of velocity and diffusion coefficient of the bulk solution, we define the macroscopic Peclet number $\mathrm{Pe_L} := v_{ref}L/\mathcal{D}_{ref}$ as

the dimensionless parameter whose magnitude quantifies the ratio between convective and diffusive effects. Assume these are of the same order of magnitude so that $\mathrm{Pe_L} = \mathcal{O}(1)$. Furthermore, to control the cluster/micropore fluxes within a fixed volume as $\epsilon \to 0$, it is also necessary to rescale the Onsager's coefficients $\{\boldsymbol{L}^{\epsilon}_{IJ}, I, J = P, C, E\}$. Following Arbogast and coworkers [2, 4] and Douglas and Arbogast [24], within the context of rigid fractured media, this is properly accomplished adopting the scaling $\boldsymbol{L}^{\epsilon}_{IJ}$ of $\mathcal{O}(\epsilon^2)$. The square of the perturbation parameter plays the role of turning the aggregates progressively less permeable and diffusive as $\epsilon \to 0$ and consequently prevents the degeneration of the cluster/micropore mass transfer as $\epsilon \to 0$ (see [2, 24] for details). Making use of these scaling arguments, we rewrite Onsager's reciprocity relations along with the momentum and constitutive law for the bulk fluid in the form

$$\mathbf{v}^{\epsilon}_D = -\epsilon^2\left(\boldsymbol{L}^{\epsilon}_{PP}\nabla\, P^{\epsilon}_b + \boldsymbol{L}^{\epsilon}_{PC}RT\nabla\, \ln C^{\epsilon}_b + \boldsymbol{L}^{\epsilon}_{PE}\nabla\, \Psi^{\epsilon}_f\right)$$

$$\boldsymbol{J}^{\epsilon}_d = -\epsilon^2\left(\boldsymbol{L}^{\epsilon}_{CP}\nabla P^{\epsilon}_b + \boldsymbol{L}^{\epsilon}_{CC}RT\nabla \ln C^{\epsilon}_b + \boldsymbol{L}^{\epsilon}_{CE}\nabla\Psi^{\epsilon}_f\right)$$

$$\boldsymbol{I}^{\epsilon}_e = -\epsilon^2\left(\boldsymbol{L}^{\epsilon}_{EP}\nabla P^{\epsilon}_b + \boldsymbol{L}^{\epsilon}_{EC}RT\nabla \ln C^{\epsilon}_b + \boldsymbol{L}^{\epsilon}_{EE}\nabla\Psi^{\epsilon}_f\right)$$

and

$$\epsilon^2\mu\triangle \boldsymbol{V}^{\epsilon}_f - \nabla P^{\epsilon}_f = 0$$

$$\boldsymbol{\sigma}^{\epsilon}_f = -P^{\epsilon}_f\boldsymbol{I} + 2\,\epsilon^2\,\mu\,\boldsymbol{\mathcal{E}}\left(\boldsymbol{V}^{\epsilon}_f\right). \tag{5.2}$$

We also consider the scaling analysis of the averaging relations Eq. 5.1. Recalling that the ratio between volume and area of the periodic cell scales with $\mathcal{O}(\epsilon^3)/\mathcal{O}(\epsilon^2)$, we have $|Y^{\epsilon}|/|\partial Y^{\epsilon}_{fs}|$ of $\mathcal{O}(\epsilon)$. Thus, considering the transformation of the integration domain to the reference unit cell Y, we have

$$\frac{\partial}{\partial t}\left(\frac{1}{|Y|}\int_Y f^{\epsilon}dY\right) = \frac{1}{|Y|}\int_Y \frac{\partial f^{\epsilon}}{\partial t}dY + \frac{1}{\epsilon\,|Y|}\int_{\partial Y_{fs}} f^{\epsilon}\,\frac{\partial \mathbf{u}^{\epsilon}}{\partial t}\cdot\boldsymbol{N}\,\mathrm{d}\Gamma \tag{5.3}$$

$$\nabla\cdot\left(\frac{1}{|Y|}\int_Y \boldsymbol{g}^{\epsilon}dY\right) = \frac{1}{|Y|}\int_Y \nabla\cdot\boldsymbol{g}^{\epsilon}dY - \frac{1}{\epsilon\,|Y|}\int_{\partial Y_{fs}}\boldsymbol{g}^{\epsilon}\cdot\boldsymbol{N}\,\mathrm{d}\Gamma\,. \tag{5.4}$$

5.2 Matched asymptotic expansions

The formal homogenization procedure is accomplished by considering every property depending on both global and local length scales in the form $f = f(\boldsymbol{x}, \boldsymbol{y})$, with $\boldsymbol{x}$ and $\boldsymbol{y}$ denoting the macroscopic and microscopic coordinates, respectively. By a straightforward application of the chain rule to a function $f = f(\mathbf{x}, \mathbf{y})$ with $\mathbf{y} = \mathbf{x}/\epsilon$, the differential operator ∇ is replaced by $\nabla_x + \epsilon^{-1}\nabla_y$. Postulate two-scale asymptotic expansions for the set ν^{ϵ} of unknowns $\{\boldsymbol{\sigma}_t, \boldsymbol{\sigma}_e, \mathbf{u}, \phi, \mathbf{v}_D, P_b, C_b, \Psi_b, \boldsymbol{J}_t, \boldsymbol{J}_d, \boldsymbol{I}_e, V_{\mathrm{match}}\}$ and $\{\boldsymbol{\sigma}_f, P_f, C_f, \overline{\Psi}_f, \boldsymbol{V}_f, \boldsymbol{J}_f, \boldsymbol{J}_{fd}, \boldsymbol{I}_f\}$ in terms of the perturbation parameter ϵ

$$\nu^{\epsilon} = \nu^0 + \epsilon\,\nu^1 + \epsilon^2\nu^2 + \ldots \tag{5.5}$$

with the coefficients ν^i, Y periodic in $\boldsymbol{y}$. Insert the expansions Eq. 5.5 into the set of microscopic governing equations with the differential operator ∂/∂_x replaced by $\partial/\partial_x + \epsilon^{-1}\partial/\partial_y$. After a formal matching of the successive powers of ϵ, we obtain a recursive system of equations. For the bulk fluid in the micropore system, the different orders of perturbation read as follows:

$$\boldsymbol{\sigma}^0_f = -P^0_f\,\boldsymbol{I}, \qquad \nabla_y\cdot\boldsymbol{\sigma}^0_f = -\nabla_y P^0_f = 0,$$

$$\nabla_x\cdot\boldsymbol{\sigma}^0_f + \nabla_y\cdot\boldsymbol{\sigma}^1_f = 0 \tag{5.6}$$

$$\mu\triangle_{yy}\boldsymbol{V}^0_f - \nabla_y P^1_f - \nabla_x P^0_f = 0, \qquad \nabla_y\cdot\boldsymbol{V}^0_f = 0,$$

$$\nabla_x\cdot\boldsymbol{V}^0_f + \nabla_y\cdot\boldsymbol{V}^1_f = 0 \tag{5.7}$$

$$\nabla_y\cdot\left(\mathcal{D}_f\nabla_y C^0_f + \Delta_f C^0_f\nabla_y\overline{\Psi}^0_f\right) = 0,$$

$$\nabla_y\cdot\left[\Delta_f\nabla_y C^0_f + \mathcal{D}_f C^0_f\nabla_y\overline{\Psi}^0_f\right] = 0 \tag{5.8}$$

$$\nabla_y\cdot\left(2C^0_f\boldsymbol{V}^0_f - \mathcal{D}_f\left(\nabla_x C^0_f + \nabla_y C^1_f\right) - \Delta_f C^0_f\left(\nabla_x\overline{\Psi}^0_f + \nabla_y\overline{\Psi}^1_f\right)\right) - \nabla_x\cdot\left(\mathcal{D}_f\nabla_y C^0_f + \Delta_f C^0_f\nabla_y\overline{\Psi}^0_f\right) = 0; \tag{5.9}$$

$$\boldsymbol{J}^0_{fd} = -\mathcal{D}_f\left(\nabla_x C^0_f + \nabla_y C^1_f\right) - \Delta_f C^0_f\left(\nabla_x\overline{\Psi}^0_f + \nabla_y\overline{\Psi}^1_f\right),$$

$$\nabla_x\cdot\boldsymbol{I}^0_f + \nabla_y\cdot\boldsymbol{I}^1_f = 0 \tag{5.10}$$

$$\nabla_y\cdot\left[\Delta_f\left(\nabla_x C^0_f + \nabla_y C^1_f\right) + \mathcal{D}_f C^0_f\left(\nabla_x\overline{\Psi}^0_f + \nabla_y\overline{\Psi}^1_f\right)\right] + \nabla_x\cdot\left(\Delta_f\nabla_y C^0_f + C^0_f\,\mathcal{D}_f\nabla_y\overline{\Psi}^0_f\right) = 0 \tag{5.11}$$

$$\boldsymbol{I}_f^0 = -F\Big[\Delta_f\left(\nabla_x C_f^0 + \nabla_y C_f^1\right) + C_f^0 \mathcal{D}_f\left(\nabla_x \overline{\Psi}_f^0 + \nabla_y \overline{\Psi}_f^1\right)\Big]. \tag{5.12}$$

$$2\frac{\partial C_f^0}{\partial t} + \nabla_x\cdot\left(2C_f^0 \boldsymbol{V}_f^0 + \boldsymbol{J}_{fd}^0\right) + \nabla_y\cdot\left(2\left(C_f \boldsymbol{V}_f\right)^1 + \boldsymbol{J}_{fd}^1\right) = 0. \tag{5.13}$$

In addition, let $\varphi^0 = \varphi^0(C_b^0, \phi^0)$ be the solution of the Poisson–Boltzmann Eq. 3.15 problem with C_b replaced by C_b^0 and let $\{v_E^0, v_C^0\}$ satisfying the flow problems Eqs. 3.26 and 3.30 with φ replaced by φ^0. Denoting $\{\boldsymbol{L}_{IJ}^0, G_c^0, \boldsymbol{\Pi}^0\}$ as the ϵ^0 order of the corresponding coefficients depending in a nonlinear fashion on $\{C_b^0, \phi^0\}$ through the nanoscopic closure problems in Eq. 3.39, (with $\{\varphi, v_E, v_C\}$ replaced by $\{\varphi^0, v_E^0, v_C^0\}$), the set of perturbed equations for the clay clusters (3.38) reads as

$$\nabla_y\cdot\left(\boldsymbol{C}\boldsymbol{\mathcal{E}}_y\left(\mathbf{u}^0\right)\right) = 0, \qquad \nabla_y\cdot\boldsymbol{\sigma}_t^0 = 0,$$
$$\nabla_x\cdot\boldsymbol{\sigma}_t^0 + \nabla_y\cdot\boldsymbol{\sigma}_t^1 = 0 \tag{5.14}$$

$$\boldsymbol{\sigma}_t^0 = -P_b^0\boldsymbol{I} + \boldsymbol{\sigma}_e^0 - \boldsymbol{\Pi}^0, \quad \boldsymbol{\sigma}_e^0 = \boldsymbol{C}\left[\boldsymbol{\mathcal{E}}_x\left(\mathbf{u}^0\right) + \boldsymbol{\mathcal{E}}_y\left(\mathbf{u}^1\right)\right] \tag{5.15}$$

$$\mathbf{v}_D^0 = 0, \quad \boldsymbol{J}_d^0 = 0, \quad \boldsymbol{I}_e^0 = 0 \tag{5.16}$$

$$\nabla_y\cdot\mathbf{v}_D^1 + \nabla_y\cdot\frac{\partial\mathbf{u}^1}{\partial t} = -\nabla_x\cdot\frac{\partial\mathbf{u}^0}{\partial t} \tag{5.17}$$

$$\frac{\partial\phi^0}{\partial t} = \left(1-\phi^0\right)\left(\nabla_x\cdot\frac{\partial\mathbf{u}^0}{\partial t} + \nabla_y\cdot\frac{\partial\mathbf{u}^1}{\partial t}\right) - \phi^1\nabla_y\cdot\frac{\partial\mathbf{u}^0}{\partial t} \tag{5.18}$$

$$\frac{\partial\phi^0}{\partial t} + \left(1-\phi^0\right)\nabla_y\cdot\mathbf{v}_D^1 + \phi^1\nabla_y\cdot\frac{\partial\mathbf{u}^0}{\partial t} = 0 \tag{5.19}$$

$$\frac{\partial}{\partial t}\left(\phi^0 G_c^0 C_b^0\right) + \nabla_y\cdot\left(2C_b^0\mathbf{v}_D^1 + \boldsymbol{J}_d^1\right) - \phi^0 G_c^0 C_b^0\nabla_y\cdot\mathbf{v}_D^1 = 0, \ \nabla_y\cdot\boldsymbol{I}_e^1 = 0 \tag{5.20}$$

$$\mathbf{v}_D^1 = -\boldsymbol{L}_{PP}^0\nabla_y P_b^0 - \boldsymbol{L}_{PC}^0 RT\nabla_y \ln C_b^0 - \boldsymbol{L}_{PE}^0\nabla_y\Psi_b^0 \tag{5.21}$$

$$\boldsymbol{J}_d^1 = -\boldsymbol{L}_{CP}^0\nabla_y P_b^0 - \boldsymbol{L}_{CC}^0 RT\nabla_y \ln C_b^0 - \boldsymbol{L}_{CE}^0\nabla_y\Psi_b^0 \tag{5.22}$$

$$\boldsymbol{I}_e^1 = -\boldsymbol{L}_{EP}^0\nabla_y P_b^0 - \boldsymbol{L}_{EC}^0 RT\nabla_y \ln C_b^0 - \boldsymbol{L}_{EE}^0\nabla_y\Psi_b^0. \tag{5.23}$$

Furthermore, denoting $\langle\cdot\rangle_y \equiv |Y|^{-1}\int_{Y_\alpha}\cdot dY_\alpha$ $(\alpha = f, s)$, the mean value operator over the reference cell Y, the $\mathcal{O}(\epsilon^0)$ of the averaging relations Eqs. 5.3 and 5.4, and the mass balance Eq. 2.26 are given by

$$\left\langle\frac{\partial f^0}{\partial t}\right\rangle_y = \frac{\partial\langle f^0\rangle_y}{\partial t} - \frac{1}{|Y|}\int_{\partial Y_{fs}}\left(f\frac{\partial\mathbf{u}}{\partial t}\right)^1\cdot\boldsymbol{N}\mathrm{d}\Gamma \tag{5.24}$$

$$\left\langle\nabla_x\cdot\boldsymbol{g}^0 + \nabla_y\cdot\boldsymbol{g}^1\right\rangle_y = \nabla_x\cdot\left\langle\boldsymbol{g}^0\right\rangle_y + \frac{1}{|Y|}\int_{\partial Y_{fs}}\boldsymbol{g}^1\cdot\boldsymbol{N}\mathrm{d}\Gamma. \tag{5.25}$$

and

$$\frac{\partial}{\partial t}\left(\phi^0 G_c^0 C_b^0\right) + \nabla_x\cdot\boldsymbol{J}_t^0 + \nabla_y\cdot\boldsymbol{J}_t^1 = 0 \tag{5.26}$$

with $\boldsymbol{J}_t^0 = \phi^0 G_c^0 C_b^0\frac{\partial\mathbf{u}^0}{\partial t}$ and

$$\boldsymbol{J}_t^1 = 2C_b^0\mathbf{v}_D^1 + \boldsymbol{J}_d^1 + \left(\phi G_c C_b\frac{\partial\mathbf{u}}{\partial t}\right)^1.$$

Finally, denoting $\boldsymbol{V}_{fs}^0 := \boldsymbol{V}_f^0 - \partial\mathbf{u}^0/\partial t$, $L_{PC}^{\infty 0} := L_{PC}^\infty(C_f^0)$ and $L_{PE}^{\infty 0} := L_{PE}^\infty(C_f^0)$, the different orders of boundary conditions Eqs. 4.9–4.13 and 4.15 are

$$\boldsymbol{V}_{fs}^0\cdot\boldsymbol{N} = 0, \qquad \mathbf{v}_D^1\cdot\boldsymbol{N} = \left(\boldsymbol{V}_f^1 - \frac{\partial\mathbf{u}^1}{\partial t}\right)\cdot\boldsymbol{N},$$
$$\boldsymbol{V}_{fs}^0\cdot\boldsymbol{\tau} = V_{\text{match}}^0 \tag{5.27}$$

$$\boldsymbol{V}_{fs}^0\cdot\boldsymbol{\tau} = -\Big[\boldsymbol{L}_{PE}^{\infty 0}\left(\nabla_x\Psi_f^0 + \nabla_y\Psi_f^1\right) + \frac{RT}{C_f^0}\boldsymbol{L}_{PC}^{\infty 0}\left(\nabla_x C_f^0 + \nabla_y C_f^1\right)\Big]\cdot\boldsymbol{\tau} \tag{5.28}$$

$$\boldsymbol{C}\boldsymbol{\mathcal{E}}_y\left(\mathbf{u}^0\right)\boldsymbol{N} = 0, \left(\boldsymbol{\sigma}_t^1 - \boldsymbol{\sigma}_f^1\right)\boldsymbol{N} = 0, \ \left(\boldsymbol{\sigma}_e^0 - \boldsymbol{\Pi}^0\right)\boldsymbol{N} = 0 \tag{5.29}$$

$$P_b^0 = P_f^0, \quad C_b^0 = C_f^0, \quad \Psi_b^0 = \Psi_f^0 \tag{5.30}$$

$$\left(\mathcal{D}_f\nabla_y C_f^0 + \Delta_f C_f^0\nabla_y\overline{\Psi}_f^0\right)\cdot\boldsymbol{N} = 0,$$
$$\left(\Delta_f\nabla_y C_f^0 + \mathcal{D}_f C_f^0\nabla_y\overline{\Psi}_f^0\right)\cdot\boldsymbol{N} = 0 \tag{5.31}$$

$$\Big[2C_f^0\boldsymbol{V}_{fs}^0 - \mathcal{D}_f\left(\nabla_x C_f^0 + \nabla_y C_f^1\right) - \Delta_f C_f^0\left(\nabla_x\overline{\Psi}_f^0 + \nabla_y\overline{\Psi}_f^1\right)\Big]\cdot\boldsymbol{N} = 0 \tag{5.32}$$

$$\Big[\Delta_f\left(\nabla_x C_f^0 + \nabla_y C_f^1\right) + \mathcal{D}_f C_f^0\left(\nabla_x\overline{\Psi}_f^0 + \nabla_y\overline{\Psi}_f^0\right)\Big]\cdot\boldsymbol{N} = 0 \tag{5.33}$$

$$\boldsymbol{J}_d^1 \cdot \boldsymbol{N} = \boldsymbol{J}_{fd}^1 \cdot \boldsymbol{N}, \qquad \boldsymbol{I}_e^1 \cdot \boldsymbol{N} = \boldsymbol{I}_f^1 \cdot \boldsymbol{N} \tag{5.34}$$

$$\left(\boldsymbol{J}_d^1 + 2(\mathbf{v}_D C_b)^1\right) \cdot \boldsymbol{N} = \left(\boldsymbol{J}_{fd}^1 + 2(C_f \boldsymbol{V}_{fs})^1\right) \cdot \boldsymbol{N} \tag{5.35}$$

and the initial conditions at $\mathcal{O}(\epsilon^0)$

$$C_b^0 = C_f^0 = \overline{C}; \quad \phi^0 = \overline{\phi}, \quad \nabla_x \cdot \mathbf{u}^0 = \nabla_y \cdot \mathbf{u}^1 = 0, \quad t = 0 \tag{5.36}$$

Next, we formally collect our homogenized results.

5.2.1 Nonoscillatory variables

From Eq. 5.6b, we have $P_f^0(\boldsymbol{x}, \boldsymbol{y}, t) = P_f^0(\boldsymbol{x}, t)$. Also note that $\mathbf{u}^0$, C_f^0 and $\overline{\Psi}_f^0$ satisfy the Neumann problems given by Eqs. 5.14a and 5.8 along with boundary conditions Eqs. 5.29a and 5.31, whose solution is $\mathbf{u}^0(\boldsymbol{x}, \boldsymbol{y}, t) = \mathbf{u}^0(\boldsymbol{x}, t)$, $C_f^0(\boldsymbol{x}, \boldsymbol{y}, t) = C_f^0(\boldsymbol{x}, t)$, and $\overline{\Psi}_f^0(\boldsymbol{x}, \boldsymbol{y}, t) = \overline{\Psi}_f^0(\boldsymbol{x}, t)$. Hence, our set of nonoscillatory variables (depending only on $(\boldsymbol{x}, t)$) is $\{P_f^0, C_f^0, \overline{\Psi}_f^0, \mathbf{u}^0\}$. Furthermore, using the divergence theorem for the last term in the RHS of Eq. 5.25, we obtain the commuting property

$$\langle \nabla_x \cdot \boldsymbol{g}^0 \rangle_y = \nabla_x \cdot \langle \boldsymbol{g}^0 \rangle_y . \tag{5.37}$$

5.2.2 Closure relations for the fluctuations

We begin by deriving the closure problem for C_f^1 and Ψ_f^1. Recalling that local hydrodynamic dispersion in the bulk fluid was neglected, the diffusion coefficients $\{\mathcal{D}_f, \Delta_f\}$ are constants. Thus, given $C_f^0 = C_f^0(\boldsymbol{x}, t)$ and $\Psi_f^0 = \Psi_f^0(\boldsymbol{x}, t)$, combine Eq. 5.9 with Eq. 5.11 and the local incompressibility constraint Eq. 5.7b to obtain

$$\nabla_y \cdot \left(\mathcal{D}_f \nabla_y C_f^1 + \Delta_f C_f^0 \nabla_y \overline{\Psi}_f^1\right) = 0,$$

$$\nabla_y \cdot \left(\mathcal{D}_f C_f^0 \nabla_y \overline{\Psi}_f^1 + \Delta_f \nabla_y C_f^1\right) = 0$$

By further manipulating the above result, using boundary conditions Eqs. 5.32, 5.33, and 5.27a, we are left with the local Neumann problems for $\{C_f^1, \overline{\Psi}_f^1\}$

$$\begin{array}{l|l} \triangle_{yy} C_f^1 = 0 \quad \text{in} \quad Y_f & \triangle_{yy} \overline{\Psi}_f^1 = 0 \quad \text{in} \quad Y_f \\ \left(\nabla_y C_f^1 + \nabla_x C_f^0\right) \cdot \boldsymbol{N} = 0 & \left(\nabla_y \overline{\Psi}_f^1 + \nabla_x \overline{\Psi}_f^0\right) \cdot \boldsymbol{N} = 0 \\ \text{on} \quad \partial Y_{fs} . & \text{on} \quad \partial Y_{fs} . \end{array}$$

By linearity, the solution can be represented as

$$C_f^1 = \boldsymbol{f}(\boldsymbol{y}) \cdot \nabla_x C_f^0 + \hat{C}(\boldsymbol{x}, t), \quad \overline{\Psi}_f^1 = \boldsymbol{f}(\boldsymbol{y}) \cdot \nabla_x \overline{\Psi}_f^0 + \hat{\Psi}(\boldsymbol{x}, t) \tag{5.38}$$

where $\boldsymbol{f}$ is the classical tortuosity vectorial function satisfying the cell problem

$$\begin{aligned} \triangle_{yy} \boldsymbol{f} &= 0 \qquad \text{in} \quad Y_f \\ \left(\nabla_y \boldsymbol{f} + \boldsymbol{I}\right) \cdot \boldsymbol{N} &= 0 \qquad \text{on} \quad \partial Y_{fs} . \end{aligned} \tag{5.39}$$

Using Eq. 5.38 in Eqs. 5.10 and 5.12, the averaged flux of species and electric current are given by

$$\boldsymbol{J}_{FD}^0 := \langle \boldsymbol{J}_{fd}^0 \rangle_y = -\left(\boldsymbol{D}_{eff} \nabla_x C_f^0 + \boldsymbol{\Delta}_{eff} C_f^0 \nabla_x \overline{\Psi}_f^0\right) \tag{5.40}$$

$$\boldsymbol{I}_F^0 := \langle \boldsymbol{I}_f^0 \rangle_y = -F\left(\boldsymbol{\Delta}_{eff} \nabla_x C_f^0 + \boldsymbol{D}_{eff} C_f^0 \nabla_x \overline{\Psi}_f^0\right) \tag{5.41}$$

where $\boldsymbol{D}_{eff} := \mathcal{D}_f \langle \boldsymbol{I} + \nabla_y \boldsymbol{f} \rangle_y$ and

$$\boldsymbol{\Delta}_{eff} := \Delta_f \langle \boldsymbol{I} + \nabla_y \boldsymbol{f} \rangle_y \tag{5.42}$$

are the macroscopic diffusion coefficients of the species in the bulk solution. It is worth noting that, in the absence of hydrodynamic dispersion, $\boldsymbol{f}$ is constant for a periodic medium. Thus, by invoking the above closure problem (5.42), $\boldsymbol{D}_{eff}$ and $\boldsymbol{\Delta}_{eff}$ are also constants.

5.2.3 Overall mass balance of the solutes

We are now ready to derive the overall macroscopic mass balance of the species. To this end, we begin by averaging the transport Eqs. 5.26 and 5.20a, use Eqs. 5.24 and 5.25 with $\{f, \boldsymbol{g}\} = \{2C_f, 2C_f \boldsymbol{V}_f + \boldsymbol{J}_{fd}\}$ and $\{\phi G_c C_b, \boldsymbol{J}_t\}$, respectively. Recalling the nonoscillatory behavior of C_f^0, so that $\langle C_f^0 \rangle_y = n_f C_f^0$, with $n_f := |Y_f|/|Y|$ denoting the macroscopic porosity, we have (recall that $\boldsymbol{N}$ was chosen outward to Y_s)

$$\begin{aligned} &2\frac{\partial}{\partial t}\left(n_f C_f^0\right) + \nabla_x \cdot \left(2C_f^0 \langle \boldsymbol{V}_f^0 \rangle_y + \langle \boldsymbol{J}_{fd}^0 \rangle_y\right) \\ &\quad = -\frac{1}{|Y|} \int_{\partial Y_{fs}} \left(2C_f^0 \boldsymbol{V}_{fs}\right)^1 + \boldsymbol{J}_{fd}^1 \cdot \boldsymbol{N} \, d\Gamma \\ &\frac{\partial}{\partial t}\left(\langle \phi^0 G_c^0 C_b^0 \rangle_y\right) + \nabla_x \cdot \langle \boldsymbol{J}_t^0 \rangle_y \\ &\quad = \frac{1}{|Y|} \int_{\partial Y_{fs}^0} \left(2C_b^0 \mathbf{v}_D^1 + \boldsymbol{J}_d^1\right) \cdot \boldsymbol{N} \, d\Gamma \end{aligned}$$

By adding the above results, using boundary conditions Eqs. 5.35 and 5.34a and definition Eq. 5.40, we obtain

$$\begin{aligned} &\frac{\partial}{\partial t}\left(2\, n_f C_f^0 + \left\langle \phi^0 \, G_c^0 \, C_b^0 \right\rangle_y\right) \\ &\quad + \nabla_x \cdot \left(2\, C_f^0 \, \boldsymbol{V}_{DF}^0 + \left(2\, n_f C_f^0 + \left\langle \phi^0 \, G_c^0 \, C_b^0 \right\rangle_y\right) \frac{\partial \mathbf{u}^0}{\partial t}\right) \\ &\quad = -\nabla_x \cdot \boldsymbol{J}_{FD}^0 \end{aligned} \tag{5.43}$$

where $\boldsymbol{V}^0_{DF} := \langle \boldsymbol{V}^0_{fs} \rangle_y = \langle \boldsymbol{V}^0_f \rangle_y - n_f \partial \mathbf{u}^0 / \partial t$ is the Darcian velocity of the bulk fluid relative to the solid phase. To express the above result in a more concise form, introduce the overall macroscopic ion concentration in both cluster and micropore systems as $2C^0_T := \langle C^0_t \rangle_y$ with

$$C^0_t := \begin{cases} 2C^0_f & \text{in} \quad Y_f \\ \phi^0 \left(C^0_+ + C^0_- \right) = \phi^0 G^0_c C^0_b & \text{in} \quad Y_s \end{cases} \tag{5.44}$$

so that

$$2C^0_T = 2n_f C^0_f + \left\langle \phi^0 G^0_c C^0_b \right\rangle_y . \tag{5.45}$$

Using the above definition and the constitutive law Eq. 5.40 in Eq. 5.43, we obtain

$$\begin{aligned} 2\frac{\partial}{\partial t}\left(n_f C^0_f\right) + \nabla_x \cdot \left(2C^0_f \boldsymbol{V}^0_{DF} + 2C^0_T \frac{\partial \mathbf{u}^0}{\partial t} \right) \\ = -\nabla_x \cdot \left(\boldsymbol{D}_{eff} \nabla_x C^0_f + \boldsymbol{\Delta}_{eff} C^0_f \nabla_x \overline{\Psi}^0_f \right) \\ = -\frac{\partial}{\partial t} \left\langle \phi^0 G^0_c C^0_b \right\rangle_y . \end{aligned} \tag{5.46}$$

The above result shows a macroscopic convection–diffusion equation for the concentration of the species in the bulk solution with an additional source/sink mass transfer term in the RHS, which quantifies the interchange of the solutes between micropores and aggregates. One may clearly observe electrochemical effects manifested in the mass transfer through the EDL storativity parameter G^0_c. Because $G^0_c \geq 2$, this coefficient acts to enhance the adsorption/desorption process. In the case of nonionic species discussed in Arbogast [2] and Douglas and Spagnuolo [23], we have $\overline{\varphi}^0 = 0$ and $G^0_c = 2$, which shows adsorption solely due to the existence of the secondary intracluster porosity ϕ^0.

5.2.4 Macroscopic conservation of charge

The macroscopic equation governing conservation of charge can be derived in a straightforward fashion. By averaging the second equations in Eqs. 5.10 and 5.20 using definition Eq. 5.41b for the macroscopic current and boundary condition Eq. 5.34b, we have

$$\begin{aligned} \nabla_x \cdot \boldsymbol{I}^0_F = \nabla_x \cdot \left\langle \boldsymbol{I}^0_f \right\rangle_y = -\left\langle \nabla_y \cdot \boldsymbol{I}^1_f \right\rangle_y = \frac{1}{|Y|} \int_{\partial Y_{fs}} \boldsymbol{I}^1_f \cdot \boldsymbol{N} \mathrm{d}\Gamma \\ = \frac{1}{|Y|} \int_{\partial Y_{fs}} \boldsymbol{I}^1_e \cdot \boldsymbol{N} \mathrm{d}\Gamma \\ = \frac{1}{|Y|} \int_{Y_s} \nabla_y \cdot \boldsymbol{I}^1_e \mathrm{d}Y = 0 . \end{aligned}$$

Because the electroneutrality condition precludes the transient accumulation of electrical charges, like Eq. 3.14, the above result shows a divergence macroscopic free current in the micropores. Together with the constitutive law Eq. 5.41, the above result gives

$$\nabla_x \cdot \left(\boldsymbol{\Delta}_{eff} \nabla_x C^0_f + C^0_f \boldsymbol{D}_{eff} \nabla_x \overline{\Psi}^0_f \right) = 0 \tag{5.47}$$

Let $\boldsymbol{J}^0_f$ be the overall convective/diffusive flux of species in the bulk fluid. Recalling that $\boldsymbol{D}_{eff}$ and $\boldsymbol{\Delta}_{eff}$ are constants, by eliminating the term involving the electric potential in the above result and substituting back in Eq. 5.46, we obtain the decoupled form of the homogenized transport equation

$$\frac{\partial}{\partial t}\left(n_f C^0_f\right) + \nabla_x \cdot \boldsymbol{J}^0_f = -\frac{\partial}{\partial t} \left\langle \phi^0 \langle \cosh \overline{\varphi}^0 \rangle^l_z C^0_b \right\rangle_y \tag{5.48}$$

$$\boldsymbol{J}^0_f := C^0_f \boldsymbol{V}^0_{DF} + C^0_T \frac{\partial \mathbf{u}^0}{\partial t} - \boldsymbol{D}^\star_{eff} \nabla_x C^0_f \tag{5.49}$$

with the effective diffusivity given by

$$2\boldsymbol{D}^\star_{eff} := \boldsymbol{D}^{-1}_{eff} \left(\boldsymbol{D}^2_{eff} - \boldsymbol{\Delta}^2_{eff} \right) \tag{5.50}$$

Thus, given C^0_f solution of Eqs. 5.48 and 5.49, the component involving this quantity in Eq. 5.47 can be treated as a source term in a Poisson-type problem for $\overline{\Psi}^0_f$. It is worth noting that, when the difference between cation and anion diffusivities decreases, $\boldsymbol{D}^2_{eff} >> \boldsymbol{\Delta}^2_{eff}$, which implies $\boldsymbol{D}^\star_{eff} \approx \boldsymbol{D}_{eff}/2$.

5.2.5 Macroscopic Darcy's law

To derive the macroscopic form of Darcy's law for the movement of the bulk solution in the micropores, we begin by using the closure relations Eq. 5.38 in the slip boundary condition Eq. 5.28 to obtain

$$\begin{aligned} \boldsymbol{V}^0_{fs} \cdot \boldsymbol{\tau} = -\Big[L^{\infty 0}_{PE} (\boldsymbol{I} + \nabla_y \boldsymbol{f}) \nabla_x \Psi^0_f \\ + \frac{RTL^{\infty 0}_{PC}}{C^0_f} (\boldsymbol{I} + \nabla_y \boldsymbol{f}) \nabla_x C^0_f \Big] \cdot \boldsymbol{\tau} \quad \text{on} \quad \partial Y_{fs} . \end{aligned} \tag{5.51}$$

Thus, given the nonoscillatory potentials $\{P^0_f, C^0_f, \Psi^0_f, \mathbf{u}^0\}$, combine the two former equations in Eq. 5.7 with boundary conditions Eq. 5.27a and the above

result to obtain a local periodic Stokes problem for $\{\boldsymbol{V}^0_{fs}, P^1_f\}$ with slip boundary condition

$$\mu \triangle_{yy} \boldsymbol{V}^0_{fs} - \nabla_y P^1_f = \nabla_x P^0_f$$

$$\nabla_y \cdot \boldsymbol{V}^0_{fs} = 0 \qquad \text{in} \quad Y_f$$

$$\boldsymbol{V}^0_{fs} \cdot \boldsymbol{N} = 0 \qquad \text{on} \quad \partial Y_{fs}$$

$$\boldsymbol{V}^0_{fs} \cdot \boldsymbol{\tau} = -\Big[L^{\infty 0}_{PE} (\boldsymbol{I} + \nabla_y \boldsymbol{f}) \nabla_x \Psi^0_f + (RT) \left(C^0_f\right)^{-1} L^{\infty 0}_{PC} (\boldsymbol{I} + \nabla_y \boldsymbol{f}) \nabla_x C^0_f \Big] \cdot \boldsymbol{\tau} \quad \text{on} \quad \partial Y_{fs} \tag{5.52}$$

To derive Darcy's law, we decompose the relative velocity and pressure fluctuation into their hydraulic, chemico-osmotic and electro-osmotic components $\boldsymbol{V}^0_{fs} = \boldsymbol{V}^0_p + \boldsymbol{V}^0_c + \boldsymbol{V}^0_e$ and $P^1_f = P^1_p + P^1_c + P^1_e$. The pair $\{\boldsymbol{V}^0_p, P^1_p\}$ satisfies the classical local Stokes problem driven only by a macroscopic pressure gradient

$$\mu \triangle_{yy} \boldsymbol{V}^0_p - \nabla_y P^1_p = \nabla_x P^0_f$$

$$\nabla_y \cdot \boldsymbol{V}^0_p = 0 \qquad \text{in} \quad Y_f$$

$$\boldsymbol{V}^0_p = 0 \qquad \text{on} \quad \partial Y_{fs} \tag{5.53}$$

whereas the electro- and chemico-osmotic components satisfy

$$\mu \triangle_{yy} \boldsymbol{V}^0_e - \nabla_y P^1_e = 0$$
$$\nabla_y \cdot \boldsymbol{V}^0_e = 0, \qquad \text{in} \quad Y_f$$
$$\boldsymbol{V}^0_e \cdot \boldsymbol{N} = 0, \quad \boldsymbol{V}^0_e \cdot \boldsymbol{\tau} = -L^{\infty 0}_{PE} (\boldsymbol{I} + \nabla_y \boldsymbol{f}) \nabla_x \Psi^0_f \cdot \boldsymbol{\tau} \quad \text{on} \quad \partial Y_{fs} \tag{5.54}$$

and

$$\mu \triangle_{yy} \boldsymbol{V}^0_c - \nabla_y P^1_c = 0$$

$$\nabla_y \cdot \boldsymbol{V}^0_c = 0 \qquad \text{in} \quad Y_f$$

$$\boldsymbol{V}^0_c \cdot \boldsymbol{N} = 0, \; \boldsymbol{V}^0_c \cdot \boldsymbol{\tau} = -RT \left(C^0_f\right)^{-1} L^{\infty 0}_{PC} \left(\boldsymbol{I} + \nabla_y \boldsymbol{f}\right) \nabla_x C^0_f \cdot \boldsymbol{\tau} \quad \text{on} \quad \partial Y_{fs} \tag{5.55}$$

Problem Eq. 5.53 for $(\boldsymbol{V}^0_p, P^1_p)$ is nothing but the classical closure problem for the hydraulic conductivity [7, 59]. Following classical superposition arguments for linear problems, denote $\{\boldsymbol{e}_j\}$, $(j = 1, 2, 3)$ as an orthonornal basis and define the periodic characteristic tensorial functions $\boldsymbol{\kappa}_p$, with vectorial components $\boldsymbol{\kappa}^j_p$ $(j = 1, 2, 3)$, and the scalars $\widetilde{p_p}^j$ as the solution of the canonical problems

$$\mu \triangle_{yy} \boldsymbol{\kappa}^j_p - \nabla_y \widetilde{p_p}^j = -\boldsymbol{e}_j$$

$$\nabla_y \cdot \boldsymbol{\kappa}^j_p = 0, \quad \text{in} \quad Y_f \qquad j = 1, 2, 3$$

$$\boldsymbol{\kappa}^j_p = 0 \qquad \text{on} \quad \partial Y_{fs} \tag{5.56}$$

Furthermore, by invoking the closure problem Eq. 5.39 for the tortuosity function $\boldsymbol{f}$, one may verify that problems Eqs. 5.54 and 5.55 admit solutions of the type

$$\boldsymbol{V}^0_e = -L^{\infty 0}_{PE} (\boldsymbol{I} + \nabla_y \boldsymbol{f}) \nabla_x \Psi^0_f,$$

$$\boldsymbol{V}^0_c = -RT \left(C^0_f\right)^{-1} L^{\infty 0}_{PC} (\boldsymbol{I} + \nabla_y \boldsymbol{f}) \nabla_x C^0_f,$$

$$P^1_j = P^1_j(\boldsymbol{x}, t) \quad j = e, c$$

Exploiting linearity after averaging, we obtain the modified form of Darcy's law for the bulk fluid

$$\boldsymbol{V}^0_{DF} := \left\langle \boldsymbol{V}^0_{fs} \right\rangle_y = -\boldsymbol{K}_P \nabla_x P^0_f - \boldsymbol{K}_C \nabla_x C^0_f - \boldsymbol{K}_E \nabla_x \Psi^0_f,$$

with $\boldsymbol{K}_P := \langle \boldsymbol{\kappa}_p \rangle$ and $\boldsymbol{K}_E := L^{\infty 0}_{PE} \langle \boldsymbol{I} + \nabla_y \boldsymbol{f} \rangle_y$,

$$\boldsymbol{K}_C := \frac{RT L^{\infty 0}_{PC}}{C^0_f} \langle \boldsymbol{I} + \nabla_y \boldsymbol{f} \rangle_y. \tag{5.57}$$

In a similar fashion to its two-scale counterpart in Eq. 2.25 for overlapping EDLs, the above result shows (in addition to a pressure gradient) bulk flow driven by gradients in concentration (chemico-osmosis) and electric potential (electro-osmosis). On the other hand, one may observe crucial differences between the two- and three-scale closure problems for the electro- and chemico-osmotic conductivities. Unlike the homogenization of the modified Stokes problem (3.6) in the nanopores with overlapping EDLs, whose homogenized form of Darcy's law for parallel particles is given by Eq. 3.33, the solution of the closure problems for $\boldsymbol{K}_C$ and $\boldsymbol{K}_E$ is simply given by the corresponding values for thin double layers $L^{\infty 0}_{PC}$ and $L^{\infty 0}_{PE}$ modified by the tortuosity factor $\nabla_y \boldsymbol{f}$.

5.2.6 Overall mass balance

We now derive the overall macroscopic mass balance. By averaging Eqs. 5.7c and 5.17 using boundary

condition Eq. 5.27b along with Eq. 5.37, the divergence theorem, and the periodicity, we get

$$\begin{aligned}\langle \nabla_x \cdot \boldsymbol{V}_f^0\rangle_y &= \nabla_x\cdot\langle \boldsymbol{V}_f^0\rangle_y = -|Y|^{-1}\int_{Y_f}\nabla_y\cdot\boldsymbol{V}_f^1\,\mathrm{d}Y\\ &= |Y|^{-1}\int_{\partial Y_{fs}}\boldsymbol{V}_f^1\cdot\boldsymbol{N}\,\mathrm{d}\Gamma\\ &= |Y|^{-1}\int_{\partial Y_{fs}}\left(\mathbf{v}_D^1+\frac{\partial\mathbf{u}^1}{\partial t}\right)\cdot\boldsymbol{N}\,\mathrm{d}\Gamma\\ &= \left\langle\nabla_y\cdot\mathbf{v}_D^1+\nabla_y\cdot\frac{\partial\mathbf{u}^1}{\partial t}\right\rangle_y = -\left\langle\nabla_x\cdot\frac{\partial\mathbf{u}^0}{\partial t}\right\rangle_y\\ &= -\nabla_x\cdot\left\langle\frac{\partial\mathbf{u}^0}{\partial t}\right\rangle_y = -\nabla_x\cdot\left((1-n_f)\frac{\partial\mathbf{u}^0}{\partial t}\right).\end{aligned}$$

In terms of the macroscopic Darcy's velocity, $\boldsymbol{V}_{DF}^0$, the above result can be rewritten as

$$\nabla_x\cdot\frac{\partial\mathbf{u}^0}{\partial t}+\nabla_x\cdot\boldsymbol{V}_{DF}^0=0 \tag{5.58}$$

which shows the same form of the two-scale result Eq. 2.4. Whence, the overall mass balance for locally incompressible media that commonly appear in the governing equations of Poromechanics applies to both single and double porosity media.

5.2.7 Overall momentum balance

To derive the overall momentum balance, we average Eqs. 5.14c and 5.6c and use boundary condition Eq. 5.29b together with the constitutive laws Eqs. 5.6a and 5.15a to obtain

$$\begin{aligned}\nabla_x\cdot\langle\boldsymbol{\sigma}_t^0\rangle_y &= \nabla_x\cdot\langle\boldsymbol{\sigma}_e^0\rangle_y-\nabla_x\langle P_b^0\rangle_y-\nabla_x\cdot\langle\boldsymbol{\Pi}^0\rangle_y\\ &= -\frac{1}{|Y|}\int_{Y_s}\nabla_y\cdot\boldsymbol{\sigma}_t^1\,\mathrm{d}Y\\ &= -\frac{1}{|Y|}\int_{\partial Y_{fs}}\boldsymbol{\sigma}_t^1\boldsymbol{N}\,\mathrm{d}\Gamma=-\frac{1}{|Y|}\int_{\partial Y_{fs}}\boldsymbol{\sigma}_f^1\boldsymbol{N}\,\mathrm{d}\Gamma\\ &= \frac{1}{|Y|}\int_{Y_f}\nabla_y\cdot\boldsymbol{\sigma}_f^1\,\mathrm{d}Y=\langle\nabla_x Pf^0\rangle_y=\nabla_x\left(n_f P_f^0\right)\end{aligned}$$

where the divergence theorem, periodicity, and Eq. 5.37 have also been used. Hence, denoting $n_s := 1-n_f$ as the macroscopic volume fraction of the clusters, we get

$$\nabla_x\cdot\left[\langle\boldsymbol{\sigma}_e^0\rangle_y-\langle\boldsymbol{\Pi}^0\rangle_y-\left(\langle P_b^0\rangle_y-(1-n_s)P_f^0\right)\boldsymbol{I}\right]=0 \tag{5.59}$$

where the macroscopic averaging of the representation Eqs. 3.36–3.37 for $\boldsymbol{\Pi}$ furnish at $\mathcal{O}(\epsilon^0)$

$$\begin{aligned}\langle\boldsymbol{\Pi}^0\rangle_y &= \langle\Pi^0\rangle_y\,\boldsymbol{n}\otimes\boldsymbol{n}=\langle\Pi_d^0\rangle_y\,\boldsymbol{n}\otimes\boldsymbol{n}\\ &= 2RT\left[\langle C_b^0\cosh\overline{\varphi}_0\rangle_y-\langle C_b^0\rangle_y\right]\boldsymbol{n}\otimes\boldsymbol{n}.\end{aligned} \tag{5.60}$$

To express Eq. 5.59 in a more compact form, denote P_0 as the excess in hidden bulk phase pressure of the clay clusters relative to its micropore counterpart

$$P_0 := P_b^0-P_f^0(\boldsymbol{x},t)\quad\text{with}$$

$$\langle P_0\rangle_y=|Y|^{-1}\int_{Y_s}\left(P_b^0-P_f^0\right)\mathrm{d}Y=\langle P_b^0\rangle_y-n_s P_f^0. \tag{5.61}$$

Making use of the above definitions, we collect the local microscopic relations in Eqs. 5.14b and 5.15 along with boundary conditions Eqs. 5.29c and 5.30a to obtain

$$\begin{aligned}&\nabla_y\cdot\left(\boldsymbol{C}\boldsymbol{\mathcal{E}}_y(\mathbf{u}^1)\right)-\nabla_y P_0-\nabla_y\cdot\boldsymbol{\Pi}^0=0 \quad \text{in}\quad Y_s\\ &\left[\boldsymbol{C}\left(\boldsymbol{\mathcal{E}}_x(\mathbf{u}^0)+\boldsymbol{\mathcal{E}}_y(\mathbf{u}^1)\right)-\boldsymbol{\Pi}^0\right]\boldsymbol{N}=0 \quad \text{on}\quad \partial Y_{fs}\\ &P_0=0 \quad \text{on}\quad \partial Y_{fs}.\end{aligned}$$

The above linear coupling between mechanical and electro-chemical effects suggests an additive decomposition for the fluctuating displacement. We then split $\mathbf{u}^1$ in a purely expansive component $\mathbf{u}_\pi^1$, induced by the transmissibility of $\boldsymbol{\Pi}^0$ between adjacent clusters, and the remaining poroelastic component $\mathbf{u}_e^1 := \mathbf{u}^1-\mathbf{u}_\pi^1$ as

$$\begin{array}{l|l}\nabla_y\cdot\left(\boldsymbol{C}\boldsymbol{\mathcal{E}}_y(\mathbf{u}_e^1)\right) & \nabla_y\cdot\left(\boldsymbol{C}\boldsymbol{\mathcal{E}}_y(\mathbf{u}_\pi^1)\right)\\ \quad-\nabla_y P_0=0 \quad \text{in}\quad Y_s & \quad-\nabla_y\cdot\boldsymbol{\Pi}^0=0 \quad \text{in}\quad Y_s\\ \left(\boldsymbol{C}\left(\boldsymbol{\mathcal{E}}_x(\mathbf{u}^0)\right.\right. & \left(\boldsymbol{C}\boldsymbol{\mathcal{E}}_y(\mathbf{u}_\pi^1)\right.\\ \quad\left.\left.+\boldsymbol{\mathcal{E}}_y(\mathbf{u}_e^1)\right)\right)\boldsymbol{N}=0 & \quad\left.-\boldsymbol{\Pi}^0\right)\boldsymbol{N}=0 \quad \text{on}\quad Y_{fs}.\\ P_0=0 \quad \text{on}\quad Y_{fs} & \end{array} \tag{5.62}$$

It should be noted that by invoking the nanoscopic representation Eqs. 3.36 and 3.37 at $\mathcal{O}(\epsilon^0)$ for $\boldsymbol{\Pi}^0$, with

$\overline{\varphi}^0$ solution of the $\mathcal{O}(\epsilon^0)$–Poisson–Boltzmann problem shows $\mathbf{u}_\pi^1$ fully determined by Eq. 5.62b parametrized by the pair $\{C_b^0.\phi^0\}$.

By invoking the constitutive law Eq. 5.15b, the contact stresses inherit the above decomposition. This suggests the following definitions for the macroscopic contact stress tensor $\boldsymbol{\sigma}_E^0$ and effective swelling stress $\boldsymbol{\Pi}_{eff}^0$

$$\begin{aligned}\boldsymbol{\sigma}_E^0 &:= \left\langle \boldsymbol{C}\left(\boldsymbol{\mathcal{E}}_x\left(\mathbf{u}^0\right)+\boldsymbol{\mathcal{E}}_y\left(\mathbf{u}_e^1\right)\right)\right\rangle_y - \langle P_0\rangle_y \boldsymbol{I},\\ \boldsymbol{\Pi}_{eff}^0 &:= -\left\langle \boldsymbol{C}\boldsymbol{\mathcal{E}}_y\left(\mathbf{u}_\pi^1\right)-\boldsymbol{\Pi}^0\right\rangle_y \end{aligned} \tag{5.63}$$

which, when combined with Eq. 5.15, gives $\langle \boldsymbol{\sigma}_t^0\rangle_y = n_s P_b^0 \boldsymbol{I} + \boldsymbol{\sigma}_E^0 - \boldsymbol{\Pi}_{eff}^0$. Using the above definitions and Eq. 5.61 in Eq. 5.59 gives

$$\nabla_x\cdot\boldsymbol{\sigma}_T^0 = 0, \quad \text{where}$$

$$\boldsymbol{\sigma}_T^0 := -P_f^0\boldsymbol{I}+\boldsymbol{\sigma}_E^0-\boldsymbol{\Pi}_{eff}^0 = -n_f P_f^0\boldsymbol{I}+\left\langle\boldsymbol{\sigma}_t^0\right\rangle_y \tag{5.64}$$

denotes the overall macroscopic stress tensor. Like the two-scale result (Eq. 2.22), the above equation represents the modified Terzaghi's decomposition at the macroscale with $\boldsymbol{\Pi}_{eff}^0$ identified with the upscaled version of $\boldsymbol{\Pi}^0$ governing the repulsive force between adjacent clusters. The double micro/nano down-scaling provided by Eqs. 5.63b, 5.62b, and 5.60 brings new information on the constitutive behavior of $\boldsymbol{\Pi}_{eff}^0$. In particular, one may observe from Eq. 5.62b that $\boldsymbol{\Pi}_{eff}^0$ incorporates two different components arising from the macroscopic averaging of the EDL contribution $\boldsymbol{\Pi}^0$ and the fluctuation of the electrochemical displacement $\mathbf{u}_\pi^1$. This latter component captures the transmissibility of the disjoining stresses between adjacent clusters. It is worth observing that such transmissibility requires clusters touching each other; otherwise, the terms involving $\mathbf{u}_\pi^1$ and $\boldsymbol{\Pi}^0$ in definition Eq. 5.63b would cancel out, implying $\boldsymbol{\Pi}_{eff}^0 = 0$. This fact highlights the essential feature underlying the survival of swelling stresses in the three-scale, which strongly relies on the balance between disjoining and contact forces. The contact between adjacent clusters leads to the variability of $\boldsymbol{\Pi}^0$ within each cluster and to the consequent appearance of the term involving the divergence of this quantity in Eq. 5.62b.

5.2.8 Mass balance of the clusters

To close the system of macroscopic governing equations, it remains to derive a mass balance for the clay clusters to compute the evolution of the porosity n_f. To this end, in Eq. 5.24, we select f equal to the macropore distribution function $\gamma(\boldsymbol{y}) := 1$ if $\boldsymbol{y}\in Y_f$ and $\gamma(\boldsymbol{y}) := 0$ if $\boldsymbol{y}\in Y_s$. Thus, with $f^0=\gamma$, $f^1=0$, and $\langle f^0\rangle_y = n_f$, using the divergence theorem and the mass balance of the solid phase Eq. 5.18, we get (recall again that $\boldsymbol{N}$ was chosen outward to Y_s)

$$\begin{aligned}\frac{\partial n_f}{\partial t} &= \frac{1}{|Y|}\int_{\partial Y_{fs}}\frac{\partial \mathbf{u}^1}{\partial t}\cdot\boldsymbol{N}\mathrm{d}\Gamma = -\left\langle\nabla_y\cdot\frac{\partial\mathbf{u}^1}{\partial t}\right\rangle_y\\ &= (1-n_f)\left(\nabla_x\cdot\frac{\partial\mathbf{u}^0}{\partial t}-\left\langle\frac{1}{(1-\phi^0)}\frac{\partial\phi^0}{\partial t}\right\rangle_y^s\right)\end{aligned} \tag{5.65}$$

where $\langle\cdot\rangle_y^s := |Y_s^{-1}|\int_{Y_s}\cdot dY_s = (1-n_f)\langle\cdot\rangle_y$ denotes the intrinsic volume averaging over the solid phase. The above result is the three-scale mass balance of the clay clusters. Unlike its two-scale counterpart for incompressible particles Eq. 2.5, the RHS describes the deformation of the compressible aggregates by the sum of two components. The first, involving the divergence of the displacement, incorporates the deformation induced by the relative movement of adjacent clusters, whereas the latter fluctuating component, involving the intracluster porosity, captures the local consolidation process within each cluster due to secondary drainage of the electrolyte solution in the nanopores.

5.3 Summary of the three-scale model of dual-porosity type

Let $\boldsymbol{C}$ be the elastic modulus of the particles and let $\{\overline{\varphi}^0, \boldsymbol{f}, \boldsymbol{\kappa}_p\}$ be the set of variables composed of the EDL potential and characteristic functions satisfying Eqs. 3.15, 5.39, and 5.56, respectively. Furthermore, denote $\{Ł_{IJ}^0, G_c^0, \boldsymbol{\Pi}^0\}$ as the microscopic electrochemical parameters of the clusters satisfying the cell problems Eq. 3.39 at $\mathcal{O}(\epsilon^0)$. Finally, let $\{\boldsymbol{D}_{eff}, \boldsymbol{\Delta}_{eff}, \boldsymbol{D}_{eff}^\star, \boldsymbol{K}_P, \boldsymbol{K}_C, \boldsymbol{K}_E$, and $\boldsymbol{\Pi}_{eff}^0\}$ be the set of macroscopic coefficients defined by the closure relations Eqs. 5.42, 5.50, 5.57, and 5.63b and C_T^0 the overall concentration of solutes given by Eq. 5.45. Application of the formal homogenization procedure leads to the following dual-porosity model: Find $\{\mathbf{u}^0, \boldsymbol{\sigma}_E^0, P_f^0, C_f^0, \Psi_f^0, n_f, \boldsymbol{V}_{DF}^0, \boldsymbol{J}_f^0$, and $\boldsymbol{I}_F^0\}$ func-

tions of $(\boldsymbol{x}, t)$ and $\{P_0,\ \mathbf{u}_e^1,\ \mathbf{u}_\pi^1,\ \phi^0,\ \mathbf{v}_D^1,\ C_b^0,\ \Psi_b^0,\ \boldsymbol{I}_e^1,$ and $\boldsymbol{J}_d^1\}$ functions of $(\boldsymbol{x}, \boldsymbol{y}, t)$ such that

$$
\begin{cases}
\nabla_x \cdot \boldsymbol{\sigma}_E^0 - \nabla_x P_f^0 - \nabla_x \cdot \boldsymbol{\Pi}_{eff}^0 = 0 \\
\boldsymbol{\sigma}_E^0 = -\langle P_0 \rangle_y \boldsymbol{I} + \boldsymbol{C}(1-n_f)\boldsymbol{\mathcal{E}}_x(\mathbf{u}^0) + \boldsymbol{C}\langle \boldsymbol{\mathcal{E}}_y\left(\mathbf{u}_e^1\right)\rangle_y \\
\nabla_x \cdot \dfrac{\partial \mathbf{u}^0}{\partial t} + \nabla_x \cdot \boldsymbol{V}_{DF}^0 = 0 \\
\boldsymbol{V}_{DF}^0 = -\boldsymbol{K}_P \nabla_x P_f^0 - \boldsymbol{K}_C \nabla_x C_f^0 - \boldsymbol{K}_E \nabla_x \Psi_f^0 \quad \text{in } \Omega, t>0 \\
\dfrac{\partial n_f}{\partial t} - \left(1-n_f^0\right)\nabla_x \cdot \dfrac{\partial \mathbf{u}^0}{\partial t} = -\left\langle \dfrac{1}{\left(1-\phi^0\right)} \dfrac{\partial \phi^0}{\partial t} \right\rangle_y \\
\dfrac{\partial}{\partial t}\left(n_f C_f^0\right) + \nabla_x \cdot \boldsymbol{J}_f^0 = -\dfrac{\partial}{\partial t}\left\langle \phi^0 \langle \cosh \overline{\varphi}^0 \rangle_z^l C_b^0 \right\rangle_y \\
\nabla_x \cdot \boldsymbol{I}_F^0 = 0 \\
\boldsymbol{J}_f^0 = 2\, C_f^0 \boldsymbol{V}_{DF}^0 + C_T^0 \dfrac{\partial \mathbf{u}^0}{\partial t} - \boldsymbol{D}_{eff}^{\star} \nabla_x C_f^0 \\
\boldsymbol{I}_F^0 = F\left(\boldsymbol{\Delta}_{eff} \nabla_x C_f^0 + \boldsymbol{D}_{eff} C_f^0 \nabla_x \Psi_f^0\right) \quad .
\end{cases}
\tag{5.66}
$$

and

$$
\begin{cases}
\nabla_y \cdot \left(\boldsymbol{C}\boldsymbol{\mathcal{E}}_y\left(\mathbf{u}_e^1\right)\right) - \nabla_y P_0 = 0 \\
\nabla_y \cdot \left(\boldsymbol{C}\boldsymbol{\mathcal{E}}_y\left(\mathbf{u}_\pi^1\right)\right) - \nabla_y \cdot \boldsymbol{\Pi}^0 = 0 \\
\nabla_y \cdot \mathbf{v}_D^1 + \nabla_y \cdot \dfrac{\partial \mathbf{u}_e^1}{\partial t} + \nabla_y \cdot \dfrac{\partial \mathbf{u}_\pi^1}{\partial t} = -\nabla_x \cdot \dfrac{\partial \mathbf{u}^0}{\partial t} \\
\dfrac{\partial \phi^0}{\partial t} + \left(1-\phi^0\right)\nabla_y \cdot \mathbf{v}_D^1 = 0 \qquad \text{in} \quad Y_s,\ t>0 \\
\dfrac{\partial}{\partial t}\left(\phi^0 G_c^0 C_b^0\right) + \nabla_y \cdot \left(2\, C_b^0\, \mathbf{v}_D^1 + \boldsymbol{J}_d^1\right) - \phi^0 G_c^0 C_b^0 \nabla_y \cdot \mathbf{v}_D^1 = 0 \\
\nabla_y \cdot \boldsymbol{I}_e^1 = 0 \\
\mathbf{v}_D^1 = -\boldsymbol{L}_{PP}^0 \nabla_y P_0 - \boldsymbol{L}_{PC}^0\, RT \nabla_y \ln C_b^0 - \boldsymbol{L}_{PE}^0 \nabla_y \Psi_b^0 \\
\boldsymbol{J}_d^1 = -\boldsymbol{L}_{CP}^0 \nabla_y P_0 - \boldsymbol{L}_{CC}^0\, RT \nabla_y \ln C_b^0 - \boldsymbol{L}_{CE}^0 \nabla_y \Psi_b^0 \\
\boldsymbol{I}_e^1 = -\boldsymbol{L}_{EP}^0 \nabla_y P_0 - \boldsymbol{L}_{EC}^0\, RT \nabla_y \ln C_b^0 - \boldsymbol{L}_{EE}^0 \nabla_y \Psi_b^0
\end{cases}
\tag{5.67}
$$

with the following boundary conditions on the cluster/micropore interface and initial conditions

$$
\begin{cases}
-\boldsymbol{C}\boldsymbol{\mathcal{E}}_y\left(\mathbf{u}_e^1\right)\boldsymbol{N} = \boldsymbol{C}\boldsymbol{\mathcal{E}}_x\left(\mathbf{u}^0\right)\boldsymbol{N} \\
-\boldsymbol{C}\boldsymbol{\mathcal{E}}_y\left(\mathbf{u}_\pi^1\right)\boldsymbol{N} = \boldsymbol{\Pi}^0 \boldsymbol{N}, \qquad \text{on} \quad \partial Y_{fs} \\
P_0 = 0, \quad C_b^0 = C_f^0, \quad \Psi_b^0 = \Psi_f^0 \\
\nabla_x \cdot \mathbf{u}^0 = \nabla_y \cdot \mathbf{u}^1 = 0, \quad t = 0\,, \\
C_b^0 = C_f^0 = \overline{C},\ \phi = \overline{\phi},\ n_f = \overline{n}_f, \qquad t = 0\,,
\end{cases}
\tag{5.68}
$$

along with boundary conditions on the outer frontier of the macroscopic medium $\partial\Omega$. It should be noted that, once $P_f^0 = P_f^0(\boldsymbol{x}, t)$, the hydraulic driving force $\nabla_y P_b^0$ in Onsager's relations in Eq. 5.67 was replaced by $\nabla_y P_0 = \nabla_y (P_b - P_f)$. After solving for P_0, the averaged bulk phase pressure of the electrolyte solution can be computed within the postprocessing approach $\langle P_b^0 \rangle_y = \langle P_0 \rangle_y + (1-n_f) P_f^0$.

The above results show a three-scale model of dual-porosity type wherein the swelling clay is represented by three overlaying nano-, micro-, and macrocontinua: The effective medium is governed by the macroscopic Eq. 5.66 posed in the domain Ω. This global system describes the evolution of a porous medium composed of micropores occupied by the bulk solution where macroscopic Darcy's flow, ion transport, and electric current take place. This system appears locally coupled with the microscopic governing equations (5.67) posed in each cluster domain Y_s. Moreover, the microscale coefficients are represented by local problems posed in a periodic nanocell Z_l with idealized nanogeometry of parallel particles. The local problems represent the influence of the micro- and nanostructures upon each macroscopic location $\boldsymbol{x}$.

The essential feature underlying the dual-porosity model is the accurate representation of the adsorption/desorption of the species by the clay clusters, which is measured by the source term in the RHS of Eq. 5.46. Compared to the adsorption of nonionic species, the influence of electrical effects on adsorption is manifested through the EDL storativity G_c^0. Within our three-scale portrait of the swelling medium, the computation of this quantity along with the other effective electrochemical parameters is accomplished by performing a double averaging of the electrochemistry of the electrolyte solution in the nanopores.

Finally, it should be noted that, because the nanoscale closure problems are stationary, the dual-porosity model appears ruled by two disparate time scales associated with the transient phenomena at micro- and macroscales. In the context of the modified Green's functions technique, it has been shown in Arbogast [5] that, in the linear case, the simultaneous micro-/macroequations are equivalent to a single macroscopic model exhibiting fading memory effects in the effective constitutive laws. When applied to double porosity poroelastic media, this equivalence shows effective stresses given by a viscoelastic constitutive law represented in terms of an hereditary integral with memory (see Murad et al. [52] and Murad and Cushman [51]).

6 Quasisteady model

We shall henceforth discuss a simplified version of the dual-porosity model, which is derived assuming that nonequilibrium phenomena within the clay clusters occur in a much shorter time scale compared to the one associated with flow and transport in the micropores. Within this time-scale assumption, we consider fast transient phenomena in the aggregates so that they reach equilibrium instantaneously when perturbed by the thermodynamic processes taking place in the

micropore system. Under this local equilibrium scenario, microscopic flow and ion transport in the clay clusters are neglected, and consequently, the time evolution of the clusters is dictated by a sequence of steady states, each one at local equilibrium with the bulk solution in the micropores. Whence the nature of the mass interchange between clusters and micropores reduces to that of an instantaneous adsorption/desorption process. This approach gives rise to the so-called quasisteady models, which have been proposed for double-porosity systems under the assumption of disparity between the time scales associated with global and local phenomena [22, 23]. The main feature underlying a quasisteady model is that the macroscopic system follows a regular evolution process, whereas local exchanges between the two media are regarded stationary. A typical example of a system governed by this reduced model is the fractured media with small-sized matrix blocks (see Douglas et al. [22]).

In the notation that follows, we adopt the additional superscript "∞" to designate the corresponding variable under the quasisteady approximation. Within the current context, local equilibrium is enforced by neglecting the local variability of the potentials within the clusters by dropping the terms $\{\nabla_y P_b^{0\infty}, \nabla_y C_b^{0\infty} \nabla_y, \Psi_b^{0\infty}\}$ in Eq. 5.67. Together with the Dirichlet boundary conditions in Eq. 5.68, this assumption enforces the equality with the corresponding potentials in the micropore system. This yields

$$P_b^{0\infty}(\boldsymbol{x}, \boldsymbol{y}, t) = P_f^{0\infty}(\boldsymbol{x}, t); \qquad C_b^{0\infty}(\boldsymbol{x}, \boldsymbol{y}, t) = C_f^{0\infty}(\boldsymbol{x}, t);$$

$$\Psi_b^{0\infty}(\boldsymbol{x}, \boldsymbol{y}, t) = \Psi_f^{0\infty}(\boldsymbol{x}, t) \tag{6.1}$$

which, when combined with the reciprocity relations in Eq. 5.67, implies in the absence of the local Onsager's fluxes $\mathbf{v}_D^{1\infty} = \boldsymbol{J}_d^{1\infty} = \boldsymbol{I}_e^{1\infty} = 0$. Thus, under the above assumptions, the convection–diffusion–reaction Eqs. 5.48 and 5.49 reduce to

$$\frac{\partial}{\partial t}\left(n_f^{\infty} C_f^{0\infty}\right) + \nabla_x \cdot \left(C_f^{0\infty} \boldsymbol{V}_{DF}^{0\infty} + \frac{1}{2} C_T^{0\infty} \frac{\partial \mathbf{u}^{0\infty}}{\partial t}\right)$$

$$- \nabla_x \cdot \left(\boldsymbol{D}_{eff}^{\star} \nabla_x C_f^{0\infty}\right) = -\frac{1}{2}\frac{\partial}{\partial t}\left(\langle \phi^{0\infty} G_c^{0\infty} \rangle_y C_f^{0\infty}\right)$$

$$= -\frac{1}{2}\frac{\partial}{\partial t}\left(\langle \phi^{0\infty} G_c^{0\infty} \rangle_y^s \left(1 - n_f^{\infty}\right) C_f^{0\infty}\right)$$

where $G_c^{0\infty} := \langle \cosh \overline{\varphi}^{0\infty} \rangle_z^l$ with $\overline{\varphi}^{0\infty}$ satisfying que quasisteady version of the one-dimensional Poisson–Boltzmann problem Eq. 3.15 at $\mathcal{O}(\epsilon^0)$

$$\tilde{\varepsilon_0}\tilde{\varepsilon}\frac{d^2\varphi^{0\infty}}{\mathrm{d}z^2} = 2FC_f^{0\infty}(\boldsymbol{x}, t)\sinh\overline{\varphi}^{0\infty}. \tag{6.2}$$

Defining the sorbed concentration $C_S^{0\infty} := 0.5\, C_f^{0\infty} \langle \phi^{0\infty} G_c^{0\infty} \rangle_y^s$, we obtain the following reactive transport system in terms of $\{C_f^{0\infty}, C_S^{0\infty}\}$

$$\begin{cases} \dfrac{\partial}{\partial t}\left(n_f^{\infty} C_f^{0\infty}\right) + \nabla_x \cdot \left(C_f^{0\infty} \boldsymbol{V}_{DF}^{0\infty} + C_T^{0\infty} \dfrac{\partial \mathbf{u}^{0\infty}}{\partial t}\right) \\ -\nabla_x \cdot \left(\boldsymbol{D}_{eff}^{\star} \nabla_x C_f^{0\infty}\right) = -\dfrac{\partial}{\partial_t}\left(C_S^{0\infty}\left(1 - n_f^{\infty}\right)\right) \\ C_S^{0\infty} = K_d C_f^{0\infty} \end{cases}$$

where

$$K_d := \frac{1}{2}\langle \phi^{0\infty} G_c^{0\infty} \rangle_y^s = \left\langle \phi^{0\infty} \langle \cosh \overline{\varphi}^{0\infty} \rangle_z^l \right\rangle_y^s$$

$$= \left\langle \langle \cosh \overline{\varphi}^{0\infty} \rangle_z \right\rangle_y^s \tag{6.3}$$

denotes the partition coefficient. Thus, under the quasisteady approximation, the movement of the species is dictated by a macroscopic convection–diffusion–reaction equation with an adsorption/desorption source term, which governs the instantaneous immobilization of the solutes in the nanopores of the aggregates. The above system can also be represented in the form

$$\frac{\partial}{\partial t}\left(RC_f^{0\infty}\right) + \nabla_x \cdot \left(C_f^0 \boldsymbol{V}_{DF}^0 + C_T^{0\infty} \frac{\partial \mathbf{u}^{0\infty}}{\partial t}\right)$$

$$= \nabla_x \cdot \left(\boldsymbol{D}_{eff}^{\star} \nabla_x C_f^{0\infty}\right)$$

where R designates the retardation factor defined as

$$R := n_f^{\infty} + \left(1 - n_f^{\infty}\right) K_d\,. \tag{6.4}$$

A notable consequence of our three-scale approach is the above representations for K_d and R, which provide new insight in the physics of adsorption/desorption phenomena in charged clays. The nanoscopic representation Eq. 6.3 shows direct correlation between the magnitude of K_d and the electrochemistry of the electrolyte solution whose electric potential distribution in the nanopores is ruled by the Poisson–Boltzmann problem Eq. 6.2. It is worth noting that the quasisteady model for transport of nonionic species discussed in Douglas and Spagnuolo [23] can easily be recovered by dropping the EDL contribution, setting $\overline{\varphi}^{0\infty} = 0 \rightarrow G_c^{0\infty} = 2$. This implies that, in the absence of electrochemical effects, K_d reduces to a purely geometric quantity defined by the averaging of the secondary porosity $\langle \phi^{0\infty} \rangle_y^s$.

The quasisteady approximation for flow and transport also implies stationary of the closure problems of the poromechanics. In fact, using assumption Eq. 6.1a ($P_0 = 0$) in Eq. 5.62a and exploring linearity yields the stationary closure relation for the fluctuating displacement.

$$\mathbf{u}_e^{1\infty}(\boldsymbol{x},\ \boldsymbol{y},\ t) = \boldsymbol{\xi}(\boldsymbol{y})\left[\boldsymbol{\mathcal{E}}_x\left(\mathbf{u}^{0\infty}(\boldsymbol{x},t)\right)\right] + \widehat{\mathbf{u}}(\boldsymbol{x},t) \tag{6.5}$$

where the third-order tensor $\boldsymbol{\xi}$ satisfies the canonical cell problem

$$\boldsymbol{\nabla}_y\cdot(\boldsymbol{C}\boldsymbol{\mathcal{E}}_y(\boldsymbol{\xi})) = 0 \quad \text{in } Y_s \tag{6.6}$$

$$\left(\boldsymbol{C}\boldsymbol{\mathcal{E}}_y(\boldsymbol{\xi})\right)\boldsymbol{N} = -(\boldsymbol{C}\boldsymbol{I}\otimes\boldsymbol{I})\boldsymbol{N} \quad \text{on } \partial Y_{fs} \tag{6.7}$$

with $\boldsymbol{I}\otimes\boldsymbol{I}$ denoting the unity fourth-order tensor with components $\delta_{ij}\delta_{kl}$ (here δ designates the Kronecker delta symbol). Defining the effective elastic modulus

$$\boldsymbol{C}_{eff} := \left\langle \boldsymbol{C}(\boldsymbol{I}\otimes\boldsymbol{I} + \boldsymbol{\mathcal{E}}_y(\boldsymbol{\xi}))\right\rangle_y \tag{6.8}$$

we then have using Eqs. 6.5 and 6.1a in Eq. 5.63

$$\boldsymbol{\sigma}_E^{0\infty} = \boldsymbol{C}_{eff}\boldsymbol{\mathcal{E}}_x\left(\mathbf{u}^{0\infty}\right) \tag{6.9}$$

which reproduces the classical linear elastic law for the contact stress. Furthermore, using Eqs. 5.60 and 6.1b in Eq. 5.63b, we obtain

$$\begin{aligned}\left\langle \boldsymbol{\Pi}^{0\infty}\right\rangle_y &= \left\langle \Pi^{0\infty}\right\rangle_y \boldsymbol{n}\otimes\boldsymbol{n}\\ &= 2RTC_f^{0\infty}(\boldsymbol{x},t)\left(1-n_f^{\infty}\right)\left(\left\langle\cosh\overline{\varphi}_0\right\rangle_y^s - 1\right)\boldsymbol{n}\otimes\boldsymbol{n}\end{aligned} \tag{6.10}$$

$$\begin{aligned}\boldsymbol{\Pi}_{eff}^{0\infty} &= -\boldsymbol{C}\langle\boldsymbol{\mathcal{E}}_y(\mathbf{u}_\pi^{1\infty})\rangle_y\\ &\quad +2RTC_f^{0\infty}(1-n_f^{\infty})(\langle\cosh\overline{\varphi}_0\rangle_y^s - 1)\boldsymbol{n}\otimes\boldsymbol{n}\,.\end{aligned} \tag{6.11}$$

By eliminating $\boldsymbol{\sigma}_E^{0\infty}$ and $\boldsymbol{\Pi}_{eff}^{0\infty}$ through their constitutive laws in Eqs. 6.9 and 6.11, the quasisteady version of Terzaghi's decomposition Eq. 5.64 reads

$$\begin{aligned}\boldsymbol{\sigma}_T^{0\infty} =& -P_f^{0\infty}\boldsymbol{I} + \boldsymbol{C}_{eff}\boldsymbol{\mathcal{E}}_x\left(\mathbf{u}^{0\infty}\right) + \boldsymbol{C}\left\langle\boldsymbol{\mathcal{E}}_y\left(\mathbf{u}_\pi^{1\infty}\right)\right\rangle_y\\ &- 2C_f^{0\infty}RT\left(1-n_f^{\infty}\right)\left(\left\langle\cosh\overline{\varphi}_0\right\rangle_y^s - 1\right)\boldsymbol{n}\otimes\boldsymbol{n}\end{aligned} \tag{6.12}$$

It is worth noting that, unlike the fully transient case (Eq. 5.64), where the appearance of the secondary time scale gives rise to a viscoelastic behavior for the effective stresses [52], the above quasisteady form of Terzaghi's decomposition is ruled by a single macroscopic time scale showing absence of fading memory effects.

Finally, we derive the steady form of the mass balance of the clay clusters Eq. 5.65. Using the stationary closure Eq. 6.5 in the mass balance Eq. 5.65 and defining

$$\boldsymbol{\beta} := \langle\boldsymbol{\nabla}_y\cdot\boldsymbol{\xi}\rangle_y, \qquad \gamma_\pi := \left\langle\boldsymbol{\nabla}_y\cdot\mathbf{u}_\pi^{1\infty}\right\rangle_y \tag{6.13}$$

we have

$$\frac{\partial n_f^{\infty}}{\partial t} + \boldsymbol{\beta} : \boldsymbol{\mathcal{E}}_x\cdot\left(\frac{\partial\mathbf{u}^{0\infty}}{\partial t}\right) = -\frac{\partial\gamma_\pi^{\infty}}{\partial t}\,. \tag{6.14}$$

where $\boldsymbol{A}:\boldsymbol{B} = \sum_{ij}A_{ij}B_{ij}$ denotes the classical inner product between tensors. Note that $-\boldsymbol{\beta}$ plays the role of a tensorial generalization of the Biot's poroelastic bulk modulus $Qn_f/R = \alpha - n_f$ (Biot [11]), which accounts for microscopic solid compressibility with α denoting the Biot–Willis coupling parameter [12]. The above form shows a typical mass balance for locally compressible aggregates with an additional electrochemical compressibility, which captures swelling/ shrinking of the clusters due to the instantaneous mass exchange with the bulk fluid. Finally, it should be noted that, for incompressible clusters, we have $\boldsymbol{\beta} = -Qn_f/R\boldsymbol{I} = -(1-n_f)\boldsymbol{I}$, $\alpha = 1$, and $\gamma_\pi = 0$.

6.1 Summary of the three-scale quasisteady model

Let $\varphi^{0\infty}$ be the EDL potential satisfying Eq. 6.2 and $\{\boldsymbol{K}_P, \boldsymbol{K}_C, \boldsymbol{K}_E, \boldsymbol{D}_{eff}, \boldsymbol{D}_{eff}^{\star}, \boldsymbol{\Delta}_{eff}\}$ be the same variables that appear in Eq. 5.66. Furthermore, let $\{R, \boldsymbol{C}_{eff}, \boldsymbol{\Pi}_{eff}^{0\infty}, \beta.\gamma_\pi\}$ be the new set of effective coefficients defined by the stationary closure Eqs. 6.4, 6.8, 6.11, and 6.13. The model consists in finding the macroscopic unknowns $(\boldsymbol{\sigma}_T^{0\infty}, \mathbf{u}^{0\infty}, P_f^{0\infty}, \boldsymbol{V}_{DF}^{0\infty}, n_f^{\infty}, C_f^{0\infty})$ satisfying

$$\begin{cases}\boldsymbol{\nabla}_x\cdot\boldsymbol{\sigma}_T^{0\infty} = 0\\ \boldsymbol{\sigma}_T^{0\infty} = -P_f^{0\infty}\boldsymbol{I} + \boldsymbol{C}_{eff}\boldsymbol{\mathcal{E}}_x\left(\mathbf{u}^{0\infty}\right) - \boldsymbol{\Pi}_{eff}^{0\infty},\\ \boldsymbol{\nabla}_x\cdot\dfrac{\partial\mathbf{u}^{0\infty}}{\partial t} + \boldsymbol{\nabla}_x\cdot\boldsymbol{V}_{DF}^{0\infty} = 0\\ \boldsymbol{V}_{DF}^{0\infty} = -\boldsymbol{K}_P\boldsymbol{\nabla}_x P_f^{0\infty} - \boldsymbol{K}_C\boldsymbol{\nabla}_x C_f^{0\infty} - \boldsymbol{K}_E\boldsymbol{\nabla}_x\Psi_f^{0\infty}\\ \dfrac{\partial n_f^{\infty}}{\partial t} + \boldsymbol{\beta}:\boldsymbol{\mathcal{E}}_x\cdot\dfrac{\partial\mathbf{u}^{0\infty}}{\partial t} = -\dfrac{\partial\gamma_\pi}{\partial t}\\ \dfrac{\partial}{\partial t}\left(RC_f^{0\infty}\right) + \boldsymbol{\nabla}_x\cdot\left(C_f^{0\infty}\boldsymbol{V}_{DF}^{0\infty} + C_T^{0\infty}\dfrac{\partial\mathbf{u}^{0\infty}}{\partial t}\right)\\ -\boldsymbol{\nabla}_x\cdot\left(\boldsymbol{D}_{eff}^{\star}\boldsymbol{\nabla}_x C_f^{0\infty}\right) = 0\\ \boldsymbol{\nabla}_x\cdot\left(\boldsymbol{\Delta}_{eff}\boldsymbol{\nabla}_x C_f^{0\infty} + \boldsymbol{D}_{eff}C_f^{0\infty}\boldsymbol{\nabla}_x\Psi_f^{0\infty}\right) = 0\end{cases}.$$

The stationarity of the microscopic closure problems reflects the absence of relaxation phenomena associated with secondary flow in the system of clay clusters. Whence, information available at the microscale is used to compute the time-independent effective electro-chemo-mechanical parameters.

7 Computational of the effective electro-chemical coefficients

To illustrate the potential of the three-scale approach in developing constitutive laws for the effective electrochemical parameters of the quasisteady model, in what follows, we present the numerical solution of the aforementioned closure problems. For conciseness of notation, hereafter, we omit the superscript $''0\infty''$ of the unknowns. For the type of nanostructure considered herein of parallel particles within each cluster, the integral form of the one-dimensional Poisson–Boltzmann problem Eq. 3.17 can easily be solved numerically adopting a well-established change of variables in conjunction with numerical integration of elliptic integrals. Such discretization procedure is presented in details in Moyne and Murad [50] and is omitted here for convenience. In the subsequent numerical simulations, we adopt the following values for the input data: $\sigma = -0.2\,\mathrm{Cm}^{-2}$, $R = 8.314$, $F = 96490$, $T = 293K$, $\tilde{\varepsilon} = 8.854 \times 10^{-12}$, $\tilde{\varepsilon_0} = 80$.

We begin by displaying the nanoscopic EDL potential profile parametrized by C_f and $H^\star := H/\ell_D$.

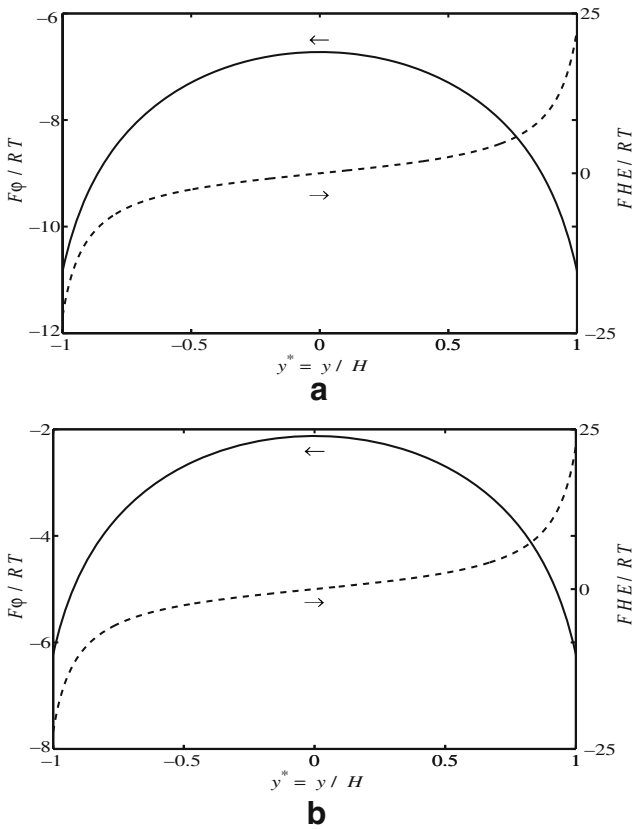

Fig. 6 Local electric potential and electric field distributions: **a** $H/L_D = 0.1$ and $C_f = 2.32 \times 10^{-4}$mol/l; **b** $H/L_D = 1.0$ and $C_f = 2.32 \times 10^{-2}$mol/l

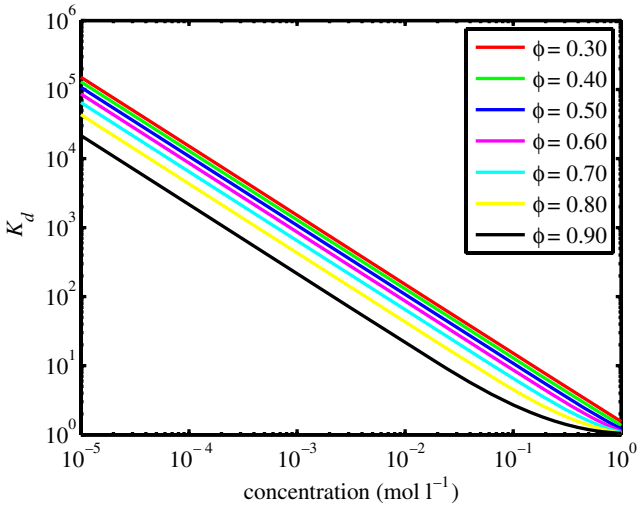

Fig. 7 Dependence of the partition coefficient on C_f for different values of the intracluster porosity ϕ

Denoting $z^* = z/H$ and $\overline{E} := FEH/RT$ a dimensionless electric field, the plots $\overline{\varphi} = \overline{\varphi}(z^*)$ and $\overline{E} = \overline{E}(z^*)$ are depicted in Fig. 6 for two values of C_f and $H^\star$. The ticks in the left and right margins show the range of values of $\overline{\varphi}$ and $\overline{E}$, respectively. As expected, in the line of symmetry ($z^* = 0$), $\overline{\varphi}$ attains maximum value and decreases negatively in a symmetric fashion toward the location of the particles $z^* = \pm 1$. Owing to symmetry, the electric field vanishes at $z^* = 0$ and behaves in a skew symmetric fashion with z^*.

The local distribution $\overline{\varphi} = \overline{\varphi}(z^*)$ is then used as input data in the numerical solution of the closure problems for the effective coefficients. By invoking the representation (6.3) for K_d, for each pair $\{C_b, \phi\}$, the average of the hyperbolic cosine of the EDL potential in the transversal direction furnishes the constitutive law $K_d = K_d(C_f, \phi)$. Figure 7 displays the logarithm of the partition coefficient K_d divided by the intracluster porosity ϕ vs C_f for different values of ϕ. As EDL effects are more pronounced for low values of C_f and ϕ, this range is characterized by high values of K_d/ϕ, which decrease asymptotically in a nearly linear fashion to the unity ($G_c = 2$ and $K_d = \phi$) at high salinity wherein EDL effects are absent. The nearly linear behavior of $\ln K_d$ with C_f suggests a power law fit $K_d = \mathcal{O}(C_f^{-\alpha})$ (for fixed ϕ) with the exponent $0 \le \alpha \le 1$ depending on C_f. To characterize more precisely the dependence $\alpha = \alpha(C_f)$, we invoke the relation $C_S = K_d C_f$ and multiply the aforementioned power-law for K_d by C_f to obtain the constitutive response of the sorbed concentration $C_S = C_S(C_f, \phi)$. Such response appears ruled by the following generalized Freundlich isotherm

$$C_S = F^*(\phi) C_f^{(1-\alpha)} \tag{7.1}$$

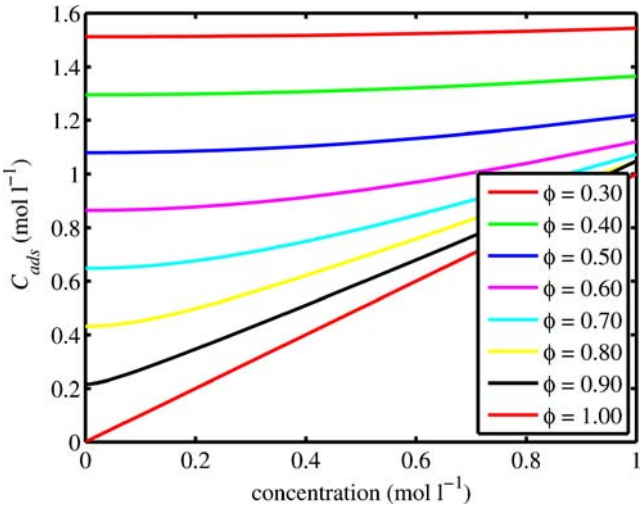

Fig. 8 Dependence of the sorbed concentration on C_f for different values of the intracluster porosity ϕ

where $F^*(\phi)$ denotes a function of the intracluster porosity with values given by the asymptotic behavior of C_S when $\alpha(C_f) \to 1$. The above form suggests the decomposition $C_S = C_S(C_f, \phi) = F^*(\phi)G^*(C_f)$ with $G^*(C_f) := C_f^{(1-\alpha)}$. The numerical plots associated with Eq. 7.1 are depicted in Fig. 8. In the range of high salinity where EDL effects vanish, $\alpha \to 0$, and therefore, adsorption is ruled by the linear isotherm $C_S = F^\star(\phi)C_f$. This asymptotic regime corresponds to the adsorption of nonionic species, which is ruled by the purely geometric quantity $K_d = F^\star(\phi) = \phi$. Conversely, when $C_f \to 0$, the EDL effects increase adsorption in a nonlinear fashion. Under the Langmuir approximation valid for low concentrations, C_S is almost insensitive to variations in C_f; i.e., $\mathrm{d}C_S/\mathrm{d}C_f \to 0$ and therefore $\alpha \to 1$ and $C_S \to F^*(\phi)$ as $C_f \to 0$. The set of discrete points $F^\star(\phi)$ are given by the intersection of the isotherms with the y axis, where each curve reaches minimum value. Such intersection can be calculated by invoking the electroneutrality condition. In fact, when $C_f \to 0$, the strength of the EDL is high and the concentration of cations is much higher than that of the anions. Thus, using the assumption $C_+ >> C_-$ in Eq. 3.5 along with the Boltzmann distribution Eq. 2.17 yields

$$\begin{aligned} q_\star = \langle q^\star \rangle_z &= F(C_+ - C_-) \approx F(C_+ + C_-) \\ &= 2FC_f\phi\langle \cosh\overline{\varphi}\rangle_z^l = -\frac{1}{|Z|}\int_{\partial Z_{ls}} \sigma \, d\Gamma \\ &= \sigma a_{fs}, \qquad \text{for } C_f \to 0 \quad \text{and} \quad \alpha \to 1 \end{aligned}$$

where $a_{fs} := |\partial Z_{ls}|/|Z| = 1/(H+\delta)$ is the surface volume fraction of the particles. For equally spaced particles, we have $\langle a_{fs}\rangle_y^s = a_{fs}$, and thus, using the above result in the three-scale representation of the partition coefficient K_d Eq. 6.3, we obtain

$$K_d = \phi\left\langle \langle \cosh\overline{\varphi}\rangle_z^l \right\rangle_y^s = \frac{\sigma a_{fs}}{2FC_f} \quad \text{for } C_f \to 0 \text{ and } \alpha \to 1.$$

Together with the relation $C_S = K_d C_f$ and the generalized Freundlich isotherm Eq. 7.1, this yields

$$C_S = F^*(\phi) = -\frac{\sigma a_{fs}}{2F} \quad \text{for} \quad C_f \to 0 \quad \alpha \to 1\,.$$

As mentioned before, the numerical values of the above asymptotic result are given by the intersection of each isotherm with the y axis in Fig. 8. Such results show F^* a decreasing function of ϕ with lower bound $F(1) = 0$.

In Figs. 9 and 10, we display the constitutive response of the effective chemico-osmotic and electro-osmotic conductivities K_C and K_E of the bulk fluid vs $\{C_f, n_f\}$. The numerical results are obtained by solving the closure problems Eq. 5.57 arising from the slip boundary conditions in conjunction with Smoluchowski's and Prieve's formulas Eqs. 3.29 and 3.32 for $\{L_{PE}^{0\infty}, L_{PC}^{0\infty}\}$ under thin double-layer approximation. In the computation of the tortuosity factor $\nabla_y \boldsymbol{f}$ in Eq. 5.57, we adopt an isotropic arrangement of spherical clusters of equally spaced particles within each cluster (Fig. 5). In this particular clay morphology, the conductivities reduce to multiple of the identity $\boldsymbol{K}_J = K_J \boldsymbol{I} (J = C, E)$ and the tortuosity can be computed by invoking the empirical relation $\langle \boldsymbol{I} + \nabla_y \boldsymbol{f}\rangle = n_f^{3/2}\boldsymbol{I}$ [25]. As displayed in Figs. 9 and 10, the magnitude of the scalars $\{K_C, K_E\}$ decreases asymptotically to zero as $C_f \to \infty$ where EDL effects vanish.

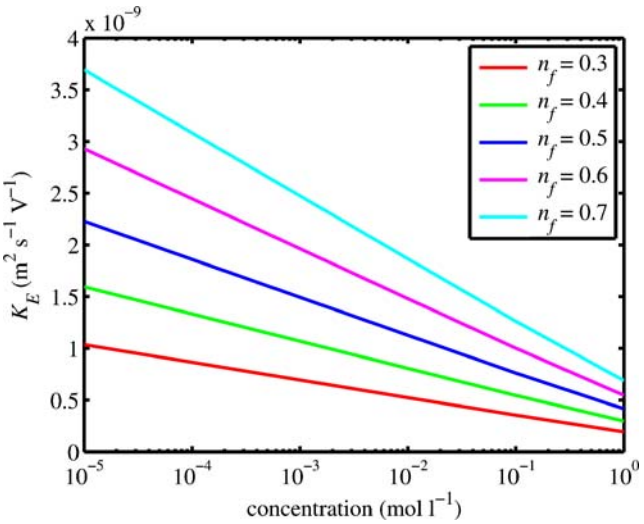

Fig. 9 Dependence of the electro-osmotic conductivity on C_f for different values of the intercluster porosity n_f

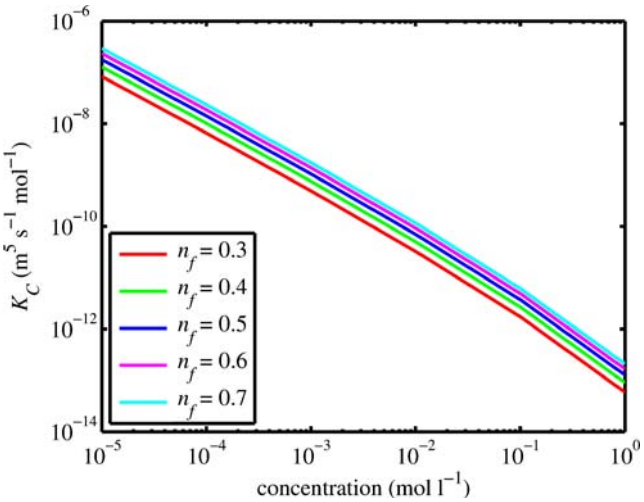

Fig. 10 Dependence of the chemico-osmotic conductivity on C_f for different values of the intercluster porosity n_f

8 Conclusions

In this work, we have successfully developed a three-scale model of dual-porosity type for expansive clays. The morphology of the swelling medium is characterized by two porous structures; the permeable clay clusters with nanopores filled by an electrolyte solution and the micropores saturated by bulk phase water. The model was rigorously derived within the asymptotic homogenization procedure applied to a microscale problem governing flow and transport of the species in the bulk solution lying in the micropores in conjunction with an electro-chemo-mechanical model for the clay aggregates based on Onsager's reciprocity relations. The effective governing equations incorporate distributed mass transfer functions between the two systems along with modified forms of Darcy's law and Terzaghi's effective stress principle. Considering a particular form of nanostructure wherein each clay cluster is composed of parallel particles, nanoscopic representations were provided for the microscale coefficients of the clay clusters in terms of the local EDL potential satisfying a Poisson–Boltzmann problem, which rules the electrochemistry of the electrolyte solution in the nanopores.

Adopting a local instantaneous equilibrium assumption between the two systems, a quasisteady version of the dual-porosity model was derived. In this simplified scenario, the general history dependency in the constitutive law inherent to the fully-transient case reduces to a local equation in time ruled by a single macroscopic time scale associated with the evolution of the macroscopic medium. In this simplified case, the constitutive behavior of the mass transfer function reduces to that of an instantaneous equilibrium adsorption/desorption process and gives rise to a retardation coefficient that appears explicitly correlated with the local distribution of the EDL potential in the nanopores. In a similar fashion, nanoscopic representations were provided for the other effective electro-chemical parameters such as electro- and chemico-osmotic permeabilities.

This bridge between electrochemical phenomena at different scales obtained herein allows us to build-up constitutive laws for the macroscopic electrochemical parameters from exploitation of the nanoscopic cell problems. Numerical simulations depicting the behavior of the effective electrochemical parameters were obtained by solving the Poisson–Boltzmann problem numerically at the nanoscale and double averaging to the macroscale.

The proposed three-scale approach captures the correct physics underlying each electro-chemo-mechanical parameter and therefore provides new insight in the multiscale modeling of swelling porous media. Although the two-scale computations were performed for a particular form of nanostructure, they provide guidance for further developments considering random geometries. Further work is in progress to incorporate more realistic irreversible elastoplastic constitutive relations including chemical hardening/softening of the solid matrix (Loret et al. [43]).

Acknowledgements This work was supported by the funding provided by *Conselho Nacional de Desenvolvimento Cientifico e Tecnologico* and by Modélisations Mathématiques et Simulations numériques liées aux problèmes de gestion des déchets nucléaires (GDR MOMAS) (*Centre National de la Recherche Scientifique*).

Appendix

Chemico-osmotic permeability of a clay cluster in the regime of thin EDL's

In this appendix we show the derivation of Eq. 3.32 for the chemico-osmotic permeability.

To this end we begin by introducing the more convenient coordinate $z' := z - H$ so that $z' = 0$ at the particle surface. Under the assumption $\ell_D << H$, electrical effects are absent away from the particle surface, which implies $\overline{\varphi} = \mathrm{d}\overline{\varphi}/\mathrm{d}z' = \mathrm{d}v_C/\mathrm{d}z' = 0$ as $z' \to \infty$. Thus, integrating Eq. 3.30 from z' to ∞ and using the thin EDL assumption, we get

$$\mu \frac{\mathrm{d}v_C}{\mathrm{d}z'} = 2\,R\,T \int_{z'}^{\infty} (\cosh\overline{\varphi} - 1)\,\mathrm{d}z' \,. \tag{8.1}$$

To compute the RHS, we make use of the identity

$$2\,(\cosh\overline{\varphi} - 1) = 4\sinh^2\frac{\overline{\varphi}}{2} = \frac{16\tanh^2\overline{\varphi}/4}{\left(1 - \tanh^2\overline{\varphi}/4\right)^2} \,. \tag{8.2}$$

Using Poisson–Boltzmann, one can relate $\tanh(\overline{\varphi}/4)$ to the dimensionless zeta potential $\overline{\zeta} := \overline{\varphi}(H)$. To this end, we multiply Eq. 3.15 by $2\,\mathrm{d}\overline{\varphi}/\mathrm{d}z'$ to obtain $\mathrm{d}/\mathrm{d}z'(d\overline{\varphi}/\mathrm{d}z')^2 = 2/\ell_D^2\,\mathrm{d}(\cosh\overline{\varphi})\;dz'$. Integrating the above result from ∞ to z' and using Eq. 8.2, we obtain

$$\left(\frac{\mathrm{d}\overline{\varphi}}{\mathrm{d}z'}\right)^2 = \frac{2}{\ell_D^2}(\cosh\overline{\varphi}-1) = \frac{4}{\ell_D^2}\sinh^2\left(\frac{\overline{\varphi}}{2}\right)$$
$$\rightarrow \frac{\mathrm{d}\overline{\varphi}}{\mathrm{d}z'} = -\frac{2}{\ell_D}\sinh\left(\frac{\overline{\varphi}}{2}\right) \rightarrow \frac{\mathrm{d}\overline{\varphi}}{\sinh(\overline{\varphi}/2)} = -\frac{2}{\ell_D}\mathrm{d}z'. \tag{8.3}$$

To integrate the above result, we adopt the change of variables $w = \tanh(\overline{\varphi}/4)\mathrm{d}w = 1/4(1-w^2)\mathrm{d}\overline{\varphi}$; $\sinh(\overline{\varphi}/2) = 2w/(1-w^2)$, which, when combined with the last equation in Eq. 8.3, gives $dw/w = -\mathrm{d}z'/\ell_D$. Hence, after integrating from 0 to z', we obtain

$$\tanh\left(\frac{\overline{\varphi}}{4}\right) = \tanh\left(\frac{\overline{\zeta}}{4}\right)\exp\left(-\frac{z'}{\ell_D}\right).$$

Moreover, denoting $A = \tanh\left(\overline{\zeta}/4\right)$, using the above result in Eq. 8.2, we get

$$2(\cosh\overline{\varphi}-1) = \frac{16A^2\exp(-2z'/\ell_D)}{\left[1-A^2\exp(-2z'/\ell_D)\right]^2}. \tag{8.4}$$

Moreover, denoting $u = A^2\exp(-2z'/\ell_D)$ with $\mathrm{d}u = -(2u/\ell_D)\mathrm{d}z'$, integrating Eq. 8.4, we obtain

$$2\int_{z'}^{\infty}(\cosh\overline{\varphi}-1)\,\mathrm{d}z' = 8\,\ell_D\int_0^u \frac{\mathrm{d}u}{(1-u)^2} = \frac{8\,\ell_D\,u}{1-u}.$$

Finally, using the above result in Eq. 8.1 yields

$$\mu\frac{\mathrm{d}v_C}{\mathrm{d}z'} = \frac{8\,R\,T\,\ell_D A^2\exp(-2z'/\ell_D)}{1-A^2\exp(-2z'/\ell_D)}$$

in which integrating from 0 to z' and using the nonslip condition at the wall yields

$$\begin{aligned} v_C(z') &= \frac{8RT\ell_D}{\mu}\int_0^{z'}\frac{A^2\exp(-2z'/\ell_D)}{1-A^2\exp(-2z'/\ell_D)}\mathrm{d}z' \\ &= -\frac{4RT\ell_D^2}{\mu}\int_{A^2}^{u}\frac{\mathrm{d}u}{1-u} \\ &= \frac{4RT\ell_D^2}{\mu}\Big[\ln(1-u)\Big]_{A^2}^{u} \\ &= \frac{4RT\ell_D^2}{\mu}\ln\left[\frac{1-\tanh^2\left(\overline{\zeta}/4\right)\exp(-2z'/\ell_D)}{1-\tanh^2\left(\overline{\zeta}/4\right)}\right]. \end{aligned} \tag{8.5}$$

In a similar fashion to Eq. 3.28, the above result shows that the magnitude of $L_{PC} = (C_b\phi/RT)\langle v_C\rangle_z^l$ given by the sum of two contributions: one solely dictated by the $\overline{\zeta}$-potential, independent of z' playing a similar role of the Smoluchowski's component of L_{PE}, which dominates the behavior of L_{PC} for $H \gg \ell_D$, and a secondary EDL component, strongly dependent on the Debye's length, which becomes pronounced when $H = \mathcal{O}(\ell_D)$. This is similar to the asymptotic regime of thin EDLs because the primary component is independent of z' and becomes equal to its averaged value L_{PC}^{∞}. Thus, under the assumption $\tanh^2(\overline{\zeta}/4)\exp(-2z'/\ell_D) << 1$, we have

$$\begin{aligned} L_{PC}^{\infty} &= -\frac{4C_b\ell_D^2\phi}{\mu}\ln\left(1-\tanh^2\left(\frac{\overline{\zeta}^{\infty}}{4}\right)\right) \\ &= \frac{8C_b\ell_D^2\phi}{\mu}\ln\left(\cosh\left(\frac{\overline{\zeta}^{\infty}}{4}\right)\right) \quad \text{for} \quad \ell_D << H. \end{aligned}$$

References

1. Achari, G., Joshi, R.C., Bentley, L.R., Chatterji, S.: Prediction of the hydraulic conductivity of clays using the electric double layer theory. Can. Geotech. J. **36**, 783–792 (1999)
2. Arbogast, T.: On the simulation of incompressible miscible displacement in a naturally fractured petroleum reservoir. R.A.I.R.O. Model. Math. Anal. Numer. **23**, 5–51 (1989)
3. Arbogast, T.: Computational aspects of dual porosity models. In: Hornung, U. (ed.) Homogenization and Porous Media. Interdisciplinary Applied Mathematics, pp. 1–27. Springer, New York (1996)
4. Arbogast, T., Douglas, J., Hornung, U.: Modeling of naturally fractured reservoirs by formal homogenization techniques. In: Dautray, R. (ed.) Frontiers in Pure and Applied Mathematics, pp. 1–19. Elsevier, Amsterdam (1991)
5. Arbogast, T.: A simplified dual-porosity model for two-phase flow. In: Russel, T.F., Ewing, R.E., Brebbia, C.A., Gray, W.G., Pindar, G.F. (eds.) Computational Methods in Water Resources, pp. 419–426. Computational Mechanics Publication, Southampton (1992)
6. Arulanandam, S., Li, D.: Liquid transport in rectangular microchannels by electroosmotic pumping. Colloids Surf. A Physicochem. Eng. Asp. **161**, 89–102 (2000)
7. Auriault, J.L.: Heterogeneous media: is an equivalent homogeneous description always possible? Int. J. Eng. Sci. **29**, 785–795 (1991)
8. Barenblatt, G.I., Zhelton, I.P., Kochina, I.N.: Basic concepts in the theory of seepage of homogeneous liquids in fissured rocks. J. Appl. Math. Mech. **24**, 1286–1303 (1960)
9. Bennethum, L.S., Cushman, J.H.: Multicomponent, multiphase thermodynamics of swelling porous media with electroquasistatics: parts I–II. Transp. Porous Media **47**(3), 309–362 (2002)
10. Bike, S.G., Prieve, C.: Electrohydrodynamics of thin double layers: a model for the streaming potential profile. J. Colloid Interface Sci. **154**(1), 87–96 (1992)
11. Biot, M.: Theory of elasticity and consolidation for a porous anisotropic soild. J. Appl. Phys. **26**, 182–185 (1955)
12. Biot, M., Willis, D.G.: The elastic coefficients of the theory of consolidation. J. Appl. Mech. **79**, 594–601 (1957)

13. Bourgeat, A., Mikelic, A., Piatnitski, A.: On the double porosity model of a single phase flow in random media. Asymptot. Anal. **34**(3–4), 311–332 (2003)
14. Callen, H.: Thermodynamics and an Introduction to Thermostatics. Wiley, New York (1985)
15. Coelho, D., Shapiro, M., Thovert, J.F., Adler, P.M.: Electroosmotic phenomena in porous media. J. Colloid Interface Sci. **181**, 169–190 (1996)
16. Corapcioglu, M.Y.: Formulation of electro-chemico-osmotic processes in soils. Transp. Porous Media **6**, 435–444 (1991)
17. Dahnert, K., Huster, D.: Comparison of the Poisson–Boltzmann model and the Donnan equilibrium of a polyelectrolyte in salt solution. J. Colloid Interface Sci. **215**, 131–139 (1999)
18. Derjaguin, B.V., Churaev, N.V., Muller, V.M.: Surface Forces. Plenum, New York (1987)
19. Derjaguin, B.V., Dukhin, S.S., Kobotkova, A.A.: Diffusiophoresis in electrolyte solutions and its role in the mechanism of film formation from rubber latexes by the method of ionic deposition. Kolloidn Z. **23**(3), 53–55 (1961)
20. Donnan, F.G.: The theory of membrane equilibria. Chem. Rev. **1**, 73–90 (1924)
21. Dormieux, L., Barboux, P., Coussy, O., Dangla, P.: A macroscopic model of the swelling phenomenon of a saturated clay. Eur. J. Mech. A Solids **14**(6), 981–1004 (1995)
22. Douglas, J., Paes Leme, P.J., Hensley, J.L.: A limit form of the equations for immiscible displacement in a fractured reservoir. Transp. Porous Media **6**, 549–565 (1991)
23. Douglas, J., Spagnuolo, A.: The transport of nuclear contamination in fractured porous media, Mathematics in the new millennium (Seoul, 2000). J. Korean Math. Soc. **38**(4), 723–761 (2001)
24. Douglas, J., Arbogast, T.: Dual porosity models for flow in naturally fractured reservoirs. In: Cushman, J.H. (ed.) Dynamics of Fluid in Hierarchical Porous Media, pp. 177–222. Academic, New York (1990)
25. Dullien, F.A.L.: Porous Media: Fluid Transport and Pore Structure. Academic, New York (1979)
26. Edwards, D.A.: Charge transport through a spatially periodic porous medium: electrokinetic and convective dispersion phenomena. Philos. Trans. R. Soc. Lond. **A353**, 205–243 (1995)
27. Eringen, A.C., Maugin, G.A.: Electrodynamics of Continua. Springer, New York (1989)
28. Fair, J.C., Osterlé, J.F.: Reverse electrodialysis in charged capillary membranes. J. Chem. Phys. **54**(8), 3307–3316 (1971)
29. Gross, R.J., Osterlé, J.F.: Membrane transport characteristics of ultrafine capillaries. J. Chem. Phys. **49**(1), 228–234 (1968)
30. Gu, W.Y., Lai, W.M., Mow, V.C.: A triphasic analysis of negative osmotic flows through charged hydrated tissues. J. Biomech. **30**(1), 71–78 (1998)
31. Gu, W.Y., Lai, W.M., Mow, V.C.: A mixture theory for charged–hydrated soft tissues containing multi-electrolytes: Passive transport and swelling behaviors. J. Biomech. Eng. **120**, 169–180 (1998)
32. Heidug, W.K., Wong, S.W.: Hydration swelling of water-adsorbing rocks: A constitutive model. Int. J. Numer. Anal. Methods Geomech. **20**, 403–430 (1996)
33. Hueckel, T.: On effective stress concepts and deformation in clays subjected to environmental loads. Can. Geotech. J. **29**, 1120–1125 (1992)
34. Hunter, R.J.: Zeta Potential in Colloid Science: Principles and Applications. Academic, New York (1981)
35. Hunter, R.J.: Introduction to Modern Colloid Science. Oxford University Press, Oxford (1994)
36. Huyghe, J.M., Janssen, J.D.: Quadriphasic mechanics of swelling incompressible porous media. Int. J. Eng. Sci. **25**(8), 793–802 (1997)
37. Israelachvili, J.: Intermolecular and Surfaces Forces. Academic, New York (1991)
38. Lambe, T.W.: A mechanistic picture of shear strength in clay. In: Proceedings of The ASCE research conference on shear strength of cohesive soils, Boulder, CO, pp. 503–532 (1960)
39. Lai, W.M., Hou, J.S., Mow, V.C.: A triphasic theory for the swelling and deformation behaviors of articular cartilage. J. Biomech. Eng. **113**, 245–258 (1991)
40. Landau, L.D., Lifshitz, E.M.: Electrodynamics of Continuous Media. Pergamon, Oxford (1960)
41. Li, D.: Electro-viscous effects on pressure-driven liquid flow in microchannels. Colloids Surf. A Physicochem. Eng. Asp. **195**, 35–57 (2001)
42. Looker, J.R., Carnie S.L.: Homogenization of the ionic transport equations in periodic porous media. Transp. Porous Media **65**, 107–131 (2006)
43. Loret, B., Hueckel, T., Gajo, A.: Chemo-mechanical coupling in saturated porous media: Elastic–plastic behavior of homoionic expansive clays. Int. J. Solids Struct. **39**, 2773–2806 (2002)
44. Low, P.F.: Structural component of the swelling pressure of clays. Langmuir **3**, 18–25 (1987)
45. Lyklema, J.: Fundamentals of Colloid and Interface Science. Academic, London (1993)
46. Mitchell, J.: Fundamentals of Soil Behavior. Wiley, New York (1993)
47. Moyne, C., Murad, M.L.: Electro-chemico-mechanical couplings in swelling clays derived from a micro/macro homogenization procedure. Int. J. Solids Struct. **39**, 6159–6190 (2002)
48. Moyne, C., Murad, M.: Macroscopic behavior of swelling porous media derived from micromechanical analysis. Transp. Porous Media, **50**, 127–151 (2003)
49. Moyne, C., Murad, M.: A two-scale model for coupled electro-chemo-mechanical phenomena and Onsager's reciprocity relations in expansive clays: I. Homogenization analysis. Transp. Porous Media, **62**(3), 333–380 (2006)
50. Moyne, C., Murad, M.: A two-scale model for coupled electro-chemo-mechanical phenomena and Onsager's reciprocity relations in expansive clays: II. Computational validation. Transp. Porous Media **63**(1), 13–56 (2006)
51. Murad, M.A., Cushman, J.C.: Thermomechanical theories for swelling porous media with microstructure. Int. J. Eng. Sci. **38**(5), 517–564 (2000)
52. Murad, M.A., Guerreiro, J.N., Loula, A. F.: Micromechanical computational modeling of secondary consolidation and hereditary creep in soils. Comput. Methods Appl. Mech. Eng. **190**(15), 1985–2016 (2001)
53. Murad, M., Moyne, C.: Micromechanical computational modeling of expansive porous media. Mecanique **330**, 865–870 (2002)
54. Newman, J. S.: Electrochemical Systems. Prentice-Hall, Englewood Cliffs (1973)
55. Prieve, D.C., Anderson, J.L., Ebel, J.P., Lowell, M.E.: Motion of a particle by chemical gradients. Part 2. Electrolytes. J. Fluid Mech. **148**, 247–269 (1984)
56. Van Olphen, H.: An Introduction to Clay Colloid Chemistry: For Clay Technologists, Geologists, and Soil Scientists. Wiley, New York (1977)
57. Rosanne, M., Paszkuta, M., Adler P.M.: Electrokinetic phenomena in saturated compact clays. J. Colloid Interface Sci. **297**, 353–364 (2006)

58. Samson, E., Marchand, J., Robert, J., Bournazel, J.: Modeling ion diffusion mechanisms in porous media. Int. J. Numer. Methods Eng. **46**, 2043–2060 (1999)
59. Sanchez-Palencia, E.: Non-Homogeneous Media and Vibration Theory. Lectures Notes in Physics. Springer, New York (1980)
60. Sasidhar, V., Ruckenstein, E.: Electrolyte osmosis through capillaries. J. Colloid Interface Sci. **82**(2), 439–457 (1981)
61. Sasidhar, V., Ruckenstein, E.: Anomalous effects during electrolyte osmosis across charged porous membranes. J. Colloid Interface Sci. **85**(2), 332–361 (1982)
62. Shang, J.Q.: Zeta potential and electroosmotic permeability of clay soils. Can. Geotech. J. **34**, 627–631 (1997)
63. Showalter, R.E.: Diffusion models with microstructure. Transp. Porous Media **6**, 567–580 (1991)
64. Slattery, J.C.: Advanced transport phenomena. In: Cambridge Series in Chemical Engineering. Cambridge University Press, New York (1999)
65. Squiries, T.M., Bazant M.Z.: Induced-charge electro-osmosis. J. Fluid Mech. **509**, 217–252 (2004)
66. Sridharan, A., Rao, G.V.: Mechanisms controlling volume change of saturated clays and the role of the effective stress concept. Geotechnique **23**(3), 359–382 (1973)
67. Szymczyk, A., Aoubiza, B., Fievet, P., Pagetti, J.: Electrokinetic phenomena in homogeneous cylindrical pores. J. Colloid Interface Sci. **116**, 285–296 (1999)
68. Yang, C., Li, D.: Analysis of electrokinetic effects on the liquid flow in rectangular microchannels. Colloids Surf. A Physicochem. Eng. Asp. **143**, 339–353 (1998)
69. Yeung, A.T., Mitchell, J.K.: Coupled fluid, electrical and chemical flows in soil. Geotechnique **43**(1), 121–134 (1993)
70. Warren, J.E., Root, P.J.: The behavior of naturally fractured reservoirs. Soc. Pet. Eng. J. **3**, 245–255 (1963)
71. Whitaker, S.: The method of volume averaging. In: Bear, J., Cheng, A., Sorek, S., Ouazar, D., Herrera, I. (eds.) Theory and Applications of Transport in Porous Media. Kluwer, Boston (1999)
72. Wilson, R.K., Aifantis, E.C.: On the theory of consolidation with double porosity. Int. J. Eng. Sci. **20**(9), 1009–1035 (1982)